Conventional and unconventional superconductivity in chalcogenides under high pressure

Dissertation zur Erlangung des Grades
„Doktor der Naturwissenschaften“
im Promotionsfach Chemie

am Fachbereich Chemie, Pharmazie und Geowissenschaften
der Johannes Gutenberg-Universität Mainz

vorgelegt von

Sergii Shylin

geboren in Severodonetsk, Die Ukraine

Mainz, 2017

Dekan: [redacted]

1. Berichterstatter: [redacted]
2. Berichterstatter: [redacted]

Tag der mündlichen Prüfung: 16.05.2017

Die vorliegende Arbeit wurde in der Zeit von Dezember 2013 bis Dezember 2016 am Institut für Anorganische und Analytische Chemie im Fachbereich Chemie, Pharmazie und Geowissenschaften der Johannes Gutenberg-Universität Mainz unter der Leitung von [redacted] angefertigt.

Mainz, Februar 2017

Hiermit versichere ich, dass ich die vorliegende Dissertation selbstständig verfasst und keine anderen als die angegebenen Hilfsmittel benutzt habe. Alle der Literatur entnommenen Stellen sind als solche gekennzeichnet.

Mainz, Februar 2017

Contents

Abstract

A superconductor is a material that can conduct electricity without resistance below a critical temperature T_c. Nowadays, technological applications of superconductors include the design of electromagnets, which are used in MRI/NMR machines, mass spectrometers, particle accelerators, and Josephson junctions, which are the building blocks of the most sensitive magnetometers, particle detectors, including superconducting bolometers and transition edge sensors, as well as low-loss power cables and power storage devices. Therefore, the investigation of high-temperature superconductors is one the most important and challenging problems in the field of solid-state physics and chemistry. Iron chalcogenides are a relatively young and promising family of superconductors. Since the nature of superconductivity in these materials is not fully understood (they are unconventional superconductors), the prospects for the development of their properties are not clear. Applying Mössbauer spectroscopy techniques in combination with magnetic susceptibility and transport measurements under pressure to the simplest systems based mainly on FeSe, we showed how magnetism and superconductivity interact in iron chalcogenides. Magnetic and/or superconducting properties of these materials can be tuned via metal doping, chalcogen substitution or chemical intercalation. Spin fluctuations in high-T_c $Li_x(NH_2)_y(NH_3)_{1-y}Fe_2Se_2$ were shown to be responsible for superconducting pairing at ambient and under applied pressure. For $FeSe_{0.5}Te_{0.5}$, the electronic phase diagram was investigated, and a structural phase transition associated with disappearance of superconductivity was described. Phase separation in $ThCr_2Si_2$-type superconductors was probed by chemical modification using Mössbauer spectroscopy. It was shown that interplay between antiferromagnetic and paramagnetic iron centres, which are responsible for superconducting pairing in $Rb_xFe_ySe_2$ series, might be tuned by doping or varying stoichiometry. In contrast to Fe-based materials, metallization of hydrogen sulfide under pressure leaded to the appearance of conventional superconductivity with T_c as high as 203 K, which is 39 K above the previous record in cuprate superconductors. The Meissner effect in H_2S under pressure of 155 GPa was demonstrated. Its fundamental parameters, critical field, London penetration depth and coherence length, were found and evidenced that H_2S under pressure is a type-II superconductor. A pronounced isotope shift of T_c in D_2S suggested an electron-phonon mechanism of superconductivity that is consistent with the Bardeen–Cooper–Schrieffer scenario. The latest says that the presence of hydrogen is a key to the record-high T_c, raising the prospect that even higher transition temperatures – possibly even approaching room temperature – will be discovered in other hydrogen-dominant systems.

List of abbreviations and symbols

HTSC – high-temperature superconductivity
T_c – critical temperature
B_c – critical field
BCS – Bardeen–Cooper–Schrieffer (theory)
NMR – nuclear magnetic resonance
ZFC – zero-field cooling
FC – in-field cooling
R – electrical resistance
ρ – electrical resistivity
χ – magnetic susceptibility
M – magnetization
V_{zz} – electric field gradient
δ – isomer shift
ΔE_Q – quadrupole splitting
B_{hf} – hyperfine field
SMS – Synchrotron Mössbauer Source
Θ_D – Debye temperature
D_F – density of states at the Fermi level
DAC – diamond anvil cell
NIS – nuclear inelastic scattering
DOS – density of states
EPMA – Electron probe micro-analysis
AFM – antiferromagnetic

1 Preface

1.1 Phenomenon of superconductivity: from Kamerlingh Onnes to nowadays

Solid state materials were divided into conductors, semiconductors and insulators long before the radio was invented [1]. For conductors that were mainly represented by pure metals, a linear resistivity dependence on temperature was known. Its linear approximation gave the negative value of resistivity in the vicinity of 0 K. However, conductivity was believed to be caused by electrons, whereas the resistance was due to their interaction with atoms. At very low temperature charge carriers should have "condensed" and resistivity increased [2]. In order to confirm this hypothesis H. Kamerlingh Onnes from Leiden in 1911 unexpectedly found a drop of the resistance for metallic mercury at liquid helium temperature [3]. The observed effect was called superconductivity, which in modern literature is defined as an ability of material to conduct electricity without resistance below a certain temperature T_c [4].

Since the discovery of the first superconductor Hg with $T_c = 4.2$ K, superconductivity is one of the most active areas in condensed matter physics and chemistry. Nowadays, a variety of elements, intermetallic compounds, alloys, and oxides show superconductivity with a maximum $T_c = 134$ K at ambient pressure [5] or even higher $T_c = 164$ K under applied pressure [6]. Some of the superconductors are already used in scientific instruments, such as superconducting quantum interference device (SQUID) or nuclear magnetic resonance (NMR), but also in our daily life (e.g., magnetic levitation vehicles, magnetic resonance imaging, and prototypes of power lines).

Several dozens superconductors have been discovered, and some significant materials with their T_c and the year of discovery are shown in Fig. 1.1. Soon after the first discovery of mercury, lead was found to be a superconductor at 7 K in 1922 [7], and niobium with a T_c of 9.5 K [8], the highest superconducting transition temperature among pure metals. In 1941, niobium nitride was found to be a superconducting compound with $T_c = 16$ K followed by the discovery of Nb_3Sn and Nb_3Ge with the superconducting transition temperature up to 23 K [9-10].

Until 1986, superconductivity with critical temperatures above 30 K was believed to be impossible according to the BCS theory, which describes superconductivity as a phonon-mediated condensation of electron pairs into a boson-like state [11]. However, this turned out to be inappropriate after the discovery of barium-doped lanthanum cuprate $(La_{1-x}Ba_x)CuO_4$ with $T_c = 35$ K by J. G. Bednorz and K. A. Müller [12]. This discovery was a start for high-T_c superconductors. Nine months later, it was found that replacement of lanthanum by yttrium in $YBa_2Cu_3O_{7-\delta}$ increased T_c drastically up to 93 K due to chemical pressure [13]. This compound can be easily obtained by the solid state synthesis at 1200 ºC:

$$4\ BaCO_3 + Y_2(CO_3)_3 + 6\ CuCO_3 + (1/2-x)\ O_2 \rightarrow 2\ YBa_2Cu_3O_{7-x} + 13\ CO_2.$$

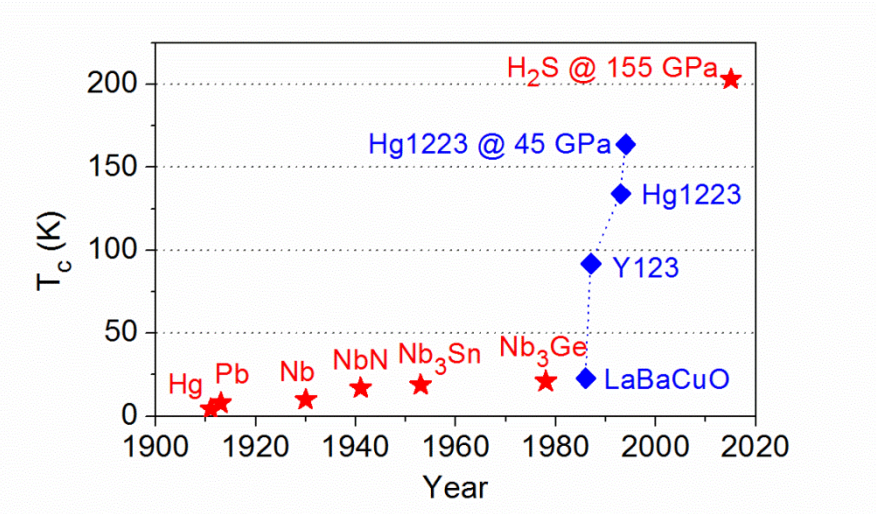

Fig. 1.1. The most significant discoveries of superconducting materials and their T_cs [1-3, 7-10]. Conventional and unconventional superconductors are shown as stars and diamonds respectively.

This discovery was noticeably significant, because the critical temperature exceeded the boiling temperature of liquid nitrogen. This is importante for applications, as the liquid nitrogen is inexpensive comparing to liquid helium. In 1988, superconducting transition temperature rose a bit more by discovery of bismuth strontium calcium cooper oxide, $Bi_2Sr_2Ca_nCu_{n+1}O_{2n+6-\delta}$, with T_c = 95 K for n = 1 and 105 K for n = 2 [14]. The same year, thallium barium calcium copper oxide, $Tl_2Ba_2Ca_{n-1}Cu_nO_{2n+4+x}$, was also discovered with a maximum T_c = 120 K (n = 3) [15]. Later on, by replacing thallium with mercury, the series of $HgBa_2Ca_{n-1}Cu_nO_{2n+2+\delta}$ superconductors was reported [16]. Their T_c is the highest known to date at ambient (T_c = 133 K [5, 17]) and under applied pressure up to 45 GPa (T_c = 164 K [6, 18]).

Cuprates were the only high temperature superconductor until 2008. After the discovery of $LaFeAsO_{1-x}F_x$ with T_c = 26 K for x = 0.11 by Y. Kamihara et al. [19], a new superconductor family, so-called Fe-based superconductors, was explored. Formally, $LaFeAsO_{1-x}F_x$ was not the first Fe-containing superconductor, because U_6Fe [20] and $Lu_2Fe_3Si_5$ [21] were discovered in the last century. However, these compounds did not receive much attention due to the relatively low transition temperature which were below 10 K. Later on, $LaFeAsO_{1-x}F_x$ showed an even higher T_c = 43 K under a pressure of 4 GPa [22]. Simultaneously, higher T_cs of up to 56 K were reported for the oxoarsenides with La replaced by rare earth elements such as Ce, Pr, Nd, and Sm [23]. This family of Fe-based superconductors is referred to as the "1111-type" phases according to the chemical composition of the parent compound. The same year, another species of Fe-based superconductors, 122-type family, $Ba_{1-x}K_xFe_2As_2$ with T_c up to 38 K [24], and 111-type family, *e.g.* LiFeAs with T_c = 18 K [25] were discovered. By the substitution of alkali metals and alkaline earth metals, the T_c values vary in a relatively large range: 32 K for $Sr_{0.6}K_{0.4}Fe_2As_2$, 21 K for $Ca_{0.6}Na_{0.4}Fe_2As_2$, 26 K for $Sr_{0.6}Na_{0.4}Fe_2As_2$ [26], *etc*.

1.2 Superconductivity in iron chalcogenides

Another important family of Fe-based superconductors – iron chalcogenides started from the 11-type phase α-FeSe, which had T_c = 8 K at ambient pressure (Fig. 1.2) [27]. A modified synthesis of FeSe (using inert atmosphere and pure reagents) led to a series of iron selenides free of impurities, iron oxides and hexagonal phase [28]. Annealing for 3 days at 750 °C, increasing the temperature to 1075 °C for 3 days, followed by cooling to 450 °C for 2 days yielded iron selenides with tetragonal structure and compositions $Fe_{1.01}Se$, $Fe_{1.02}Se$ and $Fe_{1.03}Se$. Magnetic studies showed the first two samples to be superconducting with T_c = 8.5 K and 5 K respectively, while $Fe_{1.03}Se$ is paramagnetic down to 2 K. The authors noted that the synthetic conditions, as well as the composition of the final product, significantly affect the properties of superconducting iron selenide, which, however, cannot be explained in terms of competing superconducting and magnetic transitions.

In order to understand the nature of superconductivity in FeSe detailed structural studies of the superconducting $Fe_{1.01}Se$ and non-superconducting $Fe_{1.03}Se$ were carried out with X-ray synchrotron radiation. At room temperature, both phases have an ideal tetragonal unit cell with little difference in their lattice parameters (Table 1.1). However, at 20 K $Fe_{1.01}Se$ shows a lower-symmetry diffraction peaks splitting, while $Fe_{1.03}Se$ has the same patterns as at 298 K [29]. Low-temperature phase of $Fe_{1.01}Se$ was attributed to the orthorhombic space group symmetry *Cnma* (β-FeSe). Temperature dependent structural studies have shown that the phase transition from the α to the β phase occurs around 90 K. Interestingly, the superconducting phase of $Fe_{1.01}Se$ is orthorhombic *Cnma*, i.e. the same as found for superconductors based on FeAs. Thus, the phase transition in the β-phase plays a key role in the superconducting pairing in the iron selenides and pnictides.

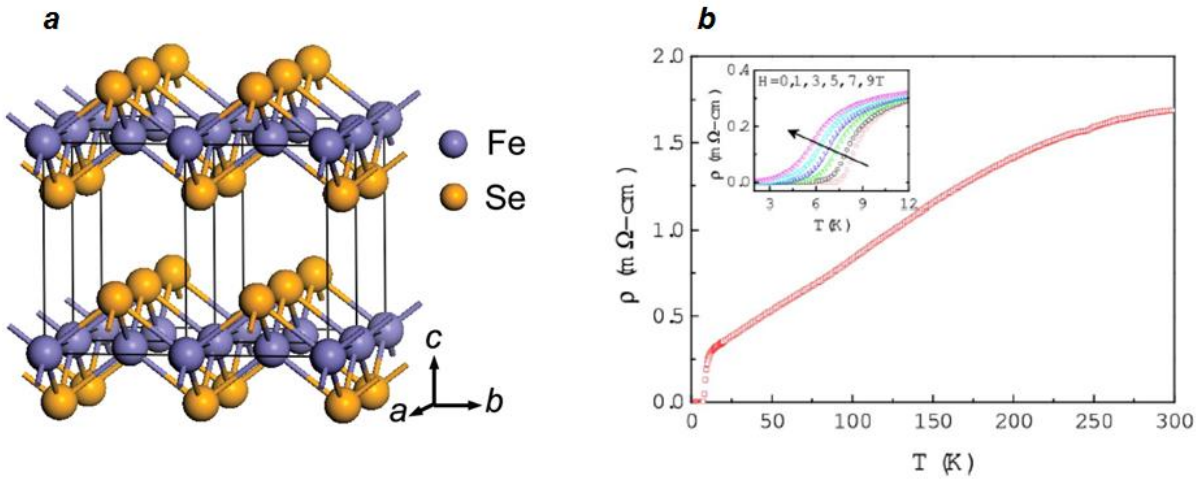

Fig. 1.2. Crystal structure (**a**) and temperature behaviour of the electrical resistivity for FeSe in zero field and in the applied field (inset) with T_c = 8 K (**b**) [27]. *Reproduced with permission from ref. 27. Copyrights 2008 NAS.*

Table 1.1. Crystallographic parameters for $Fe_{1.01}Se$ and $Fe_{1.03}Se$ at room temperature and at 20 K [29].

Compound	$Fe_{1.01}Se$		$Fe_{1.03}Se$	
Space group	*P*4/*nmm*	*Cnma*	*P*4/*nmm*	*P*4/*nmm*
T (K)	298	20	298	20
a (Å)	3.7727(1)	5.3100(2)	3.7787(1)	3.7682(1)
b (Å)		5.3344(2)		
c (Å)	5.5260(3)	5.4892(2)	5.5208(2)	5.4846(2)
Volume ($Å^3$)	78.652(7)	155.49(1)	78.827(6)	77.877(6)

After the structural phase transition had been reported for $Fe_{1.01}Se$, a number of theoretical works [30-32] appeared that associated the orthorhombic distortion of the unit cell with the emergence of a nematicity, *i.e.* unidirectional self-organized electronic state that violates the rotational symmetry of the lattice. This situation led to a significant expansion of the superconducting gap and, consequently, to the formation of Cooper pairs moving along the direction of nematic ordering without resistance [30]. The emergent nematic state was experimentally confirmed in 2015 by NMR spectroscopy [33]. Analysis of Knight shift of ^{77}Se revealed the emergence of electronic ordering in $Fe_{1.01}Se$ at T ~ 91 K. However, the question still remains enigmatic: does nematicity lead to a structural phase transition or does the phase transition generate nematic ordering?

In order to increase T_c of superconducting FeSe, Medvedev [34] and Margadonna [35] investigated its resistivity and crystal structure under high pressure. Data on the electric resistance showed that the application of external pressure leads to an increase in T_c at an initial rate of 12.6 (2) K / GPa that finishes at 8.9 GPa at a rate of 3.2(1) K / GPa, reaching T_c = 36.7 K. A further pressure increase is associated with a smooth decrease of T_c with an initial rate of ~ - 1.7 (2) K / GPa. At 15 GPa T_c = 25 K, but the electrical resistance value does not approach zero, probably due to an incomplete superconducting transition. Structural studies in high pressure cells showed that up to ~ 10 GPa FeSe is tetragonal at room temperature, showing only contraction of the lattice due to external pressure. At pressures above ~ 12 GPa structural phase transition to the hexagonal phase δ-FeSe starts, which has a higher density (volume cell 27.5 $Å^3$ vs. 31.5 $Å^3$ for the tetragonal cell at 12 GPa). The coexistence of two FeSe phases was observed in a wide range of pressure and only at p = 38 GPa diffraction reflexes of the hexagonal phase only were found. Thus, the pressure increase leads to T_c increased almost 4.5 times for β-FeSe, but above ~ 8.9 GPa due to the structural phase transition superconductivity disappears gradually (Fig. 1.3).

A Mössbauer spectrum of $Fe_{1.01}Se$ at 0.2 GPa shows a quadrupole doublet with δ = 0.44 mm/s and ΔE_Q = 0.28 mm/s. With increasing pressure the isomer shift decreases gradually, and at 7.2 GPa an additional doublet with δ = 0.84 mm/s and ΔE_Q = 0.21 mm/s appears in the spectrum [34]. The last corresponds to a new hexagonal phase, and its intensity increases with increasing pressure. The evolution of the Mössbauer spectra for $Fe_{1.01}Se$ are shown in Fig. 1.4.

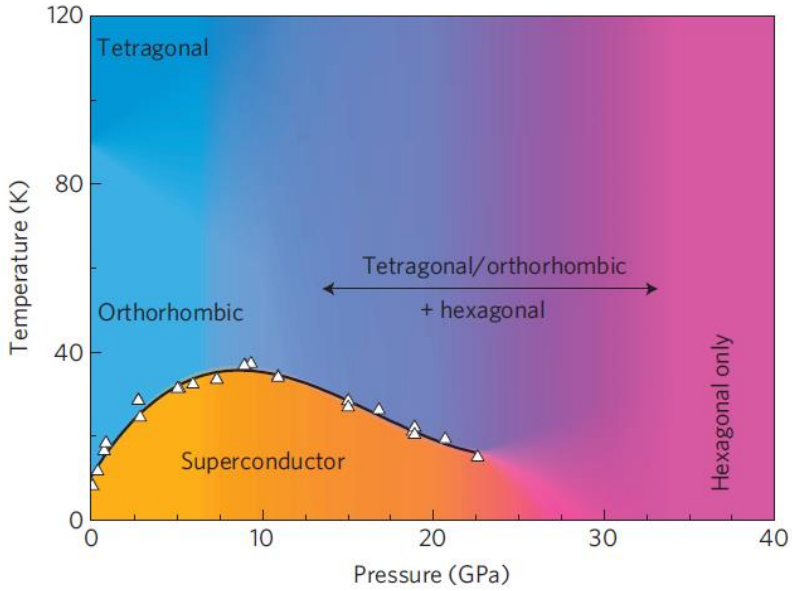

Fig. 1.3. Electronic phase diagram of FeSe in the $T_c(p)$ coordinates showing areas of tetragonal, orthorhombic and hexagonal phases existence [34]. *Reproduced with permission from ref. 34. Copyrights 2009 NPG.*

According to the BCS theory, a significant increase in T_c that is not associated with structural changes should be explained by the increase of either density of charge carriers or electron-phonon interaction energy [36]. Mössbauer spectra in the range of 0.2 - 7.2 GPa did not show a significant increase of the electron density in FeSe. This confirmed the idea of a variation of the electron-phonon interaction energy. Ksenofontov et al. studied the evolution of the phonon spectra of FeSe under high pressure [37]. When applying pressure, the acoustic modes of FeSe shifted, which would be associated with a reduction in interatomic distances in the crystal lattice (Fig. 1.5), but "Soft" modes, which would be responsible for mediating the electron-phonon coupling, were not observed.

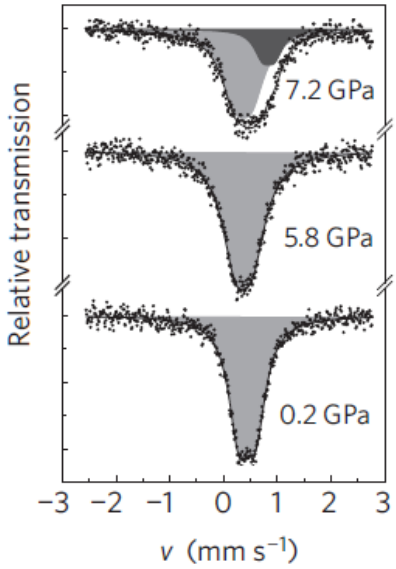

Fig. 1.4. Selected Mössbauer spectra of FeSe under pressure at room temperature. The tetragonal and hexagonal phases doublets are shown in ligh- and dark-gray respectively [34]. *Reproduced with permission from ref. 34. Copyrights 2009 NPG.*

Thus, the increase in T_c from 8 K to almost 37 K in iron(II) selenide cannot be explained within the BCS theory, which allowed to attribute FeSe to the non-conventional superconductors.

Investigation of FeSe with ^{77}Se NMR spectroscopy showed that iron selenide has similar features as superconducting iron arsenide. When approaching T_c, antiferromagnetic spin fluctuations in the material significantly increased as observed from the increase in inverse time of spin-lattice relaxation time T_1 [38]. Hydrostatic pressure increased spin fluctuations, which is associated with an increase of T_c (Fig. 1.6). Interestingly, non-superconducting $Fe_{1.03}Se$ shows no features of the relaxation time vs. temperature behaviour. The authors note that although NMR spectroscopy allowed to associate the emergence of spin fluctuations in iron selenide with the transition to the superconducting state, the method does not allow to quantify the amplitude of the fluctuations. In addition, due to the Meissner effect the relaxation time is growing rapidly in the superconducting state, which makes it impossible to observe fluctuations below T_c.

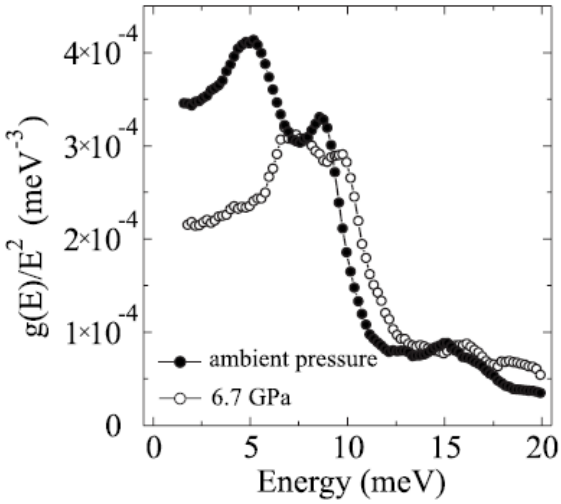

Fig. 1.5. ^{57}Fe NIS spectra of FeSe at 4.2 K showing no softening of the phonon spectrum under pressure [37]. *Reproduced with permission from ref. 37. Copyrigts 2010 APS.*

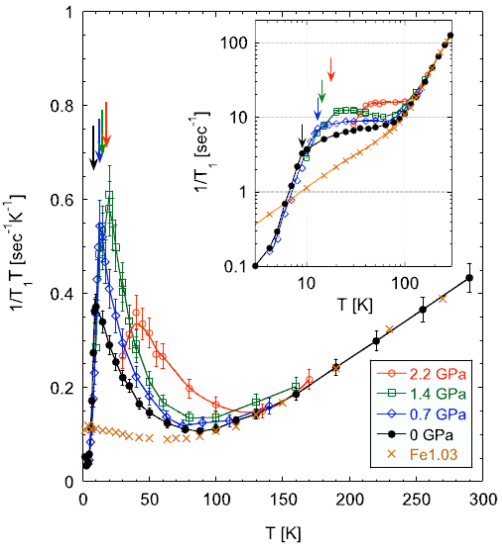

Fig. 1.6. Temperature dependences of NMR-T_1^{-1} for FeSe under pressure [38]. *Reproduced with permission from ref. 38. Copyrigts 2009 APS.*

In order to tune magnetic fluctuations, which mediate the superconducting pairing, FeSe was doped copper [39]. It has been shown that the Cu impurities lead to a metal-insulator transition, and the electric resistance of the material increases with the doping level. According to structural data, Cu ions are not included in the interplanar space of layered structure and occupy Fe positions. Accordingly, DFT calculations showed that Cu doping leads to the Anderson localization in the structure [40], which is consistent with experimental data on the electrical resistance. Measurements of the magnetic susceptibility of Cu-doped FeSe samples indicated the emergence of spin glasses at low temperatures. Thus, the appearance of uncompensated magnetic moments leads to lower values of T_c, and when more than 4 % of copper is introduced, superconductivity disappears (Fig. 1.7).

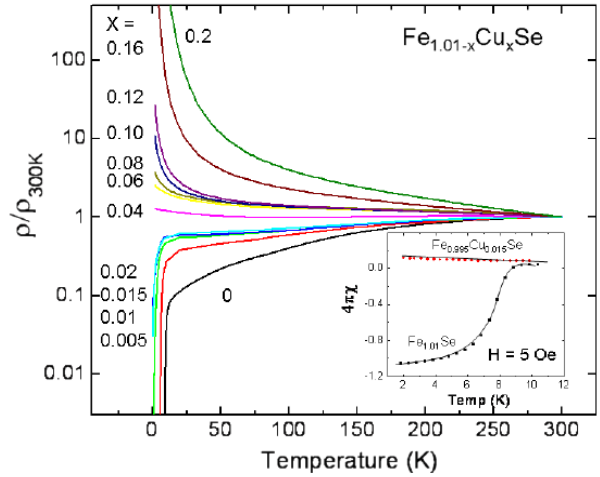

Fig. 1.7. Temperature dependences of electrical resistivity for $Cu_xFe_{1.01-x}Se$ at ambient pressure [39]. *Reproduced with permission from ref. 39. Copyrigts 2009 IOP.*

However, at relatively small pressure of ~ 1.5 GPa superconductivity in $Cu_{0.04}Fe_{0.97}Se$ is restored with T = 6.6 K [41]. At higher pressure T_c increases, reaching a maximum at 7.8 GPa (31.3 K). A further increase in pressure leads to a decrease in Tc, and at 13.7 GPa superconductivity in $Cu_{0.04}Fe_{0.97}Se$ disappears. Thus, the T_c(p) diagram for Cu-doped sample is a dome-shape that is similar to that for $Fe_{1.01}Se$ (Fig. 1.8) [34]. In both cases, the disappearance of superconductivity at high pressures is associated with a structural phase transition to the hexagonal phase, but for $Cu_{0.04}Fe_{0.97}Se$ the transition was followed only up to ~ 14 GPa, where both β and δ phases co-exist [41]. In addition, the reason for re-entrance of superconductivity at pressures of 1.5 - 7.8 GPa remains unclear.

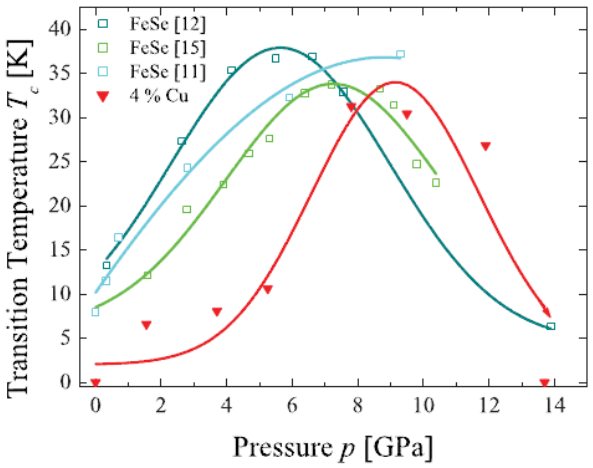

Fig. 1.8. T_c vs. pressure dependences for $Cu_{0.04}Fe_{0.97}Se$ and $Fe_{1.01}Se$ [41]. *Reproduced with permission from ref. 41. Copyrigts 2011 APS.*

Starting from metallic potassium, iron and selenium in different proportions a series of polycrystalline samples of $K_xFe_2Se_2$ (x = 0 ÷ 1) was obtained via solid-state synthesis at 700 - 750 °C [42]. These compounds have been attributed to a structural type $ThCr_2Si_2$, i.e. FeSe layers are separated by layers of potassium ions. All compounds have T_c values higher compared to the original FeSe, but the highest T_c = 30.1 K has been reported for the

compound of $K_{0.8}Fe_2Se_2$ stoichiometry. The authors note that the increase in T_c can be associated with introduction of additional carriers into FeSe layers (formal oxidation state of iron is below +2), or with structural features. Thus, the angle Se-Fe-Se is much closer to that of a regular tetrahedron for $K_xFe_2Se_2$, and FeSe layers are separated from each other at 4.10 Å (versus 2.55 Å for FeSe).

In a similar way $Cs_{0.8}Fe_2Se_{1.96}$ phase has been obtained, which also has a structural type $ThCr_2Si_2$ and T_c = 27.4 K [43]. However, the highest T_c in this series belongs to double selenide of iron and rubidium. Thus, $Rb_{0.88}Fe_{1.81}Se_2$ was obtained with T_c = 32.1 K [44]. Later, Tsurkan *et al*. studied the phase diagram for the system $Rb_{1-x}Fe_{2-y}Se_2$ and found the T_c dependence on the composition and structural parameters (Fig. 1.9) [45]. The highest T_c = 32.4 K and the most abrupt transition to the superconducting state was observed in $Rb_{0.8}Fe_{1.6}Se_2$, which became the subject of following investigations.

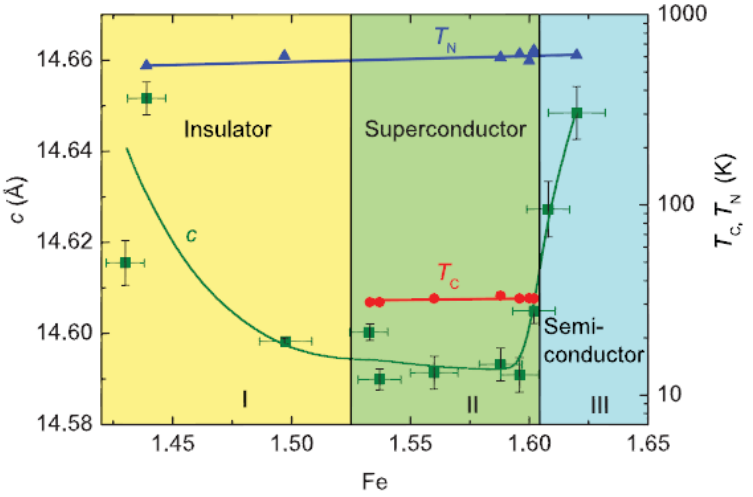

Fig. 1.9. Phase diagram for $Rb_{1-x}Fe_{2-y}Se_2$ showing T_c, T_N, c dependence on the iron content 2–y [45]. *Reproduced with permission from ref. 45. Copyrigts 2011 PRB.*

A common feature of $A_xFe_ySe_2$ (A = K, Rb, Cs) compounds is the coexistence of antiferromagnetic ordering (T_N ~ 600 K) and superconductivity that is impossible within a frameworks of BCS theory [43-45]. The explanation of this coexistence has been proposed based on NMR and structural studies of $Rb_{0.74}Fe_{1.6}Se_2$, which showed nanoscale phase separation into superconducting $Rb_{0.3}Fe_{1.6}Se_2$ (FeSe-like) and antiferromagnetic $Rb_{0.8}Fe_{1.6}Se_2$ "phases" within the same crystal structure (Fig. 1.10) [46]. Also, the phase separation was confirmed in $K_{0.8}Fe_{1.6}Se_2$ using scanning tunneling microscopy [47], high-resolution X-ray diffraction [48] and optical methods [49]. Direct quantitative observation of phase separation in $Rb_{0.8}Fe_{1.6}Se_2$ has been performed using Mössbauer spectroscopy [50]. It has been shown that magnetic phase, which gives sextet in the spectrum (88(1) % intensity) and non-magnetic phase, giving doublet (12(1) % intensity), coexist within the crystal structure. Application of an external magnetic field confirms the antiferromagnetic ordering in the dominant phase (Fig. 1.11). Under pressure superconductivity in $Rb_{0.8}Fe_{1.6}Se_2$ remains, as long as the antiferromagnetic ordering in the dominant phase exist. However, above 5 GPa the ideal order of magnetic moments is disturbed and uncompensated moments of ~ 3 μ_B appear [51]. They lead to the disappearance of superconductivity in accordance with BCS theory.

Using of thallium instead of alkali metals in synthesis leads to $TlFe_{1.6}Se_2$ with a structure type of $ThCr_2Si_2$ as well, however, in contrast to the compounds with K, Rb and Cs, neither phase separation, nor superconductivity is observed. It has semiconducting properties and is completely antiferromagnetic with T_N = 450 K [52].

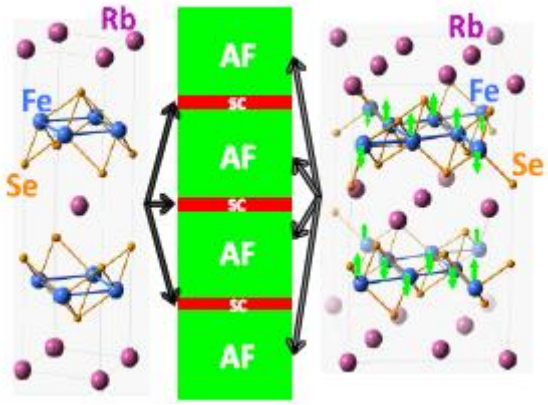

Fig. 1.10. Phase separation in $Rb_{0,74}Fe_{1,6}Se_2$: antiferromagnetic regions are separated by superconducting layers [46]. *Reproduced with permission from ref. 46. Copyrigts 2012 APS.*

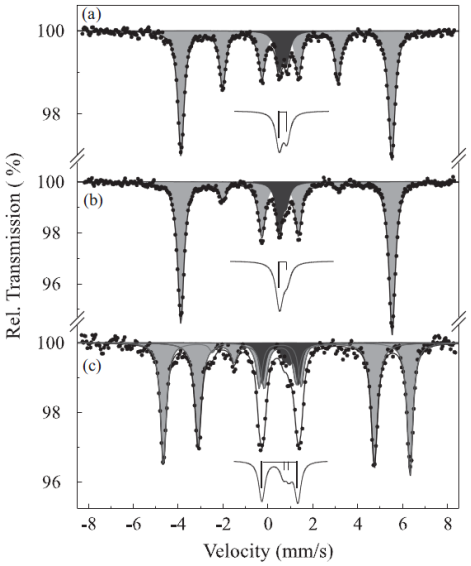

Fig. 1.11. Powder (a, c) and single crystal (b) Mössbauer spectra of $Rb_{0.8}Fe_{1.6}Se_2$ in zero and 5 T magnetic field [50]. *Reproduced with permission from ref. 50. Copyrigts 2011 APS.*

Another elegant way to improve superconducting properties of FeSe has been amonothermal intercalation, which yielded the compound $Li_x(NH_2)_y(NH_3)_{1-y}Fe_2Se_2$ (x ~ 0,6; y ~ 0,2) with T_c = 43 (1) K [53]. It represents the first HTSC from iron chalcogenides family. In contrast to $A_xFe_ySe_2$ (A = K, Rb, Cs), FeSe layers in intercalated phase has the same composition as the binary FeSe, but only separated by layers consisting of Li^+, NH_2^- ions and ammonia molecules. The crystal structure of the deuterated sample was refined by neutron diffraction (Fig. 1.12). Later Sedlmayer *et al.* showed that FeSe could be intercalated with two layers of $Li_x(NH_2)_y(NH_3)_{1-y}$ per FeSe layers, but measurements of superconducting transition failed due to unstable compound [54]. Recently, theoretical calculations have shown that T_c in the intercalated material increases due to two factors: the change of the Fermi surface topology, which is a two-dimensional, and an increase in the *d*-electron density at iron atoms [55].

There were other successful modifications of FeSe through chemical intercalation. Thus, for $Li_x(en)_yFe_{2-z}Se_2$ T_{onset} = 45 K was found, but the transition to the superconducting state is smooth, and the exact composition of the compound remains uncertain [56]. A sharp transition with T_c as high as 45 K was observed for $Li_x(py)_yFe_{2-z}Se_2$; however, attempts to obtain reliable reproducible results for FeSe, intercalated with Na, K or Rb in pyridine, was not successful [57].

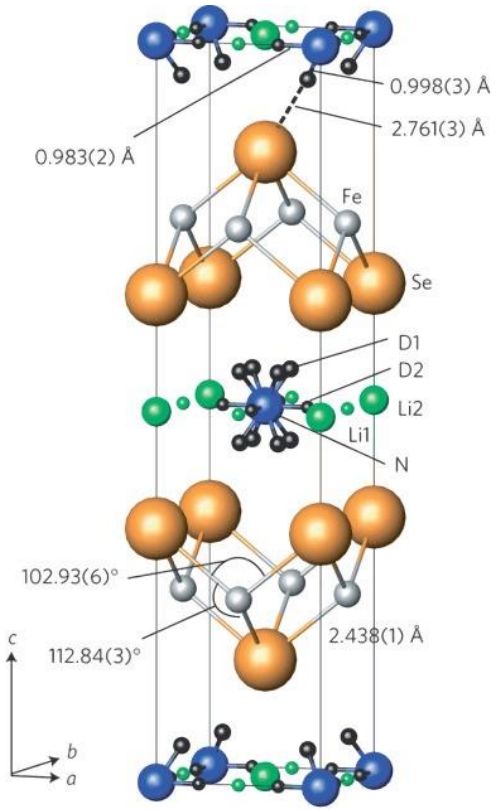

Fig. 1.12. Crystal structure of $Li_x(ND_2)_y(ND_3)_{1-y}Fe_2Se_2$ (x = 0.6; y = 0.2) [53]. *Reproduced with permission from ref. 53. Copyrigts 2013 NPG.*

1.3 Superconductivity in hydrides

According to BCS theory, compounds that are composed of light elements can potentially achieve high superconducting temperatures due to high-frequency modes in the phonon spectrum [58]. Back in 1968, Ashcroft drew attention to hydrogen, H_2, which has a high frequency of phonons and a strong electron-phonon interaction in the condensed state [59]. In this regard, search for high- and even room-temperature conventional superconductivity seems to be fruitful, since the BCS theory in the Ginzburg interpretation puts no formal limits on T_c. Later, it was expected that hydrogen under pressure had to transform to the metallic superfluid liquid that is likely to be superconducting [60]. However, the experimental work did not confirm the metallization of hydrogen at high pressure up to 300 GPa and temperatures below 100 K [61-62]. By applying pressure in a diamond-anvil cell (DAC) at room temperature Eremets *et al*. showed that above 200 GPa Raman vibration bands of hydrogen were broadened and significantly shifted to the low-frequency region, indicating strong intermolecular interactions [63]. At pressures above 220 GPa hydrogen starts to metallize, and at 260 GPa it shows a metallic conductivity. Reverse transition occurs at 200 GPa, indicating a hysteresis of the first-order phase transition of 60 GPa. Modern calculation facilities allowed to predict that metallic hydrogen should become a superconductor with a T_c of 100 - 240 K for molecular H_2, and T_c ~ 300 - 350 K in the atomic state at 500 GPa [64], but the study of electrical properties under such pressure is extremely complicated.

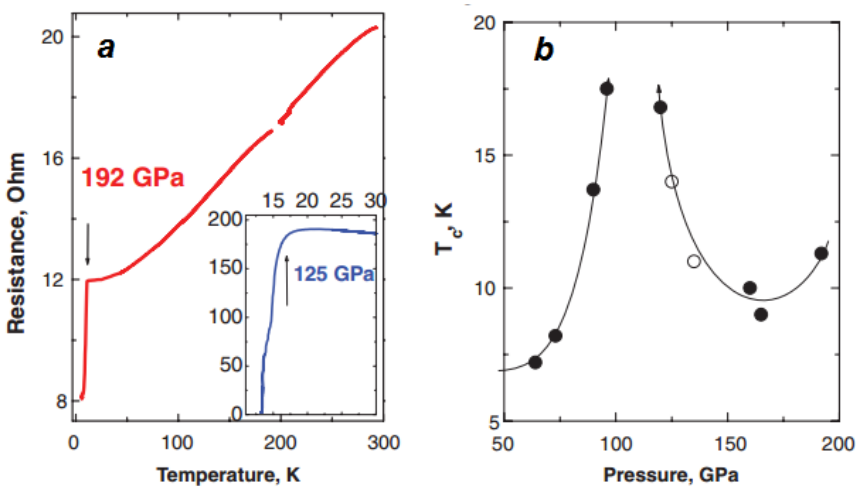

Fig. 1.13. Temperature dependences of electrical resistance under pressure of 192 and 125 GPa (**a**) and T_c(p) phase diagram (**b**) for SiH_4 [66]. *Reproduced with permission from ref. 66. Copyrigts 2008 AAAS.*

Quantum chemical calculations predicted that not only hydrogen, but also other hydrogen compounds, *e.g.* hydrides of elements of the group IV SiH_4 and SnH_4, may show superconductivity under high pressure [65]. They have high Debye temperatures and heavy elements, which provide soft modes in the phonon spectrum that enhances the electron-phonon coupling. However, only silane was experimentally confirmed to be superconducting with a relatively low T_c = 17 K in the pressure range between 96 and 120 GPa [66]. Metallization of silane started above 50 GPa; at 65 GPa SiH_4 became superconducting with T_c = 7 K; with a further pressure increase T_c raised, reached its maximum at 120 GPa and decreasesdat higher pressure (Fig. 1.13). According to structural data, metallic SiH_4 has a hexagonal close packing in which hydrogen atoms constitute a three-dimensional conductive framework.

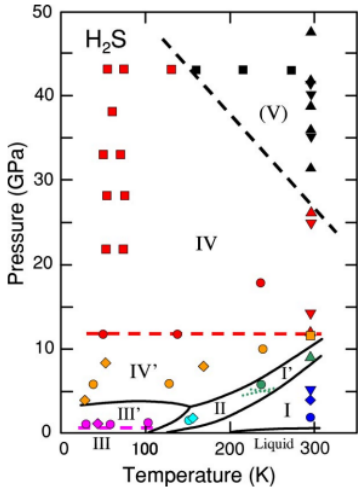

Fig. 1.14. Phase diagram for H_2S [69]. *Reproduced with permission from ref. 69. Copyrigts 2004 APS.*

Further theoretical work showed that the most abundant on the planet hydrogen compound, H_2O, metallize at extremely high pressure 800 - 1200 GPa [67]. However, its analogue, H_2S, is to transform to the metallic state at much lower pressures ~ 100 GPa and, in addition, have superconductivity with T_c = 80 K according to calculations [68]. Hydrogen sulfide has a rich phase diagram (Fig. 1.14) and at pressures above 43 GPa begins to dissociate [69]. In another study, infrared spectroscopy has revealed that at 96 GPa H_2S metallize [70]. It was suggested that the emergence of the metallic phase due to the dissociation is associated with a formation of a higher sulfur hydride and elemental sulfur. Later, Komentani *et al*. have shown that sulfur also metallize at 100 GPa and has a superconducting transition with T_c = 15 K [71]. The idea of formation of higher sulfur hydride was confirmed in an experiment, in which the H_2 and H_2S gaseous mixture

was compressed in the high pressure cell. Around 3.5 GPA, they form a common crystalline phase with intermolecular contacts $H(H_2)$ – $S(H_2S)$ [72]. It is also envisaged that H_2Se at 100 GPa is also superconducting with T_c exceeding 120 K [73]. Using modern DFT methods potential superconductivity was predicted in other hydrides under high pressure: HBr (T_c ~ 50 K) [74], TiH_2 (T_c ~ 7 K) [75], SbH_4 (T_c ~ 100 K) [76], and for binary hypothetical compound MgH_6 at 300 - 400 GPa at a record high T_c ~ 400 K [77] that should be considered with skepticism.

1.4 Conclusions and objectives

Iron(II) selenide and its derivatives constitute a relatively new and promising family of superconducting materials because of their easy synthetic access, reproducibility of properties, and the possibility to achieve high T_cs by varying their composition or applying high pressure. The increase in T_c from 8 K for FeSe to 45 K for $Li_x(py)_yFe_{2-z}Se_2$ by chemical modification or to ~ 65 K in thin films on the conductive surface, is explained by the reorganization of the Fermi surface and/or changes in electron density near the superconducting gap that is supported by calculations. However, an important task is to observe the changes in the concentration of charge carriers directly with the help of experimental techniques. In this regard, Mössbauer spectroscopy, which provides direct information about the distribution of the valence electrons around the ^{57}Fe nucleus, can be a powerful method to study the electronic effects in Fe-based superconductors. Therefore, we have chosen tetragonal FeSe, $FeSe_{0.5}Te_{0.5}$, $Rb_{0.8}Fe_{1.6}Se_2$, and a recently described intercalation product – HTSC $Li_x(NH_2)_y(NH_3)_{1-y}Fe_2Se_2$, to study the temperature behavior of the ^{57}Fe hyperfine properties.

Iron chalcogenides are unconventional superconductors, in which superconducting pairing is associated with the presence of magnetic fluctuations. On the one hand, their enhancement under pressure leads to a T_c increase, and, on the other hand, the introduction of additional magnetic moments, *e.g.* in $Cu_xFe_{1.01-x}Se$, leads to a suppression of superconductivity. To establish the role of fluctuations a detailed Mössbauer study of $Li_x(NH_2)_y(NH_3)_{1-y}Fe_2Se_2$ and $Cu_xFe_{1.01-x}Se$ in a high velocity range at ambient and under applied pressure is necessary.

For superconductors $A_xFe_ySe_2$ (A = K, Rb, Cs) of the $ThCr_2Si_2$-type structure with a relatively high T_c phase separation into antiferromagnetic and superconducting phases is known. Due to the coexistence of magnetism and superconductivity they are interesting multifunctional materials that combine two important physical properties. The interplay between magnetic and superconducting phases remains enigmatic to date. However, experimental facts show that the minimal change in one phase leads to significant changes in the other. In our opinion, an interesting task consists in the modification of antiferromagnetic matrix by introducing magnetic impurities or changing the composition and investigating the effects of such modifications on the superconducting properties in the conjugated phase.

The highest superconducting temperature known to date is 133 K at ambient pressure and 164 K under high pressure of 45 GPa for cuprate ceramics. Because the nature of

superconductivity in these materials is still not fully understood (they are not conventional superconductors), the ways towards higher T_cs are not clear. On the other hand, conventional theory of superconductivity by BCS [11] does not limit the range of T_c that is given by the equation:

$$T_c = 1{,}14 \cdot \Theta_D \cdot e^{-1/U \cdot D_F} . \qquad (1.1)$$

Thereby, to achieve the desired T_c, high-frequency lattice vibrations (expressed as the Debye temperature, Θ_D, in this equation), strong electron-phonon coupling (U) and high density of states near the Fermi level (D_F) are needed. These conditions can be met for metallic hydrogen or covalent compounds with high content of hydrogen because light H atoms provide both high-frequency modes in the phonon spectrum and strong electron-lattice interactions. Numerous density functional calculations show the potential superconductivity in many hydride compounds at extremely high pressures. We have chosen H_2S as a promising object, which is known to metallize under relatively low pressure.

2 Experimental methods

2.1 Conventional Mössbauer spectroscopy

Mössbauer spectroscopy is widely applied to study electronic effects and magnetic properties of compounds containing ^{57}Fe, ^{119}Sn, ^{151}Eu and some other nuclei that are known to have a Mössbauer effect. This method is indispensable for the characterization of Fe-based compounds with spin transition [78], ferro-, antiferro- and superparamagnetic objects [79], natural geological [80], biological [81] and even extraterrestrial materials [82]. For the family of superconductors, which is represented by iron pnictides and chalcogenides, Mössbauer spectroscopy has been widely used as well [83-85].

The method is based on the observation of the Mössbauer effect, the resonance and recoil-free absorption of electromagnetic irradiation (γ-ray) by a material containing a Mössbauer-active isotope. As a source of irradiation in conventional spectroscopy radioactive isotopes are used (*e.g.,* ^{57}Co to observe the Mössbauer effect on ^{57}Fe nuclei). If the γ-quantum energy corresponds to the difference between nuclear energy levels of ^{57}Fe with nuclear spin I = 1/2 (ground state) and I = 3/2 (excited state), the resonant absorption may be observed. The lifetime of the nucleus in the excited state is approximately 10^{-8} s, followed by either emission of γ-quantum with the same energy or relaxation to the ground state with transformation of photon energy into lattice vibrations. The probability of the latter process is defined by the Debye-Waller factor [86]. In this case, absorption can be recorded using a scintillation detector of γ-quanta. This scenario is realized when the source of γ-photons (^{57}Co) and the absorber (^{57}Fe) are in the same chemical environment; otherwise γ-quantum energy is inconsistent with the nuclear levels difference. Therefore, to observe the Mössbauer effect energy of γ-ray is modulated via accelerated movement of the source that is based on the Doppler Effect. The Mössbauer spectrum is represented as the dependence of γ-quanta transmission on the source velocity. The velocity difference between the studied and reference absorbers is called the isomer shift (δ), which is defined as:

$$\delta = \frac{24\pi(\rho+1)\{|\psi_s(0)_A|^2 - |\psi_S(0)_B|^2\}Ze^2}{\kappa(2\rho+1)(2\rho+3)\Gamma^2(2\rho+1)}\left(\frac{2Z}{a_H}\right)^{2\rho-2} R^{2\rho}\frac{\delta R}{R}, \qquad (2.1)$$

where $\psi_S(0)$ is the value of the *s*-wave at the nucleus for the investigated (A) and reference (B) sample, a_H – the Bohr radius, Γ – gyromagnetic ratio, δR/R – change of the nucleus radius after transition to the excited state, $\kappa \approx 1$ and $\rho = 0{,}98$ – constant values for ^{57}Fe. As standards metallic iron, iron(III) oxide and iron(II) nitroprusside are usually used.

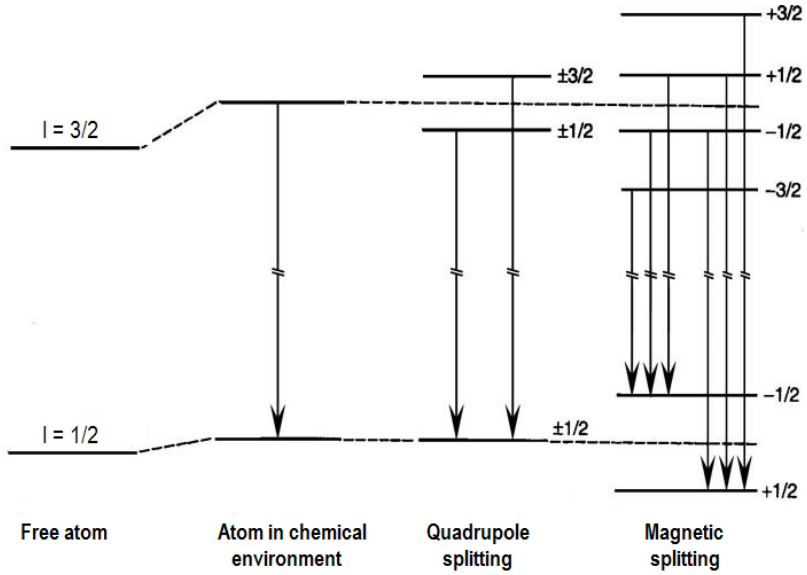

Fig. 2.1. Splitting of energy levels for the nucleus with the ground spin I = 1/2 [86].

Interaction between nuclear quadrupole moment and electric field gradient V_{zz}, in the case of non-symmetrical surrounding of the nucleus, leads to the nuclear energy levels splitting (Fig. 2.1). In the case of ^{57}Fe, a quadrupole doublet appears in the spectrum, and the difference between its components is described as the quadrupole splitting $\Delta E_Q = e^2QV_{zz}/2$. In general, the magnitude of the quadrupole interaction is given by the following expression:

$$E_Q = \frac{e^2QV_{zz}}{4I(2I-1)}[3I_z^2 - I(I+1)]\left(1+\frac{\eta^2}{3}\right)^{1/2}, \qquad (2.2)$$

where I_z is the projection of the nuclear spin on the z axis, and $\eta = (V_{xx} - V_{yy})/V_{zz}$ is the symmetry parameter that is zero in case of tetragonal distortion. In the absence of texture effects, quadrupole doublet components intensities are equal.

When the nucleus is in a magnetic field, Zeeman splitting of both ground and excited levels is observed (Fig. 2.1). Due to the selection rules for nuclear transitions $\Delta m_I = 0, \pm 1$, there are six out of eight possible transitions, which are yielded as a sextet in the Mössbauer spectrum with relative intensities 3:2:1:1:2:3. The hyperfine interaction energy depends on the magnetic field at ^{57}Fe nucleus B_{hf}:

$$E_m = -g\mu_N B_{hf} m_I, \qquad (2.3)$$

where g is the Lande factor, μ_N - nuclear Bohr magneton and m_I - quantum number. The B_{hf} value consists of an external (applied) magnetic field and the field created by electrons of ^{57}Fe atom [86].

Concluding, the main parameters of the Mössbauer spectrum are: the isomer shift, which depends on the density of *s*-electrons at the nucleus, quadrupole splitting, which is determined by the electric field gradient, and hyperfine field, which depends on the magnetic

field at the nucleus. The isomer shift is characteristic for the oxidation and spin state of iron. Quadrupole splitting reflects the distortion of coordination polyhedron. The magnetic field at the nucleus allows to estimate the magnetic moment, which is 1 μ_B per ca. 110 Oe.

^{57}Fe-Mössbauer spectra of powdered samples were recorded in transmission geometry with a ^{57}Co source embedded in a rhodium matrix using a conventional constant-acceleration Mössbauer spectrometer equipped with either nitrogen or helium cryostat. Isomer shifts are given relatively to iron metal at ambient temperature (Fig. 2.2). Simulations of the experimental data were performed with the *Recoil* software [87].

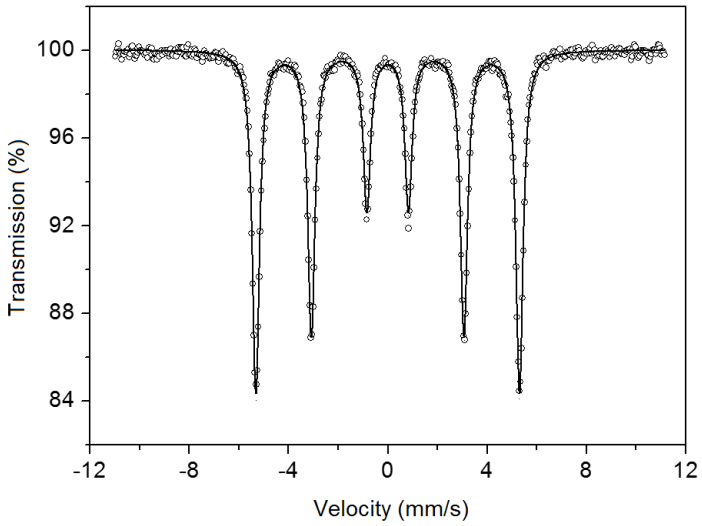

Fig. 2.2. Mössbauer spectrum of alfa-iron at room temperature used for calibration of the Mössbauer spectrometers. *The spectrum was acquired together with* [redacted]

2.2 Synchrotron Mössbauer spectroscopy

Investigation of small amounts of samples (i.e. in high-pressure cells) is possible using the Synchrotron Mössbauer Source (SMS) available at the European synchrotron (ESRF, Grenoble, France) at line ID18 [88]. The SMS is based on a nuclear resonant monochromator employing pure nuclear reflections of the iron borate ($^{57}FeBO_3$) crystal (Fig. 2.3). The source provides ^{57}Fe resonant radiation at 14.4 keV within a bandwidth of 15 neV, which is tunable in energy over a range of about 0.6 meV. In contrast to radioactive sources, the beam of γ-radiation emitted by the SMS is almost fully resonant and fully polarized, has high brilliance and can be focused to a 10x10 mm spot size. Applications include, among others, the study of very small samples under extreme conditions, for example at ultrahigh pressure or combined high pressure and high temperature, and thin films under ultrahigh vacuum. The small cross section of the beam and its high intensity allow for rapid collection of Mössbauer data. For example, the measuring time of a spectrum for a sample in a diamond anvil cell at 100 GPa is around 10 min, whereas such an experiment with a radioactive point source would take more than one week and the data quality would be considerably less.

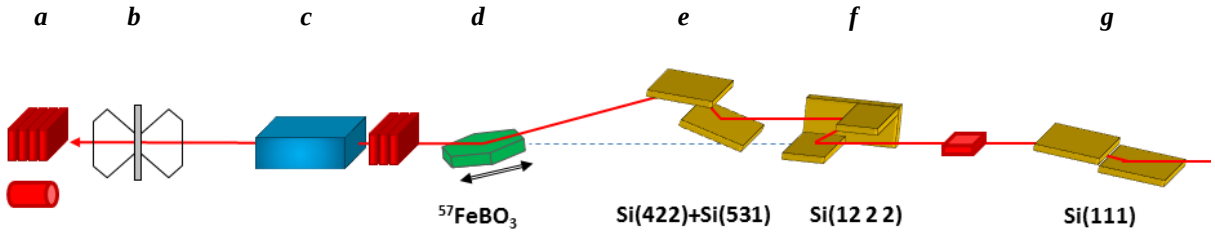

Fig. 2.3. Optical scheme of the SMS at ESRF, ID 18, that includes: γ-ray detector (**a**), high pressure cell loaded with a sample (**b**), Kirkpatrick X-ray mirrors (**c**), single crystal of $^{57}FeBO_3$ (**d**), deflector (**e**) and preliminary silicon monochromators (**f, g**). *Reproduced with permission of* [redacted]

The SMS is optimized for highest intensity and best energy resolution, which is achieved by collimation of the incident synchrotron radiation beam and thus illumination of the high-quality iron borate crystal within a narrow angular range around an optimal position of the rocking curve. The SMS is permanently located in an optics hutch and is operational immediately after moving it into the incident beam. The SMS is an in-line monochromator, i.e. the beam emitted by the SMS is directed almost exactly along the incident synchrotron radiation beam. Thus, the SMS can be easily utilized with all existing sample environments in the experimental hutches of the beamline. Owing to a very strong suppression of electronic scattering for pure nuclear reflections (~10^{-9}), SMS operation does not required any gating of the prompt electronic scattering. Thus, the SMS can be utilized in any mode of storage ring operation.

2.3 Magnetic susceptibility studies

Investigation of the magnetic susceptibility was conducted using superconducting quantum interferometer ("SQUID") that is a sensitive magnetometer designed to determine the very weak magnetic fields. The method is based on the registration of the interference of Josephson currents arising in the superconducting ring with two Josephson contacts. A studied sample passes through the ring with a constant velocity and creates a magnetic field. In this work, the SQUID MPMS-XL-5 magnetometer developed by Quantum Design was used working in a direct current mode passing through the Josephson contacts. The device was equipped with a superconducting electromagnet with a maximum magnetic field of 5 T and a cryostat with a nominal operating temperature range 1.8 - 400 K. A sample transport through a superconducting ring was performed using a piston mechanism (sample holder RSO MPMS, which provides the accuracy of the field measurements up to $5 \cdot 10^{-9}$ cm^3Oe).

Superconducting chalcogenides samples (about 10 mg) in quartz ampules were closed in a dry box and transferred in a cryostat of the interferometer, where the samples were held in a helium atmosphere under pressure of 0.1 bar, which provides the appropriate heat transfer and sample storage. The samples were normally cooled to 3 K without a magnetic field followed by switching on the magnetic field. When heating the samples at a constant velocity their magnetization was measured (ZFC). For some samples magnetization was also recorded in the cooling mode (FC). Experimental details for each sample are

described in the corresponding chapters. Magnetic susceptibility was calculated using the formula:

$$\chi = \frac{M - M_q}{m \cdot B}, \qquad (2.4)$$

where M is the raw magnetization, M_q – magnetization of the empty quartz ampule, m – mass of the sample, B – applied magnetic field.

2.4 Routine analytical methods

Powder X-ray diffraction patterns were recorded using Philips PW1730 diffractometer at room temperature using $CuK_{\alpha 1}/K_{\alpha 2}$ irradiation in the range of diffraction angles $2\theta = 5 \div 80^{o}$. Polycrystalline and single crystal samples were crushed using in a dry box with oxygen and water levels less than 0.5 ppm. To prevent oxidation, powdered samples were sealed in quartz capillaries with a diameter of 0.2 mm. Diffraction patterns were analyzed using DiffractWD software [89]. Elemental analysis (C, H, N) was performed by burning superconductor samples followed by analysis of the gas using the analyzer Vario EL III. The analysis was conducted twice for each sample, and the elements content was averaged. Infrared spectra were recorded using a spectrometer Perkin-Elmer BX II in KBr pellets in the frequency range 4000 - 400 cm^{-1}.

2.5 Studies under high pressure

Magnetic, spectroscopic, structural and resistivity measurements of the chalcogenide superconductors were investigated under high pressure. The pressure was created using various high pressure cells depending on the goal and pressure range (Fig. 2.4). A typical cell consists of two opposing diamonds, or other hard crystals, with a sample compressed between their culets. Pressure may be monitored using a reference material whose behavior under pressure is known. Common pressure standards include ruby fluorescence, and diamond Raman scattering. The uniaxial pressure supplied by the DAC may be transformed into uniform hydrostatic pressure using a pressure transmitting medium, such as synthetic oil. The pressure-transmitting medium is enclosed by a gasket and the two anvils. The sample can be viewed through the diamonds and illuminated by X-rays and visible light. In this way, X-ray diffraction and fluorescence; optical absorption and photoluminescence; Mössbauer, Raman and Brillouin scattering; positron annihilation and other signals can be measured from materials under high pressure. Magnetic field can be applied externally to the cell allowing Mössbauer spectroscopy measurements in the field. Attaching electrodes to the sample allows to perform resistivity measurements.

Fig. 2.4. High-pressure cells designed in Mainz (left to right: for magnetic studies up to 10 GPa, up to 1 GPa, up to 200 GPa loaded with H_2S, and for Mössbauer studies up to 25 GPa). *The photo is taken by the author, 2016.*

3 Unconventional superconductivity in iron selenides

3.1 Introduction

The first contribution to the chalcogenides superconductors research community was a detailed Mössbauer spectroscopy investigation of FeSe and two its intercalates with composition $Li_x(NH_2)_y(NH_3)_{1-y}Fe_2Se_2$ and $Li_x(OH)_y(H_2O)_{1-y}Fe_2Se_2$, which allowed to conclude about the leading role of magnetic fluctuations in superconducting pairing (see reprint in Chapter 3.2) [90]. The spectra of these superconductors were recorded in both low- (3 mm/s) and high- (12 mm/s) velocity ranges in the temperature range from 4.7 to 293 K.

The low-velocity spectra consist of paramagnetic doublets solely evidencing a single crystallographic position of iron in their structures. Their hyperfine parameters reflects a typical tetragonal surrounding of the central atom, which has a low spin state and formal oxidation state +2 as expected. However, variation of the parameters of three compounds indicates significant changes in electron density at the iron atoms (due to changes in the isomer shift) and in the electric field gradient (due to the changes in the quadrupole splitting). The correlation between increase in hyperfine parameters and increase in T_c of superconductors evidences that efficiency of superconducting pairing directly depends on the density of states at the Fermi level, which is formed by 3d-orbitals of iron [55].

For lithium containing superconductors a completely reversible pronounced decrease of quadrupole splitting has been observed around room temperature, while both the isomer shift and the line width do not show any anomalies. As soon as other reasons for this behaviour can be excluded, it is most likely due to the thermal activation of the Li^+ motion. In the crystal structure of $Li_x(NH_2)_y(NH_3)_{1-y}Fe_2Se_2$ reported by Burrard-Lucas et al. [53] at room temperature, Li^+ ions are disordered between two positions with occupancies of 0.25. Mössbauer spectroscopy reveals that below 240 K the Li^+ ions are arranged in the structure and do not hop between the positions providing the electric field gradient with a certain constant contribution. Upon heating Li^+ ions starts moving, and the quadrupole splitting decreases as a consequence of the decrease in their contribution to the electric field gradient. This process can be well described by the theoretical model [91] for a fluctuating field gradient.

Close inspection of Mössbauer spectra of $Li_x(NH_2)_y(NH_3)_{1-y}Fe_2Se_2$ acquired in the high velocity reveals a magnetic sextet additionally to the main quadrupole doublet (Fig. 3.1). At the lowest obtained temperature, 4.7 K, the relative intensity of the magnetic fraction is as high as 26(2) %. However, dynamic nature of the sextet indicates that magnetic moments are not static and appear as magnetic fluctuations with average lifetime ~ 10^{-7} – 10^{-8} s that is close to the observation window of Mössbauer spectroscopy. Upon heating above 20 K, the relative intensity of the magnetic subspectrum decreases and above ~ 55 K it contributes around 10 % to the total spectral intensity. In other words, in the vicinity of T_c the enhancement of magnetic fluctuations is observed (Fig. 3.2). Therefore the leading role of magnetic fluctuations in superconducting pairing mechanism in Li-intercalated FeSe becomes evident.

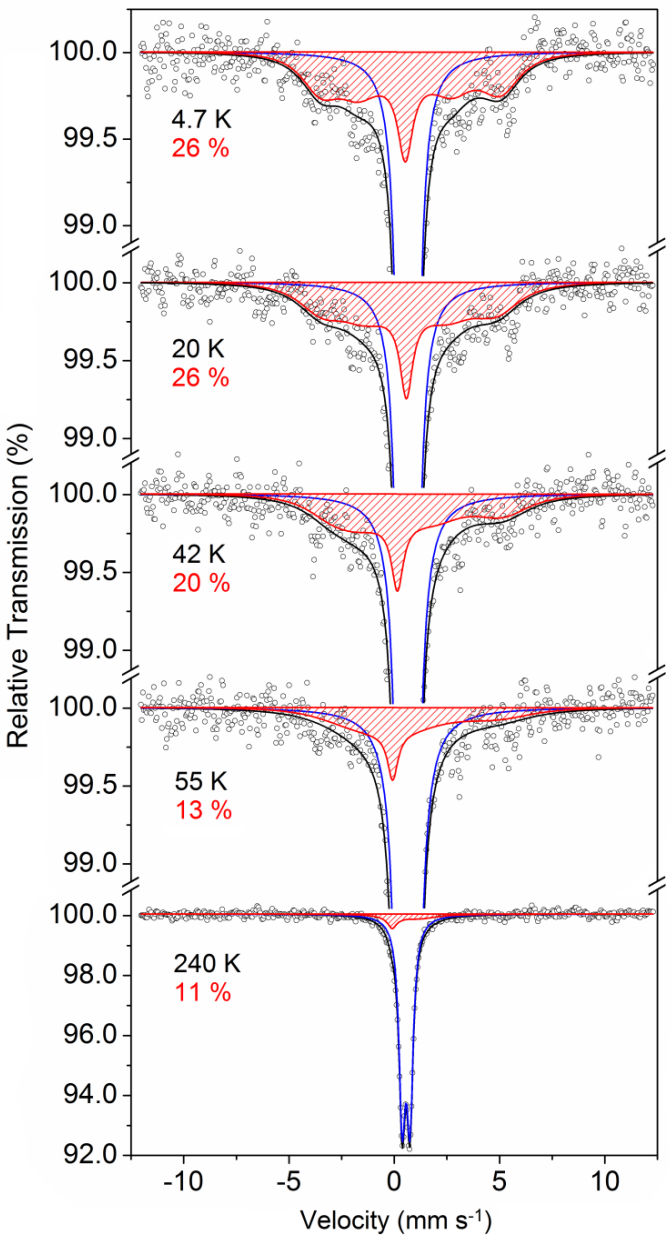

Fig. 3.1. Mössbauer spectra of $Li_x(NH_2)_y(NH_3)_{1-y}Fe_2Se_2$ showing magnetic and paramagnetic Fe sites at different temperatures. *The data were acquired together with* [redacted]

This suggestion has been further confirmed by investigation of $Li_x(NH_2)_y(NH_3)_{1-y}Fe_2Se_2$ under high pressure. At initial pressure of 0.8 GPa the temperature dependence of resistance indicates that $Li_x(NH_2)_y(NH_3)_{1-y}Fe_2Se_2$ is a semimetal with a superconducting transition temperature 40 K. Pressure increase leads to further suppression of superconductivity and at 4.8 GPa T_c = 31 K (Fig. 3.3a). At pressure above 7 GPa the sample is not superconducting and shows an R(T) dependence typical for metals. On the other hand, the relative intensity of magnetic subspectrum decreases under pressure (Fig. 3.3b). Thereby, disappearance of spin fluctuations correlates with superconductivity suppression in $Li_x(NH_2)_y(NH_3)_{1-y}Fe_2Se_2$ in contrast with pure FeSe, where both fluctuations and T_c increase under pressure [38].

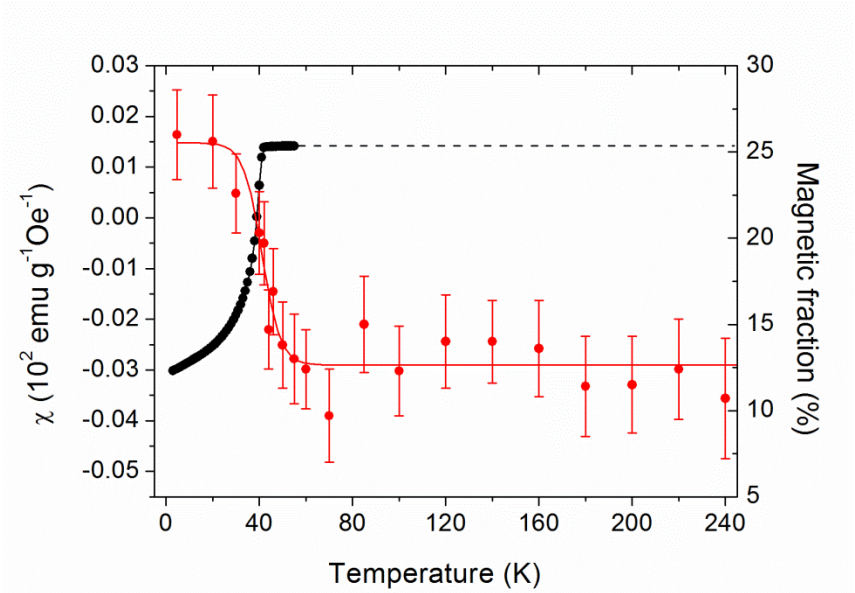

Fig. 3.2. Relative intensity of magnetic fluctuations (red) and magnetic susceptibility (black) vs. temperature for $Li_x(NH_2)_y(NH_3)_{1-y}Fe_2Se_2$. *The data were acquired together with* [redacted]

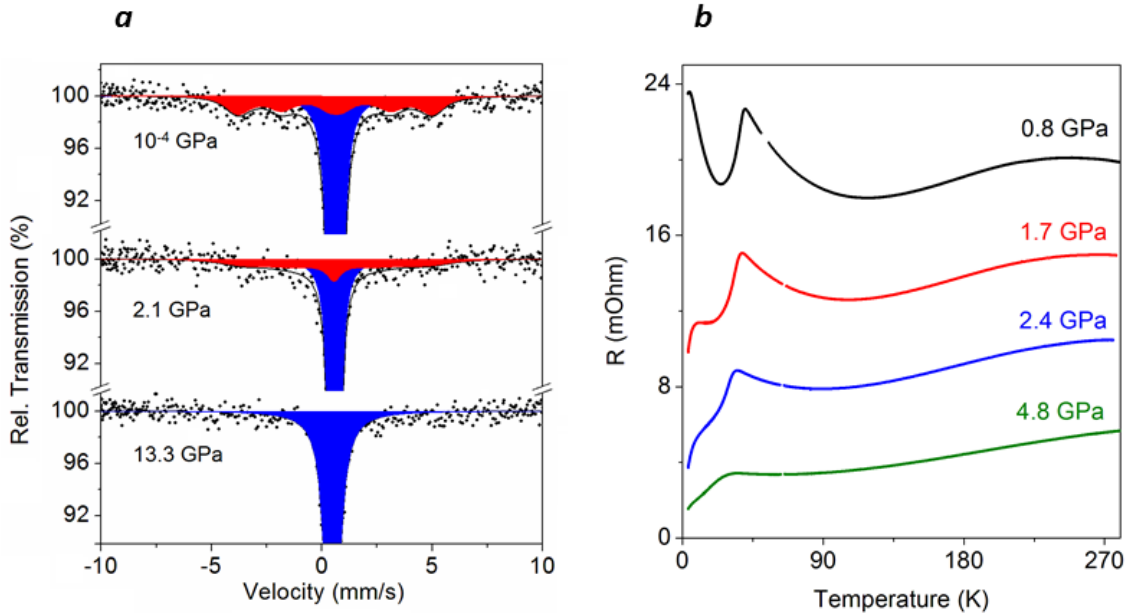

Fig. 3.3. Mössbauer spectra (**a**) and temperature dependences of resistance (**b**) of $Li_x(NH_2)_y(NH_3)_{1-y}Fe_2Se_2$ under pressure showing suppression of magnetic fluctuations and superconductivity. *The data were acquired together with* [redacted] *(Johannes Gutenberg University Mainz) (**a**) and* [redacted] *(Max Planck Institute for chemical physics of solids Dresden) (**b**).*

Additionaly to the physical pressure, superconducting properties of the material can be tuned by chemical pressure, as was followed by substitution of Se by Te with higher ionic radius [92]. This modification leads to the increase of T_c up to 14 K at ambient pressure (Fig. 3.4) in agreement with previous studies [93-99].

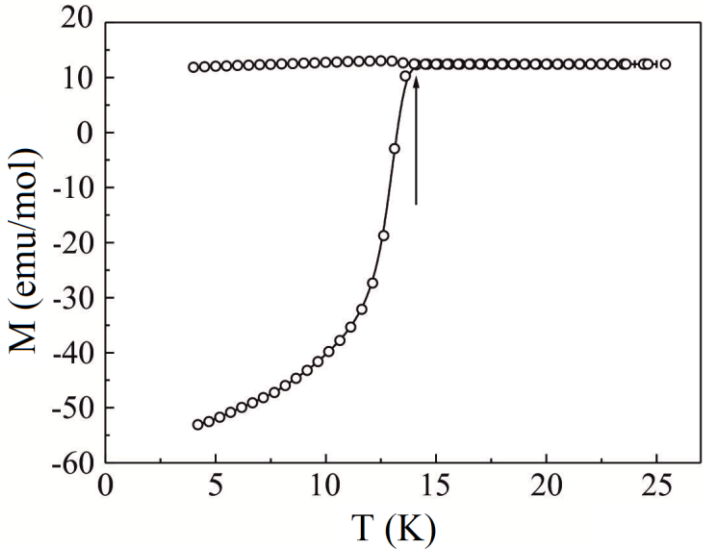

Fig. 3.4. Superconducting transition in single crystalline $FeSe_{0.5}Te_{0.5}$ recorded in ZFC/FC mode (20 Oe) showing T_c = 14 K (arrow). *The data were acquired together with* [redacted] *(Johannes Gutenberg University Mainz).*

Pressure dependent studies of $FeSe_{0.5}Te_{0.5}$ evidence a strong increase of T_c up to 20 K for pressures up to 1.3 GPa, followed by a plateau in the $T_c(p)$ dependence up to 5.0 GPa. Further pressure increase leads to a disappearance of the superconducting state around 7.0 GPa (see reprint in Chapter 3.3) [92]. As revealed by the structural measurements, appearance of the hexagonal phase under pressure correlates with disappearance of the superconducting transition in the compound above 7.0 GPa. Comparing to the parent compound FeSe, doping with Te at the elvel of 50 % does not essentially affect a structural transformation from the tetra- to hexagonal type. Thus, Te doping cannot be considered equivalent to physical pressure, despite of the big difference in ionic radii of Se and Te. The necessary precondition for superconductivity is a large number of carriers close to the Fermi energy and existing of some pairing mechanisms, which always appears in the system in a form of quantum or thermal fluctuations, *i.e.* by a sort of perturbation, which turns a pair of distinct electrons into the Cooper pair. If one assumes that all necessary conditions are fulfilled, the value of critical temperature is defined by the most stable pairing mechanism. One of the well-studied mechanisms is the electron-phonon coupling, however as it was shown by Subedi et al. [100], it cannot explain the high critical temperature achieved in FeSe under pressure.

On the other hand, different experimental studies indicate that the most important pairing mechanism in this and in similar systems could be related to magnetic fluctuations [38]. Indeed, despite that FeSe system does not exhibit long range magnetic ordering, it is on a borderline to magnetism. The constructive role of magnetic fluctuations could be concluded by comparing the T_c of FeSe (ca. 8 K at ambient pressure and maximal 37 K under pressure) to SnO, which shows a superconducting transition under pressure [101]. SnO possesses a crystal and electronic structure similar to FeSe and therefore similar nesting properties, but in contrast to FeSe is non-magnetic. The important message is that T_c in SnO also shows a maximum as a function of pressure, but compared to FeSe with a magnitude scaled down by about factor of 30. One can suggest that the functional form of $T_c(p)$ (dome-

like form) in FeSe is at large extent based on the nesting (structural) properties and less - on a particular sort of coupling mechanism. The latter however critically defines the amplitude of T_c. Obviously, the form of the $T_c(p)$ curve could be strongly influenced by a sequence of structural transformations. Thereby, the experiment on high quality single crystalline $FeSe_{0.5}Te_{0.5}$ samples confirms this idea. Critical temperature of sueprconductivity increases rapidly as a function of pressure below 2 GPa to its maximal value, and then remains almost constant up to its sudden drop at ~ 7 GPa due to the transition into the high-pressure hexagonal phase [92].

The phase separation in the family of superconducting iron chalcogenides has been probed by chemical modification of $Rb_{0.8}Fe_{1.6}Se_2$ and applying Mössbauer spectroscopy (see reprint in Chapter 3.4) [102]. Using magnetic susceptibility investigation, it has been found that $Rb_{0.8}Fe_{1.6}Se_2$ superconducts at T_c = 32 K (Fig. 3.5) as agrees with previous studies [44-45], whilst modified samples $Rb_{0.7}Fe_{1.4}Se_2$ and $Rb_{0.8}Fe_{1.56}Cu_{0.04}Se_2$ do not down to 2 K.

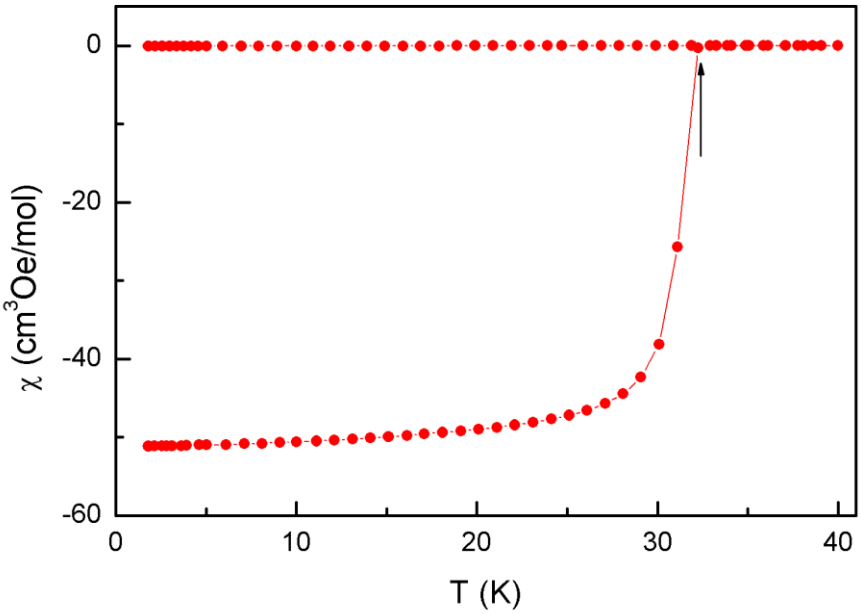

Fig. 3.5. Superconducting transition in $Rb_{0.8}Fe_{1.6}Se_2$ recorded in ZFC/FC mode (20 Oe) showing T_c = 32 K (arrow). *The data were acquired together with* [redacted]

In both $Rb_{0.7}Fe_{1.4}Se_2$ and $Rb_{0.8}Fe_{1.56}Cu_{0.04}Se_2$ the main sextet in the Mössbauer spectrum have similar hyperfine parameters to those in the parent superconducting compound $Rb_{0.8}Fe_{1.6}Se_2$. This antiferromagnetic matrix is formed independently on the deviation of the stoichiometry of iron or Cu-doping. However, the superconducting phase is very sensitive to these modifications, which lead to the disappearance of superconducting transition.

It has been found that hyperfine parameters of the Fe-based superconductors correlate with their superconducting transition temperatures (see reprint in Chapter 3.5) [103]. The isomer shift and quadrupole splitting that provide direct information about the density of states at the Fermi level are found as criteria of superconducting properties of the sample. Although superconducting pairing mechanism in iron selenides remains disputed, the Mössbauer experiment demostrates how T_c depends on the electron density of iron.

3.2. Reprint: Intercalation effect on hyperfine parameters of Fe in FeSe superconductor with T_c = 42 K

Published in: Europhysics Letters, 109 (2015), 67004.

Personal contribution: synthesis of sample **3**, preparation of the Mössbauer absorbers **1-3**, Mössbauer measurements (Figs. 3-5), magnetic susceptibility measurements (Fig. 2), treatment of the Mössbauer (**1-3**) and magnetic (**2-3**) data and the manuscript preparation were done by the author.

[redacted] designed the study, supervised the work, participated in the Mössbauer measurements (Figs. 3-5) and data treatment and contributed to writing the manuscript.

[redacted] performed the synthesis of samples **1** and **2**.

[redacted] participated in the discussion of the Mössbauer data.

[redacted] co-supervised the work.

A Letters Journal Exploring the Frontiers of Physics

March 2015

EPL, **109** (2015) 67004 www.epljournal.org
doi: 10.1209/0295-5075/109/67004

Intercalation effect on hyperfine parameters of Fe in FeSe superconductor with $T_c = 42$ K

Sergii I. Shylin[1,2], Vadim Ksenofontov[1(a)], Stefan J. Sedlmaier[3], Simon J. Clarke[3], Simon J. Cassidy[3], Gerhard Wortmann[4], Sergey A. Medvedev[5] and Claudia Felser[5]

[1] *Institute of Inorganic and Analytical Chemistry, Johannes Gutenberg-University Mainz - Staudingerweg 9, D-55099 Mainz, Germany*
[2] *Department of Chemistry, Taras Shevchenko National University of Kyiv - Volodymyrska 64/13, 01601 Kyiv, Ukraine*
[3] *Department of Chemistry, University of Oxford - Oxford OX1 3QR, UK*
[4] *Department of Physics, University of Paderborn - D-33095 Paderborn, Germany*
[5] *Max Planck Institute for Chemical Physics of Solids - D-01187 Dresden, Germany*

received 30 January 2015; accepted in final form 12 March 2015
published online 26 March 2015

PACS 74.70.Xa – Pnictides and chalcogenides
PACS 76.80.+y – Mössbauer effect; other γ-ray spectroscopy
PACS 74.62.Bf – Effects of material synthesis, crystal structure, and chemical composition

Abstract – ^{57}Fe-Mössbauer spectra of superconducting β-FeSe, the Li/NH_3 intercalate product and a subsequent sample of this intercalate treated with moist He gas have been measured in the temperature range 4.7–290 K. A correlation is established between hyperfine parameters and critical temperature T_c in these phases. A strong increase of the isomer shift upon intercalation is explained by a charge transfer from the Li/NH_3 intercalate to the FeSe layers resulting in an increase of T_c up to 42 K. A significant decrease of the quadrupole splitting above 240 K has been attributed to diffusive motion of Li^+ ions within the interlamellar space.

Introduction. – The recent development of iron-based superconductors has prompted extensive research focusing on the new synthetic approaches to high-T_c systems and on studying the superconducting pairing mechanism in these materials. Particular attention has been paid to iron chalcogenide compounds, notably the tetragonal polymorph of FeSe (β-FeSe ($T_c = 8$ K)) [1,2], where a marked increase of T_c up to 37 K has been observed under pressure [3]. An increase of T_c in FeSe-related compounds has also been obtained in a variety of its derivatives with cationic spacers between the FeSe layers consisting of alkali metal ions with the general formula $A_xFe_{2-y}Se_2$ ($A = K^+$ ($T_c = 31$ K) [4], Rb^+ ($T_c = 32$ K) [5], Cs^+ ($T_c = 27$ K) [6]). However, these compounds exhibit a complex phase separation, where only the minority of the FeSe-like regions of the bulk samples is responsible for superconductivity [7–10]. For the basic FeSe system, also the partial substitution of Se by Te results in an increase of T_c up to 13 K in $FeSe_{0.5}Te_{0.5}$, which is attributed mainly to the chemical pressure [11].

Further alternative synthesis routes of FeSe-based superconductors have been undertaken. Due to the solubility of alkali, alkaline-earth metals as well as Eu and Yb in liquid ammonia and some amines [12], one of the approaches is the intercalation reaction of FeSe under these conditions resulting in products accommodating electropositive metal ions, ammonia and amide ions between the FeSe layers. Thus, successful intercalation reactions with Li, Na, K, Ca, Sr, Ba, Yb and Eu with FeSe by the ammonothermal method at temperatures around −78 °C have been reported [13]. T_c values up to 46 K in these compounds have been found and recent computational investigations suggest that the enhancement of T_c relative to that in the FeSe parent material is a consequence of making the Fermi surface more two-dimensional and of electron doping [14]. Superconductors have also been obtained by the intercalation of alkali metals along with other molecules, notably pyridine [15], although these compounds are not yet characterised in detail. Following the ammonothermal intercalation approach, Burrard-Lucas *et al.* have characterised $Li_x(NH_2)_y(NH_3)_{1-y}Fe_2Se_2$ ($x = 0.6$; $y = 0.2$) containing Li^+ and amide ions as well as ammonia molecules

(a) E-mail: ksenofon@uni-mainz.de

acting as the spacer layer between FeSe layers, which exhibits bulk superconductivity (superconducting volume fractions of about 50%) below 43 K [16], and Sedlmaier *et al.* have identified a more ammonia-rich intercalate by probing the intercalation reaction *in situ* [17]. Using neutron powder diffraction, the crystal structure of the deuterated intercalated compounds has been unambiguously determined. It showed evidence for weak N–D$\cdots$Se hydrogen bonds and the refined compositions revealed that the amide (ND_2^-) content was lower than the Li^+ content indicating an electron transfer to the FeSe layers and, therefore, into the conducting band responsible for superconductivity. Although the superconducting mechanism in iron-based superconductors still remains enigmatic, it has been proposed that magnetic fluctuations could play a role in the pairing mechanism of superconducting charge carries [18]. Apparently, both spin fluctuations and the density of states at the Fermi level are among the major factors affecting T_c. Taking into account that the conduction band at the Fermi level is dominantly formed by Fe-3*d* orbitals, Mössbauer spectroscopy can be a useful tool to study Fe-based superconductors.

Here we report the detailed temperature-dependent ^{57}Fe-Mössbauer study of non-intercalated β-FeSe (**1**), the Li/ammonia intercalate product (**2**) and a subsequent sample of this intercalate treated with moist He gas (**3**). Our observations demonstrate that *d*-electron density on Fe ions increases upon intercalation and decreases after subsequent treatment with water vapour along with T_c. Moreover, the Mössbauer data for Li/ammonia intercalate indicate the diffusive motion of Li^+ ions within the interlayer space.

Experimental details. – The sample of tetragonal β-FeSe (**1**) was synthesized by heating a stoichiometric mixture of iron powder (Johnson-Matthey, 99.98%) and selenium shots (ALFA 99.99%) and structurally characterized as described elsewhere [2]. β-FeSe used as the precursor to **2** was synthesised in a similar way from iron powder (ALFA 99.995%) and selenium shots (ALFA 99.99%).

The intercalate $Li_x(NH_2)_y(NH_3)_{1-y}Fe_2Se_2$ (**2**) was synthesised from β-FeSe, Li metal (99%, Aldrich) and ammonia (99.98%, BOC) [16]. All manipulations of solids were performed under argon. β-FeSe and Li (molar ratio 2 : 1) were placed in a Schlenk tube and this, along with a cylinder of ammonia was connected to a Schlenk line. After evacuation of the system and cooling the Schlenk tube down to 195 K (dry ice/isopropanol bath), the valve on the ammonia cylinder was opened allowing ammonia to condense onto the reactants. The mixture was stirred for 30 min, and then the Schlenk tube was allowed to warm to room temperature enabling excess ammonia to evaporate via a mercury bubbler. After brief evacuation the powder of **2** was isolated as a black powdery solid in an argon-filled glove box.

After the Mössbauer measurements of **2** had been performed under a dry He atmosphere, **2** was partially hydrolysed in the closed sample volume of the Mössbauer cryostat by introducing moist helium gas into the sample space. After a 24 hours exposure to this moist helium atmosphere, the exchange gas was replaced and the modified sample (**3**) was kept under dry helium during subsequent measurements.

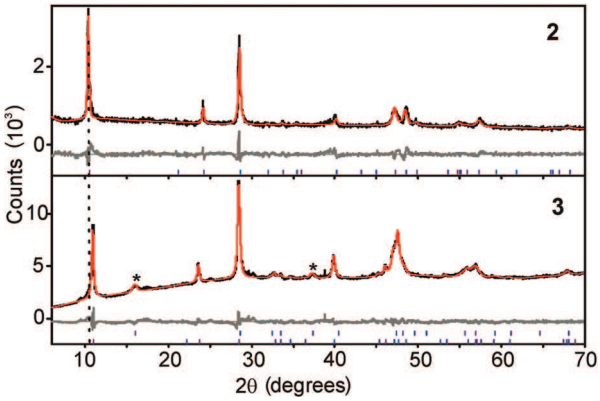

Fig. 1: (Colour on-line) X-ray powder diffraction patterns of **2** and **3**. The data (black line), Pawley-type fit (red line) and difference (grey line) are shown. Tick marks are for the main body-centred tetragonal phase (lower panel) and the FeSe-like phase in **3** (upper panel). The dotted line is used to show the shift in the 002 reflection after mild hydrolysis. The asterisks indicate reflections arising from a β-FeSe-like phase.

The purity of the samples was confirmed using a Philips PW1730 X-ray diffractometer (Cu$K\alpha_1/K\alpha_2$ radiation). Magnetic susceptibility measurements were performed using a Quantum Design SQUID magnetometer in the field of 20 Oe in the temperature range of 2–55 K using zero-field–cooled (ZFC) and field-cooled (FC) measurements. ^{57}Fe-Mössbauer spectra were recorded in transmission geometry with a ^{57}Co source in a rhodium matrix using a conventional constant-acceleration Mössbauer spectrometer equipped with a nitrogen/helium bath cryostat in the temperature range of 4.7–290 K. Isomer shifts are given relatively to an α-Fe foil at ambient temperature. Fits of the experimental Mössbauer data were performed using the Recoil software [19]. Hyperfine parameters uncertainties given in parentheses were evaluated using the covariance matrix of the fit. The absorbers were prepared by placing the powdered samples (around 30 mg) in plastic holders. All the sample preparation procedures were performed in an argon glove box with an O_2 and H_2O content below 0.5 ppm.

Results and discussion. – X-ray powder diffraction (XRPD) patterns for **2** and **3** are shown in fig. 1. The peaks observed for **2** are accounted for the $Li_x(NH_2)_y(NH_3)_{1-y}Fe_2Se_2$ superconductor phase with a structure based on that of $ThCr_2Si_2$ with a body-centred tetragonal unit cell ($a = 3.785(2)$ Å, $c = 16.914(9)$ Å) [16]. The peak shapes of this sample suggest some imperfection in the stacking of the layers. On exposure to moist helium to obtain **3**, there is evidence for partial deintercalation.

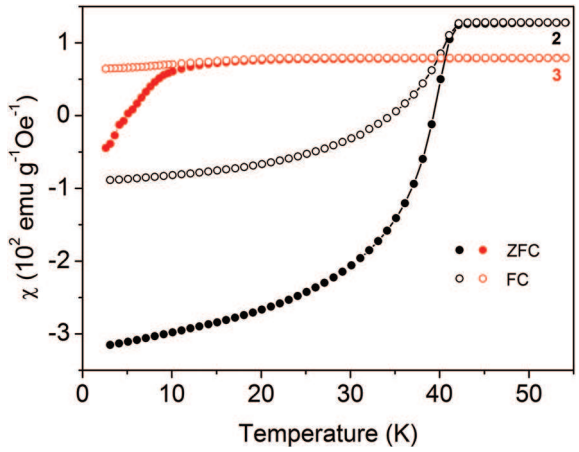

Fig. 2: (Colour on-line) Magnetic susceptibility measurements on **2** (black) and **3** (red) in the ZFC-FC mode.

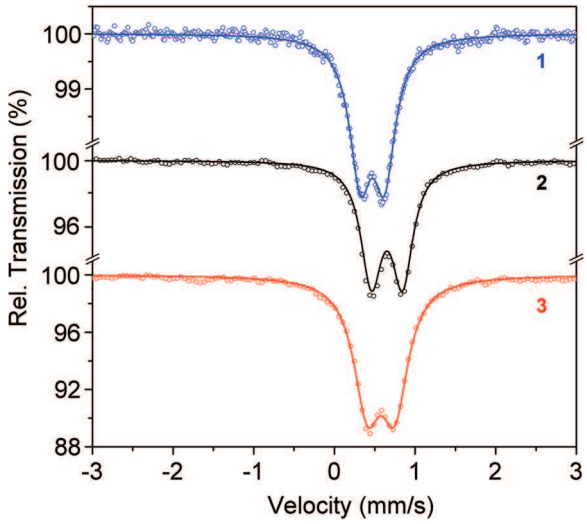

Fig. 3: (Colour on-line) Mössbauer spectra of **1** (blue), **2** (black) and **3** (red) recorded at 100 K in the ±3 mm/s velocity range.

However, the majority phase may be accounted for by using the model-independent Pawley method on a body-centred tetragonal cell ($a = 3.8572(2)$ Å, $c = 16.011(2)$ Å) with a c lattice parameter greatly reduced in comparison with sample **2**. A minor part of the sample decomposed to a phase resembling β-FeSe but with much broader Bragg peaks. Further weak reflections in the pattern of **3** could not readily be identified. The dominant phase in the powder pattern of **3** suggests that another intercalate of FeSe is produced by the gentle hydrolysis treatment.

Magnetic measurements of **1**–**3** show superconductivity in all samples. In agreement with previous studies, the non-intercalated compound (**1**) exhibits a superconducting transition at 8 K [1,2] and the intercalated one (**2**) has a transition at 42 K (fig. 2) [16]. After exposure to a moist helium atmosphere the superconducting properties of the intercalated sample change dramatically. From the susceptibility measurements, the onset transition temperature for **3** is determined to be 12 K, and the diamagnetic volume fraction noticeably decreases below T_c in comparison with **2** (fig. 2).

Mössbauer spectra of **1**–**3** recorded at 100 K are shown in fig. 3 and the derived hyperfine parameters (isomer shift δ, quadrupole splitting ΔE_Q and linewidth Γ) are summarized in table 1. All spectra consist of single paramagnetic doublets having close values of linewidth that evidence one single Fe site in the structures. ΔE_Q of **1** reflects a tetragonal structure of the parent compound and both ΔE_Q and δ indicate a low-spin (LS) state of divalent iron [2]. The parameters of its derivatives, **2** and **3**, indicate changes in electron density on the Fe nuclei (δ) as well as in the local distortion symmetry (ΔE_Q). Assuming that the FeSe layers remain intact and the first coordination sphere of Fe does not change after the intercalation procedure and after the mild hydrolysis to produce **3**, such a difference in δ means an increase in d-electron density. Indeed, taking into account the composition of **2**, $Li_x(NH_2)_y(NH_3)_{1-y}Fe_2Se_2$ ($x = 0.6$; $y = 0.2$), one

Table 1: Hyperfine parameters of **1**–**3** at 100 K.

Sample	δ (mm/s)	ΔE_Q (mm/s)	Γ (mm/s)
1	0.557(2)	0.286(3)	0.181(4)
2	0.641(2)	0.396(4)	0.178(4)
3	0.579(3)	0.337(6)	0.179(5)

can calculate the formal oxidation state of Fe to be +1.8, whilst in **1** it is +2. Apparently, the Mössbauer measurements together with the above XRPD data show that the reaction to convert **2** into **3** does not simply convert **2** back to pure FeSe. This suggests that a range of further intercalates of FeSe may exist, and may merit further investigation.

Additional information on the properties of the present samples was obtained from Mössbauer spectra recorded in the temperature range 4.7–290 K. The variation of δ with temperature is presented in fig. 4. The observed decrease of δ with increasing temperature is caused by the second-order Doppler shift, used here to derive Debye temperatures (Θ_D) by fitting the temperature dependence of δ using the Debye model [20],

$$\delta(T) = \delta(0) - \frac{9k_B T^4}{2\Theta_D^3 Mc} \int_0^{\Theta_D/T} \frac{x^3 \mathrm{d}x}{e^x - 1}, \qquad (1)$$

providing $\Theta_D = 390(5)$ K, 365(5) K and 420(5) K for **1**, **2** and **3**, respectively. Determination of Θ_D using eq. (1) results often in values, which are higher than Θ_D obtained from density of phonon states (DOS), caused by other factors, *e.g.* thermal expansion. In the present case, we derived for sample **1** a lower value, $\Theta_D = 285$ K, in our study of the local DOS using nuclear inelastic scattering

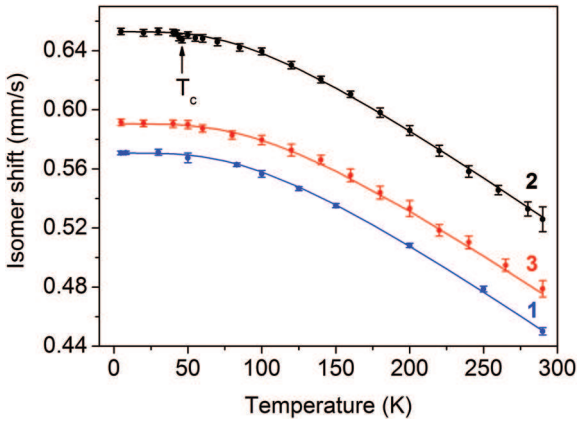

Fig. 4: (Colour on-line) Temperature dependences of the isomer shift for **1** (blue), **2** (black) and **3** (red). The fitting curves were adjusted with the Debye model (eq. (1)).

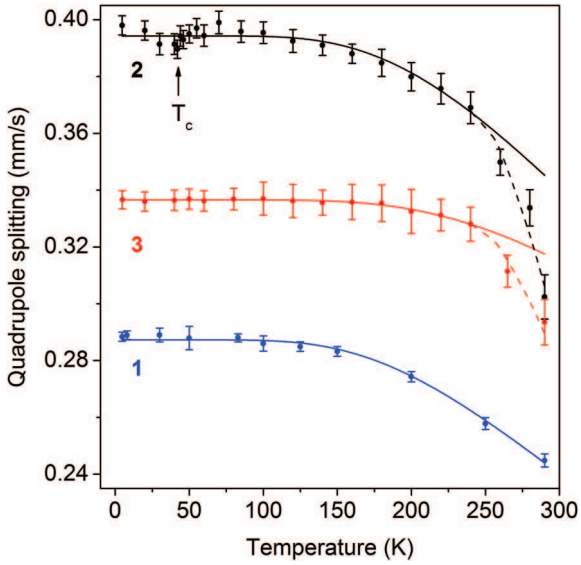

Fig. 5: (Colour on-line) Temperature dependences of the quadrupole splitting for **1** (blue), **2** (black) and **3** (red) and the fitting curves considering the tetragonal distortion of $FeSe_4$ tetrahedra (eq. (2), solid line) and for the fluctuating EFG due to the thermoactivated motion of Li^+ ions (eq. (3), dashed line).

(NIS) [21]. The comparison of the Debye temperatures of **1**–**3** indicates some softening of the phonon spectrum after intercalation to produce **2** and its hardening after subsequent mild hydrolysis to produce **3**. A similar softening of the phonon spectrum upon intercalation of FeSe has been also observed in our recent NIS measurements [22].

A marked increase of ΔE_Q by about 40% between **1** and **2** reflects a significant increase of the electric-field gradient (EFG) upon intercalation. This finding is in accordance with the crystal structure [16] indicating a larger distortion of $FeSe_4$ tetrahedra in **2**, as expressed by the variance of the polyhedral angles $\sigma^2_\Theta = 22.49$ and 32.56 for **1** and **2**, respectively. However, such an increase of ΔE_Q might be also caused by other reasons as evidenced by the Mössbauer data at different temperatures. Dependences of ΔE_Q on temperature are shown in fig. 5. A slight increase in ΔE_Q of **1** upon cooling is typical for LS Fe(II) tetrahedral compounds and can be plausibly fitted using the simplified model for tetragonal distortion in an axial electric field [23]:

$$\Delta E_Q(T) = \Delta E_Q(0) \cdot \frac{1 - e^{-E_0/k_B T}}{1 + 2e^{-E_0/k_B T}}, \qquad (2)$$

where E_0 is energy of a crystal field splitting. For **1**, a splitting value of 0.072(2) eV has been found to increase up to 0.078(2) eV after intercalation (**2**) and to 0.089(2) eV after hydrolysis treatment (**3**).

Although this model is completely appropriate and describes well the temperature dependence of ΔE_Q for **1** in the whole temperature range, an anomalous decrease of ΔE_Q above 240 K for **2** and **3** is observed. We suppose that such behaviour of ΔE_Q-*vs.*-T curves is associated with the motion of Li^+ ions. It is known that in certain cases Li-containing solids may show a mobility of Li^+ that usually is monitored by the NMR technique [24]. Herein, we observe an essential decrease of ΔE_Q above 240 K upon heating the Li-intercalated specimens **2** and **3**. Cooling then the samples, we notice that the behaviour of ΔE_Q in the region of 240–290 K is completely reversible and does not show thermal hysteresis. At the same time, δ (fig. 4), as well as the linewidth, does not show any peculiarities in this temperature region. It allows concluding that this behaviour of ΔE_Q is not caused by a structural transition or other reasons affecting the electron density on Fe nuclei. Therefore, we attribute this strong decrease of ΔE_Q above 240 K to the thermal activation of the Li^+ motion. Indeed, according to the crystal structure of **2** obtained from neutron powder diffraction measurements at 293 K, Li^+ ions are distributed over two sites (2*b*, 4*c*, *I*4/*mmm*) separated by less than 2 Å, each with fractional occupancies of ∼0.25 [16]. The large displacement ellipsoids for these ions are consistent with rapid hopping between sites at room temperature. We assume that at low temperature the Li^+ ions are arranged in an ordered array on these sites, similarly as described elsewhere [25], thereby providing a defined contribution to the EFG at the Fe sites. Above 240 K the thermoactivated motion of the Li^+ ions between their lattice sites becomes rapid enough on the timescale of the Mössbauer experiment of 10^{-8} s to lead to an averaging of the electric-field gradient caused by Li^+ ions and their contribution to the observed ΔE_Q decreases. Assuming that the Li-induced EFG fluctuates between two opposite directions, a theoretical model [26] for a fluctuating EFG has been applied to derive the activation energy E_a for the Li^+ hopping from the variation of the EFG in the region of 240–290 K:

$$\Delta E_Q^{Li}(T) = \Delta E_Q(T) \cdot \frac{1 - e^{-E_a/k_B T}}{1 + e^{-E_a/k_B T}}, \qquad (3)$$

where $\Delta E_Q^{Li}(T)$ describes the variation of the quadrupole splitting considering the Li^+ motion (dashed lines in fig. 5), and $\Delta E_Q(T)$ represents the values obtained by eq. (2) above 240 K (solid line in fig. 5). The E_a values for **2** and **3** have been determined as 0.050(14) and 0.058(7) eV.

Another observation of the present work is a small decrease of ΔE_Q for **2** near T_c as indicated in fig. 5, quite small in magnitude and comparable to the error bars, but reaching its minimum exactly at $T_c = 42\,K$ with 0.390(3) mm/s whilst being 0.396(4) mm/s at 100 K and 0.396(3) mm/s at 20 K. This small decrease may be due to the appearance of magnetic fluctuations [27] and requires further investigations since the ΔE_Q-*vs.*-T dependence for **3** does not show any noticeable anomalies between 20 and 55 K, where the sample is not superconducting. Additionally, a slight decrease of the isomer shift for **2** can be found near T_c. This feature is not observed for **1** and **3** with much lower T_c values. Hence, some variations of the hyperfine parameters of **2** in the vicinity of T_c occur, but the nature of this phenomenon should be clarified in the future.

Conclusions. – In summary, ^{57}Fe-Mössbauer studies of superconducting FeSe and its derivatives reveal that *d*-electron density on ^{57}Fe atoms increases upon intercalation with Li^+, NH_2^- and NH_3 molecules between FeSe layers concomitant with a dramatic increase in T_c. The measurements also point to an enhanced value of the quadrupole splitting for the intercalate compound. To a large extent, this increase can be assigned to the Li+ ions, which provide an additional electric-field gradient and the increase in electron density on Fe atoms resulting from the reduction of FeSe, *i.e.* "electron doping" by the Li^+ intercalation. Both δ and ΔE_Q enhancement can be considered as distinctive fingerprints of the high-T_c superconductor $Li_x(NH_2)_y(NH_3)_{1-y}Fe_2Se_2$ ($x = 0.6$; $y = 0.2$). Despite the increased density of *d*-electrons on Fe due to intercalation, we cannot conclude that this is the only reason for the rise of T_c from 8 K to 42 K. In addition, we observe small variations of the quadrupole splitting and isomer shift for **2** near T_c that might be indicative of magnetic fluctuations connected with superconducting mechanism. Finally, we report on the observation of Li^+ motion in the intercalated compounds, which may be interesting materials exhibiting both high-T_c superconductivity and Li^+ mobility.

* * *

We thank the Deutsche Forschungsgemeinschaft (DFG) for financial support provided through Grant No. KS51/2-2 (priority program SPP-1458) and a research fellowship for SJS (SE 2324/1-1). SJC thanks the UK EPSRC for financial support (Grant EP/I017844). The authors are grateful to the group of Prof. R. J. Cava (Princeton University) for the synthesis of β-FeSe.

REFERENCES

[1] Hsu F. C., Luo J. Y., Yeh K. W., Chen T. K., Huang T. W., Wu P. M., Lee Y. C., Huang Y. L., Chu Y. Y., Yan D. C. and Wu M.-K., *Proc. Natl. Acad. Sci. U.S.A.*, **105** (2008) 14262.

[2] McQueen T. M., Huang Q., Ksenofontov V., Felser C., Xu Q., Zandbergen H., Hor Y. S., Allred J., Williams A. J., Qu D., Checkelsky J., Ong N. P. and Cava R. J., *Phys. Rev. B*, **79** (2009) 014522.

[3] Medvedev S., McQueen T. M., Troyan I. A., Palasyuk T., Eremets M. I., Cava R. J., Naghavi S., Casper F., Ksenofontov V., Wortmann G. and Felser C., *Nat. Mater.*, **8** (2009) 630.

[4] Guo J., Jin S., Wang G., Wang S., Zhu K., Zhou T., He M. and Chen X., *Phys. Rev. B*, **82** (2010) 180520.

[5] Wang A. F., Ying J. J., Yan Y. J., Liu R. H., Luo X. G., Li Z. Y., Wang X. F., Zhang M., Ye G. J., Cheng P., Xiang Z. J. and Chen X. H., *Phys. Rev. B*, **83** (2011) 060512.

[6] Krzton-Maziopa A., Shermadini Z., Pomjakushina E., Pomjakushin V. Yu., Bendele M., Amato A., Khasanov R., Luetkens H. and Conder K., *J. Phys.: Condens. Matter*, **23** (2011) 052203.

[7] Ksenofontov V., Wortmann G., Medvedev S. A., Tsurkan V., Deisenhofer J., Loidl A. and Felser C., *Phys. Rev. B*, **84** (2011) 180508.

[8] Texier Y., Deisenhofer J., Tsurkan V., Loidl A., Inosov D. S., Friemel G. and Bobroff J., *Phys. Rev. Lett.*, **108** (2012) 237002.

[9] Shylin S. I., Ksenofontov V., Medvedev S. A., Tsurkan V. and Felser C., *Phase Separation in $Rb_xFe_{2-y}Se_2$ Probed by Non-stoichiometry and Cu Doping*, to be published in *J. Supercond. Nov. Magn.* (2015), DOI: 10.1007/s10948-014-2912-6.

[10] Ryan D. H., Rowan-Weetaluktuk W. N., Cadogan J. M., Hu R., Straszheim W. E., Bud'ko S. L. and Canfield P. C., *Phys. Rev. B*, **83** (2011) 104526.

[11] Gómez R. W., Marquina V., Pérez-Mazariego J. L., Escamilla R., Escudero R., Quintana M., Hernández-Gómez J. J., Ridaura R. and Marquina M. L., *J. Supercond. Nov. Magn.*, **23** (2010) 551.

[12] Somoano R. B., Hadek V. and Rembaum A. J., *Chem. Phys.*, **58** (1973) 697.

[13] Ying T. P., Chen X. L., Wang G., Jin S. F., Zhou T. T., Lai X. F., Zhang H. and Wang W. Y., *Sci. Rep.*, **2** (2012) 426.

[14] Guterding D., Jeschke H. O., Hirschfeld P. J. and Valenti R., *Phys. Rev. B*, **91** (2015) 041112.

[15] Krzton-Maziopa A., Pomjakushina E., Pomjakushin V. Yu., Rohr F., Schilling A. and Conder K., *J. Phys.: Condens. Matter*, **24** (2012) 382202.

[16] Burrard-Lucas M., Free D. G., Sedlmaier S. J., Wright J. D., Cassidy S. J., Hara Y., Corkett A. J., Lancaster T., Baker P. J., Blundell S. J. and Clarke S. J., *Nat. Mater.*, **12** (2013) 15.

[17] Sedlmaier S. J., Cassidy S. J., Morris R., Drakopoulos M., Reinhard C., Moorhouse S. J., O'Hare D., Manuel P., Khalyavin D. and Clarke S. J., *J. Am. Chem. Soc.*, **136** (2014) 630.

[18] Scalapino D. J., *Rev. Mod. Phys.*, **84** (2012) 1383.

[19] Lagarec K. and Rancourt D. G., *Nucl. Instrum. Methods Phys. Res. B*, **129** (1997) 266.
[20] Wang P., Stadnik Z. M., Żukrowski J., Thaler A., Bud'ko S. L. and Canfield P. C., *Phys. Rev. B*, **84** (2011) 024509.
[21] Ksenofontov V., Wortmann G., Chumakov A. I., Gasi T., Medvedev S., McQueen T. M., Cava R. J. and Felser C., *Phys. Rev. B*, **81** (2010) 184510.
[22] Ksenofontov V. *et al.*, *Density of phonon states in superconducting Li/NH₃ intercalated FeSe with* $T_c = 42\,K$, in preparation.
[23] Greenwood N. N. and Gibb T. C., in *Mössbauer Spectroscopy* (Chapman and Hall Ltd., London) 1971, p. 101.
[24] Deiseroth H. J., Kong S. T., Eckert H., Vannahme J., Reiner C., Zaiß T. and Schlosser M., *Angew. Chem., Int. Ed.*, **47** (2008) 755.
[25] Padma kumar P. and Yashonath S., *J. Phys. Chem. B*, **105** (2001) 6785.
[26] Gerard A. and Gradjean F., *J. Phys. Chem. Solids*, **36** (1975) 1365.
[27] Imai Y., Ahilan K., Ning F. L., McQueen T. M. and Cava R. J., *Phys. Rev. Lett.*, **102** (2009) 177005.

3.3. Reprint: Pressure effect on superconductivity in $FeSe_{0.5}Te_{0.5}$

Published in: Physica Status Solidi (b), 254 (2017), 1600161.

Personal contribution: Mössbauer measurements at ambient and high pressure (Figs. 1-2, 6-7), magnetic susceptibility measurements under pressure (Figs. 3-4), treatment of the Mössbauer and magnetic (Fig. 8) data, and the preparation of the major part of the manuscript were done by the author personally.

[redacted] designed the study, supervised the work, participated in the Mössbauer and susceptibility measurements (Figs. 1-4, 6-8) and data treatment, and contributed to writing the manuscript.

[redacted] loaded the sample in the high-pressure cell for magnetic measurements and performed structural studies of the sample (Fig. 5).

[redacted] synthesized the sample.

[redacted] participated in the discussion of magnetic, structural and Mössbauer data.

[redacted] co-supervised the work.

Phys. Status Solidi B **254**, No. 1, 1600161 (2017) / **DOI** 10.1002/pssb.201600161

physica status solidi b
www.pss-b.com
basic solid state physics

Pressure effect on superconductivity in $FeSe_{0.5}Te_{0.5}$

Sergii I. Shylin[,1,2], Vadim Ksenofontov[*,1], Pavel G. Naumov[3], Sergey A. Medvedev[3], Vladimir Tsurkan[4,5], Joachim Deisenhofer[4], Alois Loidl[4], Leslie M. Schoop[6], Taras Palasyuk[7], Gerhard Wortmann[8], and Claudia Felser[3]**

[1] Institute of Inorganic and Analytical Chemistry, Johannes Gutenberg University Mainz, Staudingerweg 9, 55099 Mainz, Germany
[2] Department of Chemistry, Taras Shevchenko National University of Kyiv, Volodymyrska 64/13, 01601 Kyiv, Ukraine
[3] Max Planck Institute for Chemical Physics of Solids, 01187 Dresden, Germany
[4] Experimental Physics V, University of Augsburg, 86159 Augsburg, Germany
[5] Institute of Applied Physics, Academy of Sciences of Moldova, MD 2028 Chisinau, Moldova
[6] Max Planck Institute for Solid State Research, 70569 Stuttgart, Germany
[7] Institute of Physical Chemistry, Polish Academy of Sciences, Kasprzaka 44/52, 01-224 Warsaw, Poland
[8] Department of Physics, University of Paderborn, 33095 Paderborn, Germany

Received 25 March 2016, revised 31 August 2016, accepted 5 September 2016
Published online 23 September 2016

Keywords high pressure, iron chalcogenides, Mössbauer spectroscopy, superconductivity, synchrotron X-ray diffraction

* Corresponding author: e-mail ksenofon@uni-mainz.de, Phone: +49 6131 39 23889, Fax: +49 6131 39 23827
** e-mail shylin@univ.kiev.ua, Phone/Fax: +38 044 239 3393

Due to the simple layered structure, isostructural FeSe and $FeSe_{0.5}Te_{0.5}$ are clue compounds for understanding the principal mechanisms of superconductivity in the family of Fe-based superconductors. High-pressure magnetic, structural and Mössbauer studies have been performed on single-crystalline samples of superconducting $FeSe_{0.5}Te_{0.5}$ with $T_c = 13.5$ K. Susceptibility data have revealed a strong increase of T_c up to 19.5 K for pressures up to 1.3 GPa, followed by a plateau in the $T_c(p)$ dependence up to 5.0 GPa. Further pressure increase leads to a disappearance of the superconducting state around 7.0 GPa. X-ray diffraction and Mössbauer studies explain this fact by a tetragonal-to-hexagonal structural phase transition. Mössbauer parameters of the non-superconducting high-pressure phase indicate less covalency of Fe–Se bonds. Based on structural and susceptibility data, we conclude about a common character of $T_c(p)$ diagrams for both FeSe and $FeSe_{0.5}Te_{0.5}$ superconductors.

1 Introduction Discovery of superconducting compounds $A_xFe_{2-y}Se_2$ with intercalated alkali elements (A = K, Rb, Cs) has extended superconducting transition temperature above 30 K and confirmed an essential research potential of FeSe-based systems [1]. The nearly stoichiometric FeSe becomes superconducting below 8 K at ambient pressure but the transition temperature can be enhanced up to 37 K by application of external pressure of ca. 9 GPa [2, 3]. Above this pressure, FeSe transforms to a hexagonal close packed NiAs-type structure that exhibits semiconducting behaviour. Variety of experiments demonstrates ambiguous relation between the crystal structures of FeSe-based compounds and their superconducting properties. For instance, the superconducting transition in $Fe_{1.01}Se$ occurs in an orthorhombic phase which appears after a subtle structural transition from the tetragonal phase at ca. 90 K [4]. Below this temperature, $Fe_{1.01}Se$ exhibits nematic ordering without long-range magnetism, which competes with emerging superconductivity [5]. In contrast, the non-superconducting composition $Fe_{1.03}Se$ remains always in the tetragonal phase. Pressure application at room temperature converts $Fe_{1.01}Se$ to the non-metallic NiAs-type polymorph around 9 GPa, which remains stable at low temperatures [2]. The substitution of Se by Te in $FeSe_{1-x}Te_x$ increases the superconducting transition temperature up to 14 K for $x = 0.5$ [6, 7]. The low-temperature structural response to pressure of orthorhombic $FeSe_{0.55}Te_{0.42}$ is different than in FeSe as evidenced by the observation of a

monoclinic structure at 2.3 GPa, the same pressure, where $T_c = 23.3$ K is found to reach its maximum [8]. Further pressure increase leads to a monotonic decrease of T_c in the monoclinic phase that exists up to a pressure of 11.9 GPa, at which superconductivity is completely suppressed. According to resistivity data, above this pressure $FeSe_{0.55}Te_{0.42}$ remains metallic [8]. Formally FeSe, $FeSe_{0.55}Te_{0.42}$, $FeSe_{0.5}Te_{0.5}$, as well as Cu-substituted FeSe, reveal similar dome-shape curves in their $T_c(p)$ diagrams limiting the range of superconductivity [2, 8, 9]. In the previous study of $FeSe_{0.5}Te_{0.5}$, it was found that T_c increases rapidly from 13.5 to 26.2 K upon applying pressures up to 2 GPa. Above 2 GPa, T_c decreases linearly and a non-superconducting metallic phase is observed at $p = 14$ GPa [10]. The authors point out that the same relationship between normalized T_c and pressure in both $FeSe_{0.5}Te_{0.5}$ and FeSe presumes universal pressure dependence in these systems, but suggest that the phase transition from the tetragonal to the hexagonal modification observed in FeSe does not occur in $FeSe_{0.5}Te_{0.5}$. Considering an interest to superconducting $FeSe_{0.5}Te_{0.5}$ compound and taking into account a scope of experimental data available [11–16], a complete $T_c(p)$ diagram reflecting the interrelation of structural, electronic and superconducting properties would be demanded. Additional experimental information is also necessary to clarify the unusual rapid growth, subsequent stagnation and disappearance of T_c in $FeSe_{1-x}Te_x$ under pressure.

It has been shown earlier that no significant pressure variations that can be responsible for the initial rapid increase of T_c with pressure occur in the phonon spectrum of FeSe [17]. In this context, the suggestion that the strong enhancement of T_c under pressure in $FeSe_{0.5}Te_{0.5}$ is mainly due to an increase of density of electronic states [18], requires further consideration. Until now the superconducting properties of powdered $FeSe_{0.5}Te_{0.5}$ samples were investigated only by resistivity measurement under pressure [8]. The disadvantage of this method is the influence of particle boundaries, distribution of particles size and percolation effects on the formation of the $T_c(p)$ curve. Magnetic susceptibility measurements of single crystals under pressure should be more appropriate to obtain a reliable $T_c(p)$ dependence. We also present here results of high-pressure structural and ^{57}Fe Mössbauer studies of superconducting single crystalline $FeSe_{0.5}Te_{0.5}$.

2 Experimental Single crystals of $FeSe_{0.5}Te_{0.5}$ were grown by Bridgman method. Details of the preparation and sample characterisation were described elsewhere [16]. The quality of the grown samples was confirmed by the X-ray diffraction and magnetic measurements.

High-pressure X-ray diffraction experiments were performed at room temperature on the BL12B2 beamline at SPring-8 synchrotron facility, Japan. For X-ray diffraction, the grained sample of $FeSe_{0.5}Te_{0.5}$ was loaded in a diamond anvil cell with at culets of diameter 450 μm and a tungsten gasket with sample chamber of diameter 150 μm. Silicon oil was used as a pressure transmitting medium. X-ray beam was collimated to 100 μm. As detector, the ADSC Quantum 210r image plate reader was set up perpendicular to the beam path. Typical accumulation time of diffraction pattern was 2 min. Cerium dioxide was used as an external standard to determine the beam centre, sample-to-detector distance, exact wavelength ($\lambda = 0.56289$ nm) and tilting angle of the image plate. Collected full-circle powder patterns were processed with FIT2D software.

Magnetic susceptibility measurements under pressure were performed using a SiC-anvil high-pressure cell made from a non-magnetic hardened Cu-Ti alloy equipped with SiC anvils. The diameter of the flat working surface of the SiC-anvil was 0.8 mm, and the diameter of the hole in the gasket was 0.3 mm. The cell allows quasihydrostatic pressures up to 12 GPa [19]. The hole was filled with the crystalline $FeSe_{0.5}Te_{0.5}$ sample and Daphne oil as a pressure transmitting medium. Pressure was measured by the Ruby scale from a small chips scattered across the sample. The pressure inhomogeneity was estimated 0.5 GPa across the sample. T_c was determined from the onset of the superconducting transition curve, i.e., from the intersection of two extrapolated straight lines drawn through the curve in the normal state and the one drawn through the steepest part of the curve in the superconducting state.

^{57}Fe-Mössbauer spectra were recorded using a constant-acceleration spectrometer and a ^{57}Co(Rh) Mössbauer source with an active spot diameter of 0.5 mm. The spectrometer was equipped with a helium bath cryostat operating in 5–300 K temperature range. The Mössbauer absorber of single crystalline $FeSe_{0.5}Te_{0.5}$ was prepared by the so-called scotch-tape technique [20], e.g., extracting thin sample layers from the crystal by a scotch tape and inserting four sample layers fixed on the tape in the absorber holder. For the Mössbauer measurements under pressure, grained ^{57}Fe-enriched (20%) $FeSe_{0.5}Te_{0.5}$ sample was loaded in a diamond anvil pressure cell with silicon oil as the pressure transmitting medium enabling quasihydrostatic pressure. The isomer shift values were quoted relative to α-Fe at 295 K.

3 Results

3.1 Mössbauer spectroscopy characterisation

Preparation of single crystal sample of $FeSe_{0.5}Te_{0.5}$ by scotch-tape technique results in a highly textured $FeSe_{0.5}Te_{0.5}$ absorber with the c axis of the tetragonal structure oriented preferentially parallel to the transmitting gamma rays. The Mössbauer spectra shown in Fig. 1 exhibit an asymmetric quadrupole doublet with an intensity ratio I_-/I_+ of about 2.1. This value allows to derive a negative sign of V_{zz}, the electric field gradient, and of the quadrupole splitting $\Delta E_Q = e^2 Q V_{zz}/2$. The derived hyperfine parameters at room temperature, isomer shift $\delta = 0.463(1)$ mm s^{-1} and $|\Delta E_Q| = 0.283(2)$ mm s^{-1}, are close to those for superconducting FeSe [21, 22] and indicate a low-spin state of divalent iron in tetrahedral chalcogen environment. The asymmetry of the quadrupole doublet arises solely from the highly textured absorber, which is strikingly demonstrated

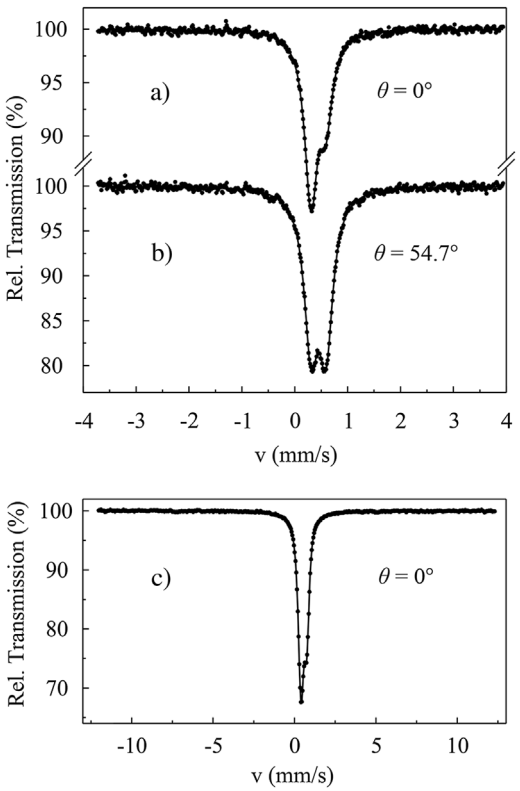

Figure 1 ^{57}Fe-Mössbauer spectra of single crystalline $FeSe_{0.5}Te_{0.5}$ acquired in transmission geometry with a wave vector of γ-rays perpendicular to the sample plane at 293 K (a) and 5 K (c); spectrum measured at magic angle $\theta = 54.7^{\circ}$ at 293 K (b).

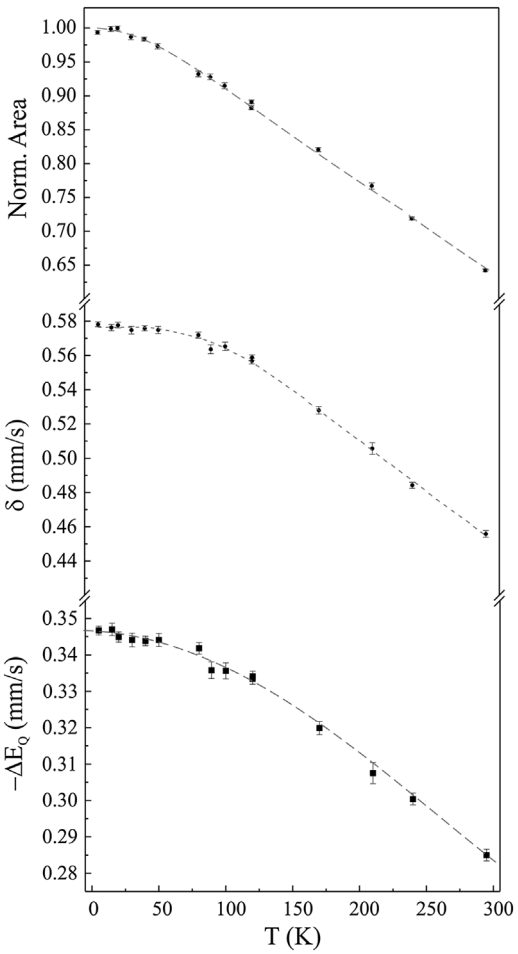

Figure 2 Temperature dependences of the normalized spectral area, δ and ΔE_Q for $FeSe_{0.5}Te_{0.5}$. Fitting details are described in the text.

by measuring the absorber tilted by 54.7°, the so-called magic angle, with respect to the gamma rays. The symmetric quadrupole doublet (Fig. 1b) exhibits an intensity ratio of 1:1, indicating absence of any impurity phases or variety of Fe sites.

The temperature-dependent spectra were measured between 5 and 295 K in the large velocity range shown in Fig. 1c and fitted with a routine using a Voigt profile (convolution of Lorentzian and Gaussian profiles) to obtain reliable values of the hyperfine parameters for the thick absorber. The derived values for the normalized spectral area, the isomer shift, δ, and the quadrupole splitting, $|\Delta E_Q|$, are plotted in Fig. 2. Experimental results do not show any feature in the vicinity of T_c and do not support any scenario of superconductivity based on anomalous softening of a phonon spectrum. The gradual decrease of δ with increasing temperature is caused by the second-order Doppler shift only and can be described by a Debye model [23]. Temperature dependence of $|\Delta E_Q|$ is also typical for iron chalcogenides and can be plausibly fitted using the simplified model for tetragonal distortion in an axial electric field [21].

3.2 Magnetic studies Figure 3 shows the temperature dependence of the normalized magnetization of

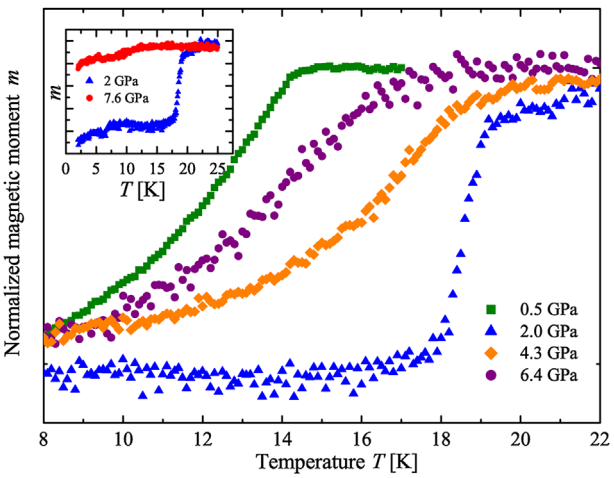

Figure 3 Selected magnetization curves of $FeSe_{0.5}Te_{0.5}$ measured at different pressures in a 20 Oe magnetic field (ZFC). Data are normalized to a maximal signal value for every pressure. At pressures above 7.6 GPa superconductivity disappears (inset).

$FeSe_{0.5}Te_{0.5}$ at various pressures in a magnetic field of 20 Oe after zero-field cooling (ZFC). A fast increase of T_c with increasing pressure is observed up to 1.3 GPa. In the pressure range of 1.3–4.8 GPa, T_c attains a value of approximately 20 K and remains essentially pressure-independent, giving rise to a distinctive plateau in the $T_c(p)$ dependence. Above 5 GPa, T_c starts to decrease reaching 17.2 K at 6.4 GPa. At 7.6 GPa, no superconductivity is observed above 2.0 K.

Comparison of the present $T_c(p)$ curve (Fig. 4) to the corresponding experimental curve obtained from resistivity measurements [10] shows that in both cases a fast increase of T_c with pressure up to 2 GPa is observed. However, this increase is more pronounced in the work of Horigane et al. [10], where maximal value of $T_{onset} = 26.2$ K is reported. The maximal value of $T_c = 19.5$ K in the present magnetization measurements is substantially lower, and a $T_c(p)$ dependence exhibits a much more flat and clear plateau. A second difference in the two studies of $FeSe_{0.5}Te_{0.5}$ is the fast disappearance of T_c above 7.6 GPa in the magnetization measurements, while from the resistivity data the loss of superconductivity is extrapolated to occur at 9.5 or 12 GPa from the T_{offset} and T_{onset} data, respectively. However, due to the small sample volume which is possible to load into the high pressure cell used for magnetization measurements it is not possible to observe small superconducting fractions of sample. The disappearance of superconductivity in our magnetization measurements looks like the disappearance of bulk superconductivity in a single crystal. Other resistivity data [8, 24] are similar to those of Ref. [10], showing a slow decrease of $T_c(p)$ dependence up to 12 GPa.

3.3 XRD studies The synchrotron X-ray powder diffraction pattern recorded at the lowest experimental pressure of 0.4 GPa and at room temperature could be indexed with a tetragonal *P*4/*nmm* lattice (anti-PbO type) with the lattice parameters $a = 3.788$ Å and $c = 5.884$ Å that is in good agreement with ambient pressure structural data [25]. The diffraction patterns indicate that tetragonal anti-PbO type structure of $FeSe_{0.5}Te_{0.5}$ remains stable at pressures below 6.5 GPa. At higher pressures, the onset of the structural phase transition occurs (Fig. 5). The presented diffraction pattern at 7.2 GPa illustrates the coexistence of the low-pressure *P*4/*nmm* phase and the high-pressure phase. The diffraction patterns of the high-pressure phase collected at 19.0 GPa can be assigned to a NiAs structure ($P6_3/mmc$), similar to the high-pressure phase in FeSe [2]. Similarly to FeSe, the phase transition is associated with significant reduction (15%) of the unit cell volume. Thus, the structural response of $FeSe_{0.5}Te_{0.5}$ on compression at room temperature observed here is identical to that of the FeSe but it differs from the phase sequence observed at low-temperature compression of $Fe_{1.03}Se_{0.57}Te_{0.43}$ [8] where pressure above ca. 3.0 GPa caused a discontinues transformation of the low-temperature orthorhombic phase into the monoclinic phase which remains stable up to 14.0 GPa.

3.4 Mössbauer studies under pressure Selected Mössbauer spectra of $FeSe_{0.5}Te_{0.5}$ at pressures up to 15.7 GPa are shown in Fig. 6. Below 5.5 GPa, a single quadrupole doublet is observed, which corresponds to the tetragonal phase. Similarly to FeSe [2], at pressure of 8.3 GPa another quadrupole doublet with $\delta = 0.51(2)$ mm s^{-1} and $|\Delta E_Q| = 0.42(3)$ mm s^{-1} appears, which should be assigned to the high-pressure hexagonal phase. The coexistence of both phases is observed up to 10.5 GPa, and at higher pressures spectra can be fitted using single

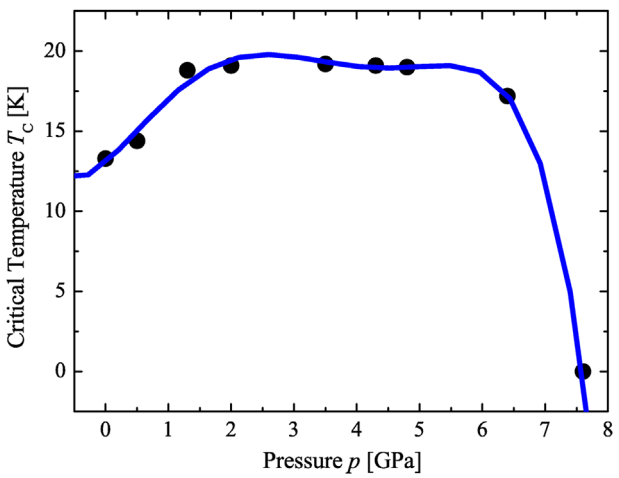

Figure 4 Pressure dependence of T_c (onset) for $FeSe_{0.5}Te_{0.5}$ obtained by magnetization measurements. Solid line is a guide to the eye.

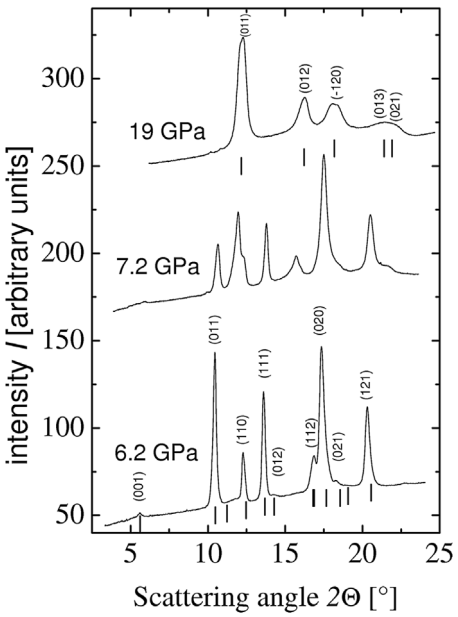

Figure 5 Room temperature synchrotron X-ray powder diffraction patterns of $FeSe_{0.5}Te_{0.5}$ recorded at 6.2 GPa (tetragonal phase), 7.2 GPa (coexisting tetragonal and hexagonal phases) and 19.0 GPa (pure hexagonal high-pressure phase).

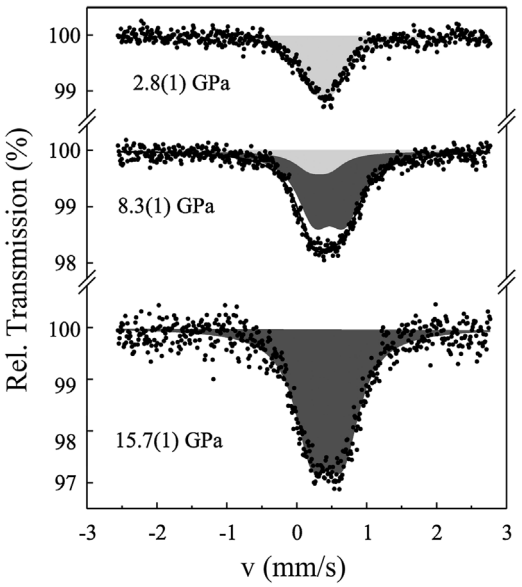

Figure 6 ^{57}Fe-Mössbauer spectra of $FeSe_{0.5}Te_{0.5}$ at 295 K measured at 2.8, 8.3 and 15.7 GPa. Light-grey shading corresponds to the tetragonal phase. The dark-grey shading indicates the doublet of the high-pressure hexagonal phase.

doublet that is consistent with the structural measurements under pressure.

Figure 7 shows the pressure dependence of the isomer shift and quadrupole splitting of iron in the tetragonal and hexagonal phases of $FeSe_{0.5}Te_{0.5}$, measured at room temperature. The rates of the hyperfine parameters changes

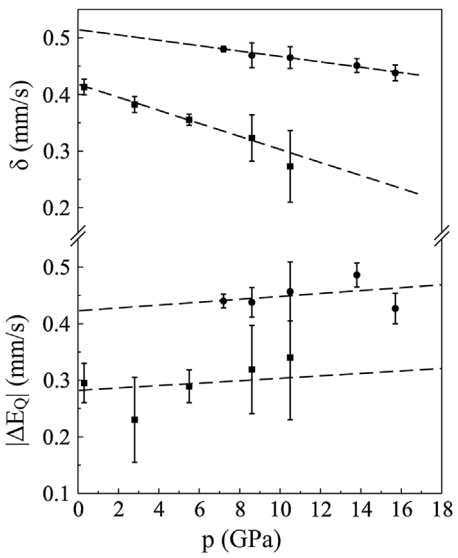

Figure 7 Pressure dependence of the isomer shifts, δ, and quadrupole splitting, $|\Delta E_Q|$, of Fe in tetragonal (closed squares) and hexagonal (closed circles) sites of $FeSe_{0.5}Te_{0.5}$ at room temperature obtained at monotonously ascending pressure. The data at 7.2 GPa, which show existence of hexagonal phase only, have been measured after releasing pressure from 15.7 GPa.

in tetragonal phase are $(\partial\delta/\partial p) = -0.011(3)$ and $(\partial\Delta E_Q/\partial p) = 0.002(1)\,\mathrm{mm\,s^{-1}\,GPa^{-1}}$. These numbers are close to the corresponding values for FeSe $(\partial\delta/\partial p) = -0.015(3)$ and $(\partial\Delta E_Q/\partial p) = 0.001(4)\,\mathrm{mm\,s^{-1}\,GPa^{-1}}$. For the hexagonal phase, pressure dependence of δ and ΔE_Q can be formally described in linear approximation by $(\partial\delta/\partial p) = -0.004(7)$ and $(\partial\Delta E_Q/\partial p) = 0.002(5)\,\mathrm{mm\,s^{-1}\,GPa^{-1}}$. The hyperfine parameters in the hexagonal phase correspond to divalent iron with less covalency comparing to the tetragonal phase similarly to FeSe [2] (Table 1).

As well as in superconducting FeSe, the distortion of the local surrounding of Fe atoms in $FeSe_{0.5}Te_{0.5}$ is higher in the high-pressure phase. A decrease of pressure exhibits a hysteresis with a width of 3.3 GPa which suggests a first-order type pressure induced structural transition. When pressure is released, the original tetragonal phase is restored without any indication of the high-pressure phase. The relatively small change of the hyperfine parameters in both tetragonal and hexagonal phases with pressure indicates a modest variation of the local surroundings of the Fe ions. A decrease in the isomer shift for both sites is observed, which corresponds to an increase in the *s*-electron density at the Fe nuclei under pressure. There are several mechanisms by which the core electron contribution $|\psi(0)|^2$ can be altered by pressure [26]. The *s*-like conduction electrons behave approximately like a free electron gas so that changes in core electron contribution should scale nearly inversely with a volume: $|\psi(0)|^2 \sim 1/V$. Summarizing Mössbauer data, the transformations seen in the spectra can be associated with a first order structural phase transition between the low-pressure tetragonal and the high-pressure hexagonal modifications of $FeSe_{0.5}Te_{0.5}$. Since superconductivity disappears above 7.6 GPa, the high-pressure phase is also stable at low temperatures, which explains the loss of superconductivity.

4 Discussion Pressure dependence of the tetragonal phase fraction obtained from Mössbauer measurements at room temperature for FeSe (closed circles) and $FeSe_{0.5}Te_{0.5}$ (open circles) together with the normalized transition temperature $T_c/T_{c,max}$ for $FeSe_{0.5}Te_{0.5}$ derived from

Table 1 Comparison of the Mössbauer parameters for $FeSe_{0.5}Te_{0.5}$ and FeSe [2, 21] in the tetragonal (t) and hexagonal (h) phases at room temperature.

parameter	$FeSe_{0.5}Te_{0.5}$	FeSe
δ_t (1 bar) [mm s^{-1}]	0.463(1)	0.450(2)
$\lvert\Delta E_Q\rvert_t$ (1 bar) [mm s^{-1}]	0.283(2)	0.245(3)
$(\partial\delta_t/\partial p)$ [mm s^{-1} GPa^{-1}]	−0.011(3)	−0.015(3)
$(\partial\Delta E_{Qt}/\partial p)$ [mm s^{-1} GPa^{-1}]	0.002(1)	0.001(4)
δ_h (8.3 GPa) [mm s^{-1}]	0.51(3)	0.58(5)
$\lvert\Delta E_Q\rvert_h$ (8.2 GPa) [mm s^{-1}]	0.42(3)	0.52(7)
$(\partial\delta_h/\partial p)$ [mm s^{-1} GPa^{-1}]	−0.004(7)	−0.005(9)
$(\partial\Delta E_{Qh}/\partial p)$ [mm s^{-1} GPa^{-1}]	0.002(5)	0.001(1)

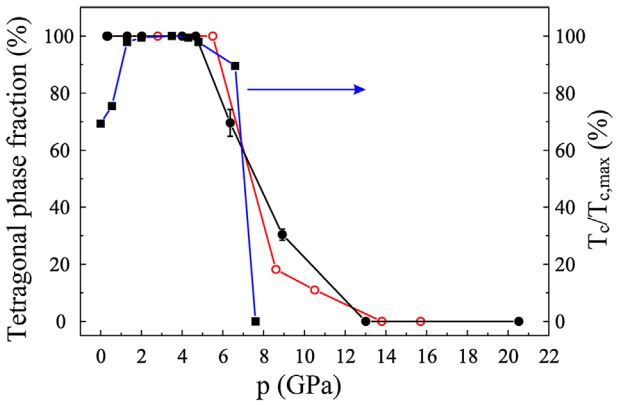

Figure 8 Pressure dependence of tetragonal phase fraction obtained from Mössbauer measurements at 295 K for FeSe [2] (closed circles) and $FeSe_{0.5}Te_{0.5}$ (open circles) together with normalized T_c for $FeSe_{0.5}Te_{0.5}$ obtained in magnetization measurements (closed squares).

magnetization measurements are presented in Fig. 8. An increase of the hexagonal phase fraction under pressure correlates with disappearance of the superconductivity in $FeSe_{0.5}Te_{0.5}$ above 8.0 GPa. Curiously, heavy doping with Te does not essentially affect a structural transformation from the tetra- to hexagonal type under pressure. Thus, Te doping cannot be considered equivalent to physical pressure, despite of the big difference in ionic radii of Se and Te. A drastic increase of T_c observed up to 1.5 GPa agrees well with previously reported data [8]. In the pressure range between 1.5 and 6.0 GPa T_c is almost pressure independent, although the lattice parameters decrease monotonously with pressure. However, in contrast to a previous study [8], pressure above 6.0 GPa applied at room temperature causes a transformation into the non-superconducting hexagonal phase.

Remarkably, neither FeSe, nor $FeSe_{0.5}Te_{0.5}$ do exhibit long-range magnetic ordering at ambient or under applied pressure in contrast to related arsenide phases [27, 28]. On the other hand, different experimental studies indicate that the superconducting pairing mechanism in FeSe and similar systems is related to magnetic fluctuations. The latter dramatically enhance under pressure leading to a strong raise of T_c in FeSe [29, 30]. In case of high quality single crystalline $FeSe_{0.5}Te_{0.5}$ reported here, T_c increases rapidly as a function of pressure ($0 < p < 2.0$ GPa) up to about its maximal value (ca. 20 K) showing similarity to FeSe. In the pressure range 2.0 GPa $< p <$ 5.0 GPa T_c remains almost constant up to its sudden drop due to the transition into the high-pressure hexagonal phase above 7.0 GPa.

5 Conclusions The pressure study of single crystalline $FeSe_{0.5}Te_{0.5}$ reveals distinct regions of $T_c(p)$ dependence presumably predetermined by miscellaneous structures. The rapid growth of T_c in the range of small pressures observed by previous studies [8] could be explained by the enhancement of magnetic fluctuations by application of pressure [29, 30]. The subsequent plateau in $T_c(p)$ dependence is fairly broad and, comparing with conductivity measurements of powder samples under pressure, could be considered more plausible. In contrast to the known pressure studies [8], we found a pressure-induced structural transformation to the hexagonal NiAs-type polymorph phase which terminates superconductivity in $FeSe_{0.5}Te_{0.5}$. Prerequisite condition of the tetragonal to hexagonal transformation is pressure application at room temperature. The first-order reversible transition has the same features as non-substituted FeSe and shows a non-equivalence of physical pressure and chemical pressure due to Te doping.

Acknowledgements This work was supported by the Deutsche Forschungsgemeinschaft (DFG) through grants KS51/2-2 and ME3652/1-2 (priority programme SPP-1458). T.P. gratefully acknowledges the support from the Polish National Science Centre within the project no. 2012/05/E/ST3/02510 (programme "SONATA BIS").

References

[1] X. Liu, L. Zhao, S. He, J. He, D. Liu, D. Mou, B. Shen, Y. Hu, J. Huang, and X. J. Zhou, J. Phys.: Condens. Matter **27**, 183201 (2015).
[2] S. Medvedev, T. McQueen, I. Troyan, T. Palasyuk, M. Eremets, R. Cava, S. Naghavi, F. Casper, V. Ksenofontov, G. Wortmann, and C. Felser, Nature Mater. **8**, 630 (2009).
[3] S. Margadonna, Y. Takabayashi, Y. Ohishi, Y. Mizuguchi, Y. Takano, T. Kagayama, T. Nakagawa, M. Takata, and K. Prassides, Phys. Rev. B **80**, 064506 (2009).
[4] T. McQueen, A. Williams, P. Stephens, J. Tao, Y. Zhu, V. Ksenofontov, F. Casper, C. Felser, and R. Cava, Phys. Rev. Lett. **103**, 57002 (2009).
[5] S.-H. Baek, D. V. Efremov, J. M. Ok, J. S. Kim, J. van den Brink, and B. Büchner, Nature Mater. **14**, 210 (2015).
[6] E. Pomjakushina, K. Conder, V. Pomjakushin, M. Bendele, and R. Khasanov, Phys. Rev. B **80**, 024517 (2009).
[7] M. Fang, H. Pham, B. Qian, T. Liu, E. Vehstedt, Y. Liu, L. Spinu, and Z. Mao, Phys. Rev. B **78**, 224503 (2008).
[8] N. Gresty, Y. Takabayashi, A. Ganin, M. McDonald, J. Claridge, D. Giap, Y. Mizuguchi, Y. Takano, T. Kagayama, Y. Ohishi, M. Takata, M. J. Rosseinsky, S. Margadonna, and K. Prassides, J. Am. Chem. Soc. **131**, 16944 (2009).
[9] L. M. Schoop, S. A. Medvedev, V. Ksenofontov, A. Williams, T. Palasyuk, I. A. Troyan, J. Schmitt, F. Casper, C. Wang, M. Eremets, R. J. Cava, and C. Felser, Phys. Rev. B **84**, 174505 (2011).
[10] K. Horigane, N. Takeshita, C.-H. Lee, H. Hiraka, and K. Yamada, J. Phys. Soc. Jpn. **78**, 063705 (2009).
[11] B. Sales, A. Sefat, M. McGuire, R. Jin, D. Mandrus, and Y. Mozharivskyj, Phys. Rev. B **79**, 094521 (2009).
[12] G. Chen, Z. Chen, J. Dong, W. Hu, G. Li, X. Zhang, P. Zheng, J. Luo, and N. Wang, Phys. Rev. B **79**, 140509 (2009).
[13] R. Khasanov, M. Bendele, A. Amato, P. Babkevich, A. Boothroyd, A. Cervellino, K. Conder, S. Gvasaliya, H. Keller, H. Klauss, H. Luetkens, V. Pomjakushin, E. Pomjakushina, and B. Roessli, Phys. Rev. B **80**, 140511 (2009).

[14] T. Taen, Y. Tsuchiya, Y. Nakajima, and T. Tamegai, Phys. Rev. B **80**, 092502 (2009).
[15] R. Hu, E. Bozin, J. Warren, and C. Petrovic, Phys. Rev. B **80**, 214514 (2009).
[16] V. Tsurkan, J. Deisenhofer, A. Günther, C. Kant, M. Klemm, H.-A. Krug von Nidda, F. Schrettle, and A. Loidl, Eur. Phys. J. B **79**, 289 (2011).
[17] V. Ksenofontov, G. Wortmann, A. Chumakov, T. Gasi, S. Medvedev, T. McQueen, R. Cava, and C. Felser, Phys. Rev. B **81**, 184510 (2010).
[18] C.-L. Huang, C.-C. Chou, K.-F. Tseng, Y.-L. Huang, F.-C. Hsu, K.-W. Yeh, M.-K. Wu, and H.-D. Yang, J. Phys. Soc. Jpn. **78**, 084710 (2009).
[19] P. Alireza and G. Lonzarich, Rev. Sci. Instrum. **80**, 023906 (2009).
[20] S. I. Shylin, V. Ksenofontov, S. A. Medvedev, V. Tsurkan, and C. Felser, J. Supercond. Nov. Magn. **28**, 1315 (2015).
[21] S. I. Shylin, V. Ksenofontov, S. J. Sedlmaier, S. J. Clarke, S. J. Cassidy, G. Wortmann, S. A. Medvedev, and C. Felser, EPL **109**, 67004 (2015).
[22] S. I. Shylin, V. Ksenofontov, S. A. Medvedev, and C. Felser, J. Supercond. Nov. Magn. **29**, 573 (2016).
[23] P. Wang, Z. M. Stadnik, J. Żukrowski, A. Thaler, S. L. Bud'ko, and P. C. Canfield, Phys. Rev. B **84** (2011) 024509.
[24] G. Tsoi, A. Stemshorn, Y. Vohra, P. Wu, F. Hsu, Y. Huang, M. Wu, K. Yeh, and S. Weir, J. Phys.: Condens. Matter **21**, 232201 (2009).
[25] M. Tegel, C. Löhnert, and D. Johrendt, Solid State Commun. **150**, 383 (2010).
[26] D. Williamson, in: Mössbauer Isomer Shifts, edited by G. Shenoy and F. Wagner (North-Holland Publishing Company, Amsterdam, 1978), p. 317.
[27] J. J. Wu, J.-F. Lin, X. C. Wang, Q. Q. Liu, J. L. Zhu, Y. M. Xiao, P. Chow, and C. Jin, Proc. Natl. Acad. Sci. USA **110**, 17263 (2013).
[28] J. J. Wu, J. F. Lin, X. C. Wang, Q. Q. Liu, J. L. Zhu, Y. M. Xiao, P. Chow, and C. Q. Jin, Sci. Rep. **4**, 3685 (2014).
[29] T. Imai, K. Ahilan, F. Ning, T. McQueen, and R. Cava, Phys. Rev. Lett. **102**, 177005 (2009).
[30] M. Bendele, A. Ichsanow, Yu. Pashkevich, L. Keller, Th. Strässle, A. Gusev, E. Pomjakushina, K. Conder, R. Khasanov, and H. Keller, Phys. Rev. B **85**, 064517 (2012).

3.4. Reprint: Phase separation in $Rb_xFe_{2-y}Se_2$ probed by nonstoichiometry and Cu-doping

Published in: Journal of Superconductivity and Novel Magnetism, 28 (2015), 1315.

Personal contribution: Mössbauer measurements (Figs. 1-4), treatment of the spectra, and the preparation of the manuscript were done by the author personally.

[redacted] designed the study, supervised the work, participated in the Mössbauer measurements (Figs. 1-4), and contributed to writing the manuscript.

[redacted] synthesized and analyzed (EPMA) the samples.

[redacted] participated in the discussion of Mössbauer data.

[redacted] co-supervised the work.

J Supercond Nov Magn (2015) 28:1315–1319
DOI 10.1007/s10948-014-2912-6

ORIGINAL PAPER

Phase Separation in $Rb_xFe_{2-y}Se_2$ Probed by Non-stoichiometry and Cu Doping

Sergii I. Shylin · Vadim Ksenofontov · Sergey A. Medvedev · Vladimir Tsurkan · Claudia Felser

Received: 31 July 2014 / Accepted: 12 November 2014 / Published online: 16 December 2014

Abstract The paper presents Mössbauer spectroscopy investigation on superconducting $Rb_{0.8}Fe_{1.6}Se_2$ exhibiting nanoscale phase separation and two its derivatives: Cu-doped $Rb_{0.8}Fe_{1.56}Cu_{0.04}Se_2$ and Fe-deficient $Rb_{0.7}Fe_{1.4}Se_2$. The spectra reveal the presence of the same dominant magnetic sextet in the samples, which is assigned to the Fe 16*i* sites of the $\sqrt{5} \times \sqrt{5} \times 1$ superstructure. This magnetic part is independent on the modification of the sample and does not undergo any changes after doping or deviation of stoichiometry. In contrast, the minor non-magnetic doublet in the spectra of $Rb_{0.8}Fe_{1.6}Se_2$, which is attributed to the superconducting nanoscale phase, is sensitive to such modifications. After doping with Cu, the relative intensity of non-magnetic doublet significantly decreases together with suppression of superconductivity. On the other hand, the Fe-deficient sample is entirely magnetically ordered below 250 K including in the minor nanoscale phase. A discussion of Mössbauer spectroscopic data and comparison with previous studies on other Fe chalcogenide analogues allow to conclude the nanosized phase separation is also observed in non-stoichiometric and doped modifications of $Rb_{0.8}Fe_{1.6}Se_2$.

Keywords Mössbauer spectroscopy · $Rb_{0.8}Fe_{1.6}Se_2$ · Cu doping · Phase separation

S. I. Shylin · V. Ksenofontov (✉)
Institute of Inorganic and Analytical Chemistry, Johannes Gutenberg-University Mainz, D-55099 Mainz, Germany
e-mail: ksenofon@uni-mainz.de

S. I. Shylin
Department of Chemistry, Taras Shevchenko National University of Kyiv, Volodymyrska 64, Kyiv 01601, Ukraine

S. A. Medvedev · C. Felser
Max Planck Institute for Chemical Physics of Solids, D-01187 Dresden, Germany

V. Tsurkan
Experimental Physics V, University of Augsburg, D-86159 Augsburg, Germany

V. Tsurkan
Institute of Applied Physics, Academy of Sciences, MD-2028, Chişinău, Republic of Moldova

1 Introduction

Layered iron chalcogenides show great potential in achieving high superconducting transition temperature. A parent compound, β-FeSe, and related Te-substituted systems with the simplest structure, consisting of FeX (X = Se, Te) layers only, exhibit a relatively low values from 8 K [1] to 13 K [2]. However, a significant increase of T_c up to 37 K has been observed for β-FeSe under pressure of ∼9 GPa [3]. The extreme sensitivity of T_c to stoichiometry in this compound has previously been demonstrated showing an influence of the magnetic defects on superconductivity [4]. No static magnetism has been observed, whereas ^{77}Se NMR studies have provided evidence for spin fluctuations [5] that are believed to play a role in the pairing mechanism [6]. Later, superconductivity in β-FeSe has been shown to be completely suppressed by various dopants at the level of only a few percent [7, 8]. Thus, the addition of very small amounts of Cu into the structure significantly has lowered T_c and even at the 3 % doping level no evidence for superconductivity has been seen. The Mössbauer measurements of the $Fe_{1.01-x}Cu_xSe$ series have implied the presence of slow magnetic fluctuations or glassy state in the system [8]. However, L. M. Schoop et al. have reported the restoration

of superconductivity in Cu-doped β-FeSe under pressure pointing to suppression of local magnetic moments [9].

The discovery of high-T_c superconductivity in chalcogenide compounds of $ThCr_2Si_2$ structure type with general formula of $A_xFe_{2-y}Se_2$ ($A = K^+$ [10], Rb^+ [11], Cs^+ [12]) at ambient pressure has been an exciting breakthrough. Due to a coexistence of superconductivity and antiferromagnetic (AFM) ordering, this family has been of a particular scientific interest. By means of scanning tunneling microscopy [13], high-resolution nanofused X-ray diffraction [14] and optical conductivity measurements [15], it has been shown that superconductivity and magnetism occur in spatially separated regions in the same crystal structure. Nanoscale phase separation in $Rb_{0.8}Fe_{1.6}Se_2$ has been also probed by Mössbauer measurements yielding the presence of both magnetic sextet (88 %) and non-magnetic quadrupole doublet (12 %) [16], whilst specific-heat measurements have revealed a superconducting volume fraction above 90 % [17]. Hereafter, we have shown that under pressure, $Rb_{0.8}Fe_{1.6}Se_2$ remains superconducting until a perfect order of the AFM matrix is suppressed [18]. Emergence of non-compensated magnetic moments of about 3 μ_B caused by pressure application has led to appearance of huge transferred magnetic fields destroying superconducting pairing in FeSe-like nanoscale phase. This observation has motivated the idea to tune superconducting properties implementing magnetic defects into the AFM phase. As described above, such defects may be due to transition metal doping or stoichiometry deviation in FeSe-like nanoscale phase. In this paper, we report detailed Mössbauer spectroscopic studies of $Rb_{0.8}Fe_{1.6}Se_2$ and two its derivatives: Cu-doped $Rb_{0.8}Fe_{1.56}Cu_{0.04}Se_2$ and Fe-deficient $Rb_{0.7}Fe_{1.4}Se_2$.

2 Experimental Details

Single crystals of $Rb_{0.8}Fe_{1.6}Se_2$ (**1**), $Rb_{0.7}Fe_{1.4}Se_2$ (**2**) and $Rb_{0.8}Fe_{1.56}Cu_{0.04}Se_2$ (**3**) were grown employing the Bridgman method. The detailed preparation conditions for **1** and **2** have been discussed elsewhere [17]. For preparation of **3**, polycrystalline FeSe synthesized from the high-purity elements (99.98 % Fe and 99.999 % Se), 99.75 % Rb and 99.998 % Cu were used as starting materials. Handling of the reaction mixture was done in a glow box with residual oxygen and water content less than 1 ppm. Single crystals of **3** were obtained by heating the mixture to 1343 K, soaking for 3 h and cooling at rate of 6 K/h. The composition of the grown sample was determined by electron probe microanalyses (EPMA) using a Cameca SX50 analyser. The concentrations of Rb, Fe and Cu elements were normalized assuming a Se concentration of two per formula unit and presented in Table 1. The single-phase composition of **3** was confirmed by X-ray powder diffraction conducted on crushed single crystals using a STOE Stadi P diffractometer with Cu Kα radiation. Direct current magnetic susceptibility measurements were made using the Quantum Design SQUID magnetometer.

^{57}Fe-Mössbauer spectra were recorded in transmission geometry with a ^{57}Co(Rh) source using a conventional constant-acceleration Mössbauer spectrometer equipped with a nitrogen/helium bath cryostat. Isomer shifts are given relatively to the α-Fe foil at ambient temperature. Simulations of the experimental data were performed with the Recoil software [9]. The absorbers of **1** and **3** were prepared by crushing small pieces of single crystals under strictly inert conditions and placing the powder between acryl platelets of the sealed sample holder. Therefore, Mössbauer spectra of **1** and **3** reveal the textured nature of the absorbers due to preferred orientation of microcrystals in the holder. The absorber of **2** was prepared by attaching thin single-crystalline flakes, separated from the bulk single crystals by the so-called scotch-tape technique. This yielded a mosaic crystal samples with the crystalline c-axis oriented perpendicular to the absorber plane and a and b axes oriented randomly within the absorber plane.

3 Results and Discussion

Mössbauer spectrum of **1** recorded at 227 K is presented in Fig. 1. The spectrum consists of a dominant magnetic sextet with 88(1) % spectral intensity of the Fe sites and of a non-magnetic quadrupole doublet with 12(1) % intensity. The hyperfine parameters of both sites ($\delta = 0.65(1)$ mm/s, $\Delta E_Q = +1.10(2)$ mm/s, $B_{hf} = 268.5(1)$ kOe for sextet; $\delta = 0.62(1)$ mm/s, $\Delta E_Q = -0.27(2)$ mm/s for doublet) are

Table 1 EPMA data for $Rb_{1-x}Fe_{2-y-z}Cu_zSe_2$. The composition of **1** and **2** is given according to [17]

Sample	Content of the element			
	Rb (1−x)	Fe (2−y − z)	Cu (z)	Se
1	0.80(3)	1.600(8)	–	2.00(3)
2	0.73(2)	1.43(2)	–	2.00(3)
3	0.80(3)	1.560(3)	0.040(2)	2.00(3)

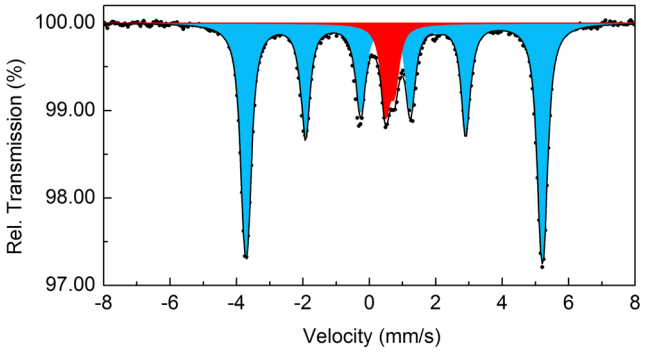

Fig. 1 Mössbauer spectrum of **1** at 227 K showing magnetic (sextet) and non-magnetic (doublet) Fe sites in final fit

close to those at 4.2 K reported in our previous communication [16]. As described therein, the magnetic subspectrum corresponds to AFM matrix where Fe atoms occupy 16*i* sites of the $\sqrt{5} \times \sqrt{5} \times 1$ phase. The non-magnetic subspectrum may be assigned either to the formally empty 4*d* sites of the $\sqrt{5} \times \sqrt{5} \times 1$ superstructure or to the non-magnetic minority phase, detected in $A_xFe_{1-y}Se_2$ superconductors by means of other techniques [13–15]. However, the most likely scenario for existing of magnetic and non-magnetic parts is that nanoscale phase separation in FeSe intercalated with Rb takes place indeed [20]. Thus, a well-resolved hyperfine spectrum of powdered **1** at 227 K with a dominant magnetic site and a non-magnetic site indicates the presence of two nanoscale phases. The magnetic sites can by perfectly adjusted by a fit analysis of Fe^{2+} ions with a non-collinear magnetic-dipole and electric quadrupole interactions. The spectrum of the textured absorber proves the orientation of the moments parallel to the crystalline *c*-axis. Whereas the AFM matrix is not superconducting, the non-magnetic Fe sites exhibiting a quadrupole doublet corresponds to the superconducting nanoscale phase [16].

Figure 2 demonstrates the Mössbauer spectrum of **3** at 180 K. The spectrum consists of the same subspectra as the non-doped specimen with close hyperfine parameters ($\delta = 0.63(3)$ mm/s, $\Delta E_Q = +1.10(3)$ mm/s, $B_{hf} = 271.7(1)$ kOe for sextet; $\delta = 0.57(3)$ mm/s, $\Delta E_Q x = -0.30(3)$ mm/s for doublet). It shows a clear evidence for a strong texture by a deviation of the line intensity ratios of the magnetic subspectra from 3:2:1:1:2:3 and of the quadrupole doublet from a 1:1 ratio as expected for a fully homogenized polycrystalline absorber. However, the relation between fractions of a magnetic sextet and non-magnetic doublet is dramatically changed in comparison with **1**. After Cu doping, the amount of Fe sites in the AFM matrix increases to 95(1) %, whereas a quadrupole doublet is only 5(1) % of total amount of Fe sites. These changes indicate that Cu substitutes Fe preferably in the non-magnetic nanoscale phase but not in the AFM $\sqrt{5} \times \sqrt{5} \times 1$ phase. Due to substitution of Fe in the phase being responsible for superconductivity, the superconducting properties of the sample are expected to be hindered. Indeed, magnetic susceptibility measurements for **3** corroborate Mössbauer data, and no evidence for superconductivity is observed above 2 K. It is evident that the introduction of copper into the non-magnetic nanoscale phase introduces local magnetic moments and, consequently, destroys superconductivity. In this regard, Cu

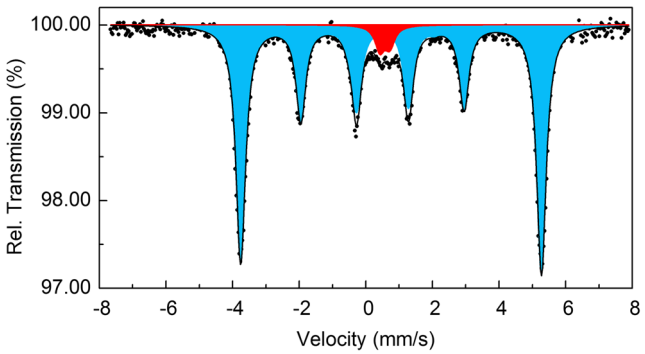

Fig. 2 Mössbauer spectrum of **3** at 180 K showing magnetic (sextet) and non-magnetic (doublet) Fe sites in final fit

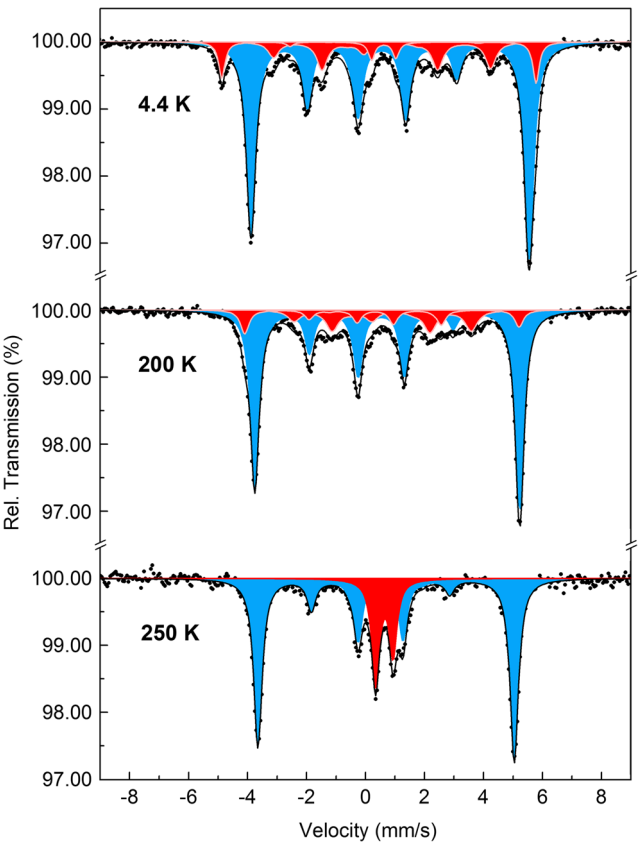

Fig. 3 Selected Mössbauer spectra of **2** showing magnetic ordering between 200 and 250 K

doping in FeSe-like nanophase in **3** has the same effect on superconducting properties as in β-FeSe [8].

In Fig. 3, Mössbauer spectra of Fe-deficient sample, **2**, at different temperatures are presented. At low temperature, the spectrum can be fitted with three magnetic sextets using a model of a mosaic absorber. The spectrum provides direct information about the high degree of orientation of Fe magnetic moments of the magnetic phase relative the crystallographic *c*-axis. This, for instance, is evidenced by the strongly reduced intensities of the lines 2 and 5 in the dominant subspectrum. The main sextet (site 1) has the same hyperfine parameters ($\delta = 0.69(1)$ mm/s, $\Delta E_q = +1.22(2)$ mm/s, $B_{hf} = 281.4(2)$ kOe) as main sextets observed for **1** and **3** and corresponds to the Fe^{2+} 16*i* sites in AFM matrix. Similar to **1**, a pronounced difference in the intensities of lines of magnetic sextets is caused by complex non-collinear quadrupole and magnetic hyperfine interactions.

The behaviour of B_{hf} for **2** is presented in Fig. 4. Upon heating up to 250 K, two minor sextets with relative intensities 15(2) % (site 2) and 11(2) % (site 3) transform into a quadrupole doublet with $\delta = 0.64(1)$ mm/s and $\Delta E_Q = 0.60(2)$ mm/s. Asymmetry of lines of the quadrupole doublet reflects, on the one hand, the mosaic structure of the absorber. On the other hand, similar to FeSe-like nanophase in **1**, this fact proves that corresponding Fe sites are incorporated together with the AFM matrix in the same crystal structure. It has been reported that Fe-deficient $Rb_xFe_{2-y}Se_2$ compound exhibit an unusual behaviour of its properties between 220 and 240 K [17]. The specific heat measurements have shown a sharp peak at 220 K; a small but clearly discernible anomaly has been observed on resistivity curves at 230–240 K and magnetic susceptibility measurements have shown a non-monotonic temperature dependence with a broad maximum at around 233 K [17]. Although it has been supposed that these anomalies have not been related to conventional AFM or FM transitions, Mössbauer spectra indicate a magnetic ordering in **2** between 200 and 250 K. Taking into account close but not equal intensities of two minor sextets, one can suppose the ferromagnetic type of ordering in the minority phase below 250 K. Relative intensity of the quadrupole doublet at 250 K is 24(2) %. At the same time, from the chemical composition of **2**, the formal amount of Fe^{3+} can be found as 28(5) %. We believe that the transforming part of the Mössbauer spectra correspond to Fe^{3+} sites exhibiting magnetic transition, whilst Fe^{2+} sites of the main AFM matrix showing magnetic stability appear as a dominant sextet. Considering that the main sextet is not sensitive to a deficit of Fe and can be fitted with the hyperfine parameters found for **1** and **3**, Fe^{3+} occupies positions in minor nanoscale phase but not in the main matrix as defects. Comparing with stoichiometric **1**, Fe-deficient **2** at low temperature reveals no non-magnetic Fe species and is entirely magnetically ordered. Therefore, **2** should not and does not exhibit superconductivity.

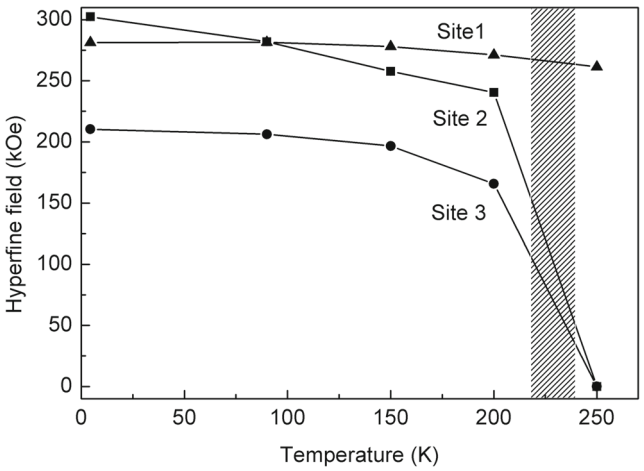

Fig. 4 Temperature dependence of the hyperfine fields for the dominant sextet (site 1) and the minor sextets (sites 2 and 3) of **2**. The temperature region (according to [17]) of magnetic ordering is *shaded*

4 Conclusion

^{57}Fe-Mössbauer measurements of powdered $Rb_{0.8}Fe_{1.56}Cu_{0.04}Se_2$ and single-crystalline $Rb_{0.7}Fe_{1.4}Se_2$ samples exhibit well-resolved hyperfine spectra consisting of a dominant AFM site and minor non-magnetic or magnetic sites. Correspondingly, in both cases the main sextet having the same parameters as a parent compound $Rb_{0.8}Fe_{1.6}Se_2$ corresponds to AFM matrix, which may be considered as a main nanoscale phase. This phase is formed independently on Cu doping or deviation of the stoichiometry of Fe ("Fe^{3+} doping"). At the same time, the minor non-magnetic Fe site of $Rb_{0.8}Fe_{1.6}Se_2$, which is assigned to superconducting nanoscale phase, is very sensitive to modification. Cu^{2+} or Fe^{3+} substitutes Fe^{2+} in non-magnetic FeSe-like nanophase that leads to decrease of Fe population or induces magnetic ordering, respectively. In both cases, it suppresses superconductivity although nanoscale phase separation into AFM matrix and minor phase presumably is conserved.

Acknowledgments The financial support provided by the Deutsche Forschungsgemeinschaft (DFG) through grants No. KS51/2-2 and ME3652/1-2 (priority program SPP-1458) is gratefully acknowledged.

Conflict of Interest The authors declare that they have no conflict of interest.

References

1. Hsu, F.C., Luo, J.Y., Yeh, K.W., Chen, T.K., Huang, T.W., Wu, P.M., Lee, Y.C., Huang, Y.L., Chu, Y.Y., Yan, D.C., Wu, M.-K.: Superconductivity in the PbO-type structure α-FeSe. Proc. Natl. Acad. Sci. **105**, 14262–14264 (2008)
2. Gómez, R.W., Marquina, V., Pérez-Mazariego, J.L., Escamilla, R., Escudero, R., Quintana, M., Hernández-Gómez, J.J., Ridaura, R., Marquina, M.L.: Effects of substituting Se with Te in the FeSe compound: structural, magnetization and Mössbauer studies. J. Supercond. Nov. Magn. **23**, 551–557 (2010)
3. Medvedev, S., McQueen, T.M., Troyan, I.A., Palasyuk, T., Eremets, M.I., Cava, R.J., Naghavi1, S., Casper1, F., Ksenofontov, V., Wortmann, G., Felser, C.: Electronic and magnetic phase diagram of β-$Fe_{1.01}Se$ with superconductivity at 36.7 K under pressure. Nat. Mater. **8**, 630–633 (2009)
4. McQueen, T.M., Huang, Q., Ksenofontov, V., Felser, C., Xu, Q., Zandbergen, H., Hor, Y.S., Allred, J., Williams, A.J., Qu, D., Checkelsky, J., Ong, N.P., Cava, R.J.: Extreme sensitivity of superconductivity to stoichiometry in $Fe_{1+\delta}Se$. Phys. Rev. B **79**, 014522 (2009)
5. Imai, T., Ahilan, K., Ning, F.L., McQueen, T.M., Cava, R.J.: Why does undopped FeSe become a high-T_c superconductor under pressure? Phys. Rev. Lett. **102**, 177005 (2009)
6. Scalapino, D.J.: A common thread: the pairing interaction for unconventional superconductors. Rev. Mod. Phys. **84**, 1383–1417 (2012)
7. Mizuguchi, Y., Tomioka, F., Tsuda, S., Yamaguchi, T., Takano, Y.: Substitution effects on FeSe superconductor. J. Phys. Soc. Jpn. **78**, 074712 (2009)
8. Williams, A.J., McQueen, T.M., Ksenofontov, V., Felser, C., Cava, R.J.: The metal-insulator transition in $Fe_{1.01-x}Cu_xSe$. J. Phys.: Condens. Matter **21**, 305701 (2009)
9. Schoop, L.M., Medvedev, S.A., Ksenofontov, V., Williams, A., Palasyuk, T., Troyan, I.A., Schmitt, J., Casper, F., Wang, C., Eremets, M., Cava, R.J., Felser, C.: Pressure-restored superconductivity in Cu-substituted FeSe. Phys. Rev. B **84**, 174505 (2011)
10. Guo, J., Jin, S., Wang, G., Wang, S., Zhu, K., Zhou, T., He, M., Chen, X.: Superconductivity in the iron selenide $K_xFe_2Se_2$ ($0 \leq x \leq 1.0$). Phys. Rev. B **82**, 180520 (2010)
11. Wang, A.F., Ying, J.J., Yan, Y.J., Liu, R.H., Luo, X.G., Li, Z.Y., Wang, X.F., Zhang, M., Ye, G.J., Cheng, P., Xiang, Z.J., Chen, X.H.: Superconductivity at 32 K in single-crystalline $Rb_xFe_{2-y}Se_2$. Phys. Rev. B **83**, 060512 (2011)
12. Krzton-Maziopa, A., Shermadini, Z., Pomjakushina, E., Pomjakushin, V.Yu., Bendele, M., Amato, A., Khasanov, R., Luetkens, H., Conder, K.: Synthesis and crystal growth of $Cs_{0.8}(FeSe_{0.98})_2$: a new iron-based superconductor with $T_c = 27$ K. J. Phys.: Condens. Matter **23**, 052203 (2011)
13. Li, W., Ding, H., Deng, P., Chang, K., Song, C., He, K., Wang, L., Ma, X., Hu, J.-P., Chen, X., Xue, Q.-K.: Phase separation and magnetic order in K-doped iron selenide superconductor. Nat. Phys. **8**, 126–130 (2012)
14. Ricci, A., Poccia, N., Campi, G., Joseph, B., Arrighetti, G., Barba, L., Reynolds, M., Burghammer, M., Takeya, H., Mizuguchi, Y., Takano, Y., Colapietro, M., Saini, N.L., Bianconi, A.: Nanoscale phase separation in the iron chalcogenide superconductor $K_{0.8}Fe_{1.6}Se_2$ as seen via scanning nanofocused x-ray diffraction. Phys. Rev. B **84**, 060511 (2011)
15. Charnukha, A., Deisenhofer, J., Pröpper, D., Schmidt, M., Wang, Z., Goncharov, Y., Yaresko, A.N., Tsurkan, V., Keimer, B., Loidl, A., Boris, A.V.: Optical conductivity of superconducting $Rb_2Fe_4Se_5$ single crystals. Phys. Rev. B **85**, 100504 (2012)
16. Ksenofontov, V., Wortmann, G., Medvedev, S.A., Tsurkan, V., Deisenhofer, J., Loidl, A., Felser, C.: Phase separation in superconducting and antiferromagnetic $Rb_{0.8}Fe_{1.6}Se_2$ probed by Mössbauer spectroscopy. Phys. Rev. B **84**, 180508 (2011)
17. Tsurkan, V., Deisenhofer, J., Günther, A., Krug von Nidda, H.-A., Widmann, S., Loidl, A.: Anisotropic magnetism, superconductivity, and the phase diagram of $Rb_{1-x}Fe_{2-y}Se_2$. Phys. Rev. B **84**, 144520 (2011)
18. Ksenofontov, V., Medvedev, S.A., Schoop, L.M., Wortmann, G., Palasyuk, T., Tsurkan, V., Deisenhofer, J., Loidl, A., Felser, C.: Phys. Rev. B **85**, 214519 (2012)
19. Lagarec, K., Rancourt, D.G.: Extended Voigt-based analytic lineshape method for determining N-dimensional correlated hyperfine parameter distributions in Mössbauer spectroscopy. Nucl. Instrum. Methods Phys. Res. B **129**, 266–280 (1997)
20. Texier, Y., Deisenhofer, J., Tsurkan, V., Loidl, A., Inosov, D.S., Friemel, G., Bobroff, J.: NMR Study in the Iron-Selenide $Rb_{0.74}Fe_{1.6}Se_2$: Determination of the Superconducting Phase as Iron Vacancy-Free $Rb_{0.3}Fe_2Se_2$. Phys. Rev. Lett. **108**, 237002 (2012)

3.5. Reprint: Correlation between T_c and hyperfine parameters of Fe in layered chalcogenide superconductors

Published in: Journal of Superconductivity and Novel Magnetism, 29 (2016), 573.

Personal contribution: Mössbauer measurements (Figs. 2-4), treatment of the spectra, and the preparation of the manuscript (incl. Fig. 1) were done by the author personally.

[redacted] designed the study, supervised the work, participated in the Mössbauer measurements (Figs. 2-4), and contributed to writing the manuscript.

[redacted] participated in the discussion of Mössbauer data.

[redacted] co-supervised the work.

J Supercond Nov Magn (2016) 29:573–576
DOI 10.1007/s10948-015-3299-8

ORIGINAL PAPER

Correlation Between T_c and Hyperfine Parameters of Fe in Layered Chalcogenide Superconductors

Sergii I. Shylin[1,2] · Vadim Ksenofontov[1] · Sergey A. Medvedev[3] · Claudia Felser[3]

Received: 10 October 2015 / Accepted: 19 November 2015 / Published online: 19 December 2015

Abstract Although pairing mechanism in unconventional superconductors is still an open question, the density of states at the Fermi level is considered to be one of the factors affecting the superconducting transition temperature. Herein, we report on ^{57}Fe-Mössbauer studies of β-FeSe, $FeSe_{0.5}Te_{0.5}$, and $Rb_{0.8}Fe_{1.6}Se_2$ superconductors as well as two intercalate products consisting of FeSe layers and a lithium-containing molecular spacer in between. In these materials, the hyperfine parameters of ^{57}Fe are directly related to the 3*d*-electron density on Fe atoms and show strong correlation with superconducting properties.

Keywords Mössbauer spectroscopy · Superconductivity · FeSe · Electron doping

1 Introduction

The recent unprecedented discovery of metallic H_2S to be a conventional superconductor with $T_{onset} = 203$ K under pressure has initiated an intensive debate regarding the origin of such a high transition temperature [1]. It has become apparent that there are no formal boundaries of T_c; thereby, room temperature superconductivity may be achieved in favorable conditions. The latest include a high electron density at the Fermi level, a strong electron-phonon coupling, high frequency of phonons, and magnetic fluctuations. In this regard, iron chalcogenides that constitute a relatively novel family of unconventional superconductors have been of a special interest since Hsu et al. have found superconductivity in FeSe [2]. Later on, high-T_c superconductivity in FeSe has been reached under pressure [3] suggesting a key role of spin fluctuations in superconducting pairing mechanism [4]. Half substitution of Se by electron-rich Te in this compound has led to an increase of T_c from 8.5 to 14.5 K at ambient pressure [5]. The superconducting properties of FeSe have been also improved by implementing different cationic spacers between FeSe layers (Fig. 1). Thus, alkali metal ions providing additional electron density at FeSe layers increase T_c up to 32 K in $A_xFe_{2-\delta}Se_2$ (A = K, Rb, Cs) [6]. The general feature of these materials is a complex phase separation, i.e., only the minor non-magnetic FeSe-like phase is responsible for superconductivity. The nanoscale phase separation in $Rb_{0.8}Fe_{1.6}Se_2$ has been probed by Mössbauer spectroscopy [7], high-resolution nanofused X-ray diffraction [8], Cu-doping [9], etc. Under external pressure, it remains superconducting until a perfect antiferromagnetic order in the magnetic phase is suppressed and non-compensated magnetic moments of ca. $3\mu_B$ appear [10].

Another elegant way to improve superconducting properties of FeSe has been an ammonothermal intercalation method. Burrard-Lucas et al. have obtained $Li_x(NH_2)_y(NH_3)_{1-y}Fe_2Se_2$ ($x = 0.6$; $y = 0.2$) containing Li^+, NH_2^- ions, and NH_3 molecules acting as the spacer between FeSe layers, which exhibits bulk superconductivity below 43 K [11]. Hereafter, 45 K superconductivity

✉ Vadim Ksenofontov
ksenofon@uni-mainz.de

1 Institute of Inorganic and Analytical Chemistry, Johannes Gutenberg-University Mainz, 55099 Mainz, Germany

2 Department of Chemistry, Taras Shevchenko National University of Kyiv, Volodymyrska 64/13, 01601 Kyiv, Ukraine

3 Max Planck Institute for Chemical Physics of Solids, 01187 Dresden, Germany

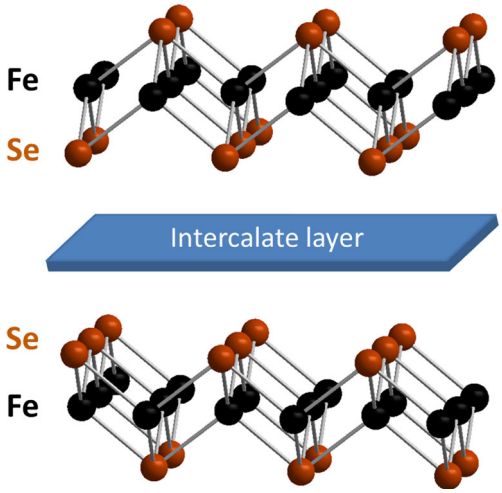

Fig. 1 Schematic representation of the structure of FeSe layered superconductors

has been reported for FeSe intercalated with pyridine [12] and ethylenediamine [13]. The recent theoretical considerations have shown that such an enhancement of T_c in the ammonia intercalate of FeSe is due to both magnetic fluctuations and electron doping [14]. The latter moves the Fermi level towards the edge of the hole bands increasing density of states (DOS) and, consequently, T_c. Bearing in mind that the conduction band at the Fermi level is formed by outer orbitals of Fe, Mössbauer spectroscopy that provides direct information about electron density on Fe atoms [15] can be an informative method to study Fe-based superconductors. In this paper, we discuss the correlation between isomer shift and quadrupole splitting, which quantify the electron density on Fe atoms, and T_c for FeSe and its derivatives.

2 Materials and Methods

The sample of a parent superconductor β-FeSe (1) was synthesized by heating a stoichiometric mixture of Fe and Se as described elsewhere [16]. The high-T_c intercalate superconductor $Li_x(NH_{3-\delta})_yFe_2Se_2$ (2) was synthesized from β-FeSe, Li, and NH_3 using ammonothermal procedure [11]. After the gentle hydrolysis treatment of 2, sample 3 was obtained and structurally characterized [17]. Starting with Fe, Se, and Te, single crystals of $FeSe_{0.5}Te_{0.5}$ (4) superconductor were grown by a Bridgman method as described by Tsurkan et al. [5]. The same technique was applied for the synthesis of $Rb_{0.8}Fe_{1.6.}Se_2$ single crystals (5) from β-FeSe and Rb [9].

^{57}Fe-Mössbauer spectra were recorded in transmission geometry with a ^{57}Co(Rh) source using a constant-acceleration Mössbauer spectrometer equipped with a bath cryostat at 85 K (samples 1, 2, 5) and at 80 K (samples 3, 4). Isomer shifts are given relatively to α-Fe at 295 K. The absorbers of 1–3 were prepared by placing the powdered samples (around 30 mg each) in sealed acryl sample holders. Absorbers of 4 and 5 were prepared by attaching thin single-crystalline flakes, separated from the bulk single crystals by the scotch-tape technique. All the sample preparation procedures were performed in an argon glove box with an O_2 and H_2O content below 0.5 ppm.

3 Results and Discussion

Mössbauer spectra of pure FeSe (1), its lithium/ammonia intercalate (2), a product of a mild hydrolysis treatment (3), and $FeSe_{0.5}Te_{0.5}$ (4) are presented in Fig. 2. The spectra show single doublets with relatively small line width of about 0.17–0.18 mm s^{-1} that confirms purity of the samples and the presence of only one Fe site in the structures. The parent compound of this family, FeSe, exhibiting the lowest $T_c = 8.5$ K has the isomer shift $\delta = 0.563(2)$ mm s^{-1} that is close to the values reported by Mizuguchi et al. [18]. After intercalation of 1 with Li^+ ions and ammonia leading to significant enhancement of superconducting transition temperature, δ increases up to 0.647(3) mm s^{-1} in 2. According to its composition $Li_x(NH_{3-\delta})_yFe_2Se_2$ [11], the positive charge of Li^+ ions is not fully compensated by NH_2^- anions; thereby, the interlayer spacer donates electron density to the FeSe layer, i.e., to 3d-orbitals of Fe. Due to the shielding, the effective s-electron density on Fe nuclei decreases that leads to an increase of δ. On the other hand, Guterding et al. point out that in FeSe the DOS near the Fermi level increases concomitantly with electron doping for d_{xy} and $d_{xz/yz}$ orbitals [14]. One can assume that the increased δ indicates an enhanced density on the Fermi level N_0 as a consequence of lithium/ammonia intercalation.

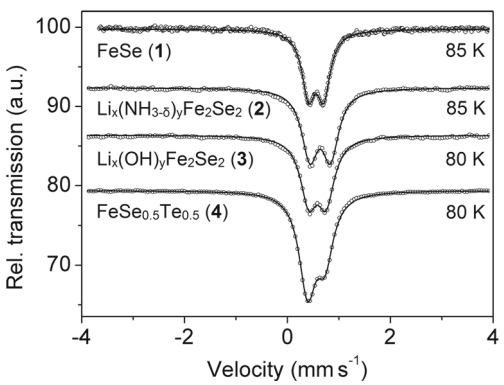

Fig. 2 Mössbauer spectra of *1–4*

It leads to improving superconducting properties as given below (V describes the interaction between the electrons and Θ_D is Debye temperature):

$$T_c \cong \Theta_D \cdot e^{-\frac{1}{N_0 V}}.$$

To verify this suggestion, we have modified the composition of the intercalate by an exposure the sample to moist helium gas. The obtained sample 3 comprises FeSe layers and modified spacer containing Li^+ ions in between. It is superconducting below 12 K and similarly to 2 shows the Li^+ ionic motion above 240 K [17]. At the same time, δ of 3 at 80 K is found to be 0.583(3) mm s^{-1} that is much closer to pure FeSe in comparison with the high-T_c intercalate 2. One can conclude that after 2 has been converted to 3, electron donor ability of the interlayer spacer is decreased due to either introduction of anions, which compensate the positive charge of Li^+ ions, or partial elimination of cations. In this regard, further studies on the composition of intercalate layers in 3 are required.

The spectrum of 4 reflects the so-called mosaic crystal type of the absorber, where the c crystalline axis being parallel to the direction of γ-rays is oriented perpendicular to the absorber plane and the a and b axes randomly lie within the sample plane. The quadrupole doublet of 4 exhibits asymmetry with an intensity ratio $I_-/I_+ =$ ca. 2.0. This allows to define the sign of quadrupole splitting to be negative. The isomer shift derived at 80 K is 0.568(3) mm s^{-1}, slightly higher than δ for 1. Although this difference is within the error, it may indicate an increase of 3d-electron density at Fe atoms via partial substitution of Se by less electronegative Te. However, one should admit that an increase of T_c up to 14.5 K may be not only due to electron doping but chemical pressure as well.

Figure 3 depicts the Mössbauer spectrum of 5 acquired in the high velocity range. The spectrum consists of a dominant magnetic sextet with 87.5(9) % intensity of the Fe sites and of a non-magnetic quadrupole doublet with 12.5(5)

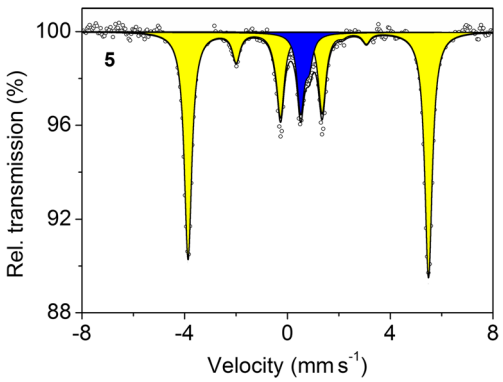

Fig. 3 Mössbauer spectrum of *5* at 85 K showing quadrupole doublet of the minor superconducting FeSe-like phase and magnetic sextet of the AFM matrix

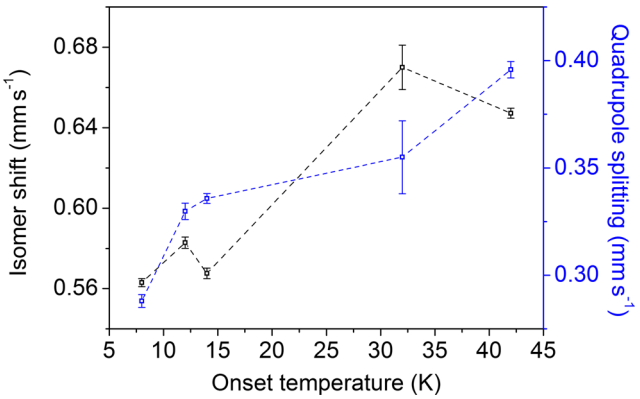

Fig. 4 Hyperfine parameters for *1–5* derived at 80–85 K as a function of superconducting transition temperature. For *5*, δ and ΔE_Q of the paramagnetic doublet are given

% intensity, which belongs to the superconducting phase [7]. The isomer shift of the doublet $\delta = 0.67(1)$ mm s^{-1} indicates the high level of electron doping due to Rb^+ ions introduced into the structure. The magnetic subspectrum corresponding to the Fe 16i sites is characterized by $\Delta E_Q = 1.23(1)$ mm s^{-1} with $\eta = 0.07(2)$ and an angle $\theta = 45(2)°$ between the main axis of the EFG and the magnetic hyperfine field $B_{hf} = 280.4(2)$ kOe.

The hyperfine parameters of FeSe based superconductors 1–5 are summarized in Fig. 4. The isomer shift that provides information about the DOS at the Fermi level can be a useful criterion of superconducting properties of the sample. Noteworthy, ΔE_Q follows T_c as well. This may be due to the fact that ΔE_Q is proportional to the EFG, which depends on the local density of electron orbitals of Fe atoms. Although other factors (e.g., magnetic fluctuations) may influence T_c, the electron density seems to be one of the important for the 1–5 series.

4 Conclusion

Mössbauer measurements of FeSe superconductor and its derivatives reveal that Fe 3d-electron density increases with electron doping via introduction of different electron-rich spacers between FeSe layers as well as partial Se substitution by Te. Although pairing mechanism in chalcogenides is still an open question, we demonstrate experimentally how T_c depends on the density of d-electrons on Fe atoms. In addition, the quadrupole splitting is also found to strongly correlate with T_c confirming that the Fermi level is primarily formed by d_{xy} and $d_{xz/yz}$ orbitals.

Acknowledgments This work was supported by the DFG within the Priority Program No. 1458 (grants KS51/2-2 and ME3652/1-2). The authors are grateful to the group of Prof. S. J. Clarke and Dr. V. Tsurkan for providing samples and to Prof. G. Wortmann for helpful discussion.

References

1. Drozdov, A.P., Eremets, M.I., Troyan, I.A., Ksenofontov, V., Shylin, S.I.: Nature **525**, 73–76 (2015)
2. Hsu, F.C., Luo, J.Y., Yeh, K.W., Chen, T.K., Huang, T.W., Wu, P.M., Lee, Y.C., Huang, Y.L., Chu, Y.Y., Yan, D.C., Wu, M.-K.: Proc. Natl. Acad. Sci. **105**, 14262–14264 (2008)
3. Medvedev, S., McQueen, T.M., Troyan, I.A., Palasyuk, T., Eremets, M.I., Cava, R.J., Naghavi, S., Casper, F., Ksenofontov, V., Wortmann, G., Felser, C.: Nat. Mater. **8**, 630–633 (2009)
4. Imai, T., Ahilan, K., Ning, F.L., McQueen, T.M., Cava, R.J.: Phys. Rev. Lett. **102**, 177005 (2009)
5. Tsurkan, V., Deisenhofer, J., Günther, A., Kant, C., Klemm, M., Krug von Nidda, H.-A., Schrettle, F., Loidl, A.: Eur. Phys. J. B **79**, 289–299 (2011)
6. Liu, X., Zhao, L., He, S., He, J., Liu, D., Mou, D., Shen, B., Hu, Y., Huang, J., Zhou, X.J.: J. Phys.: Condens. Matter **27**, 183201 (2015)
7. Ksenofontov, V., Wortmann, G., Medvedev, S.A., Tsurkan, V., Deisenhofer, J., Loidl, A., Felser, C.: Phys. Rev. B. **84**, 180508 (2011)
8. Ricci, A., Poccia, N., Campi, G., Joseph, B., Arrighetti, G., Barba, L., Reynolds, M., Burghammer, M., Takeya, H., Mizuguchi, Y., Takano, Y., Colapietro, M., Saini, N.L., Bianconi, A.: Phys. Rev. B. **84**, 060511 (2011)
9. Shylin, S.I., Ksenofontov, V., Medvedev, S.A., Tsurkan, V., Felser, C.: J. Supercond. Nov. Magn. **28**, 1315–1319 (2015)
10. Ksenofontov, V., Medvedev, S.A., Schoop, L.M., Wortmann, G., Palasyuk, T., Tsurkan, V., Deisenhofer, J., Loidl, A., Felser, C.: Phys. Rev. B **85**, 214519 (2012)
11. Burrard-Lucas, M., Free, D.G., Sedlmaier, S.J., Wright, J.D., Cassidy, S.J., Hara, Y., Corkett, A.J., Lancaster, T., Baker, P.J., Blundell, S.J., Clarke, S.J.: Nat. Mater. **12**, 15–19 (2013)
12. Krzton-Maziopa, A., Pomjakushina, E., Pomjakushin, V.Y., Rohr, F., Schilling, A., Conder, K.: J. Phys.: Condens. Matter **24**, 382202 (2012)
13. Noji, T., Hatakeda, T., Hosono, S., Kawamata, T., Kato, M., Koike, Y.: Physica C **504**, 8–11 (2014)
14. Guterding, D., Jeschke, H.O., Hirschfeld, P.J., Valenti, R.: Phys. Rev. B **91**, 041112 (2015)
15. Shylin, S.I., Gural'skiy, I.A., Bykov, D., Demeshko, S., Dechert, S., Meyer, F., Hauka, M., Fritsky, I.O.: Polyhedron **87**, 147–155 (2015)
16. McQueen, T.M., Huang, Q., Ksenofontov, V., Felser, C., Xu, Q., Zandbergen, H., Hor, Y.S., Allred, J., Williams, A.J., Qu, D., Checkelsky, J., Ong, N.P., Cava, R.J.: Phys. Rev. B. **79**, 014522 (2009)
17. Shylin, S.I., Ksenofontov, V., Sedlmaier, S.J., Clarke, S.J., Cassidy, S.J., Wortmann, G., Medvedev, S.A., Felser, C.: EPL **109**, 67004 (2015)
18. Mizuguchi, Y., Furubayashi, T., Deguchi, K., Tsuda, S., Yamaguchi, T., Takano, Y.: Physica C **470**, S338–S339 (2010)

4 Conventional superconductivity in hydrogen sulfide

4.1 Introduction

The most challenging problem in studies devoted to high-pressure superconductors is susceptibity measurements under pressure. For the investigation of hydrogen sulfide under high pressure the miniature cell was elaborated (Fig. 4.1). The composition of the alloy was selected by the combination of copper, titanium and beryllium. The main criteria were: linear magnetization behavior in the region of interest 100 – 300 K, and magnetization value close to zero. The desired properties were met for the alloy consisting of 94 % Cu, 4 % Ti and 2 % Be (Fig. 4.2).

Fig. 4.1. High-pressure cell loaded with H_2S. *The photo is taken by the author, 2015.*

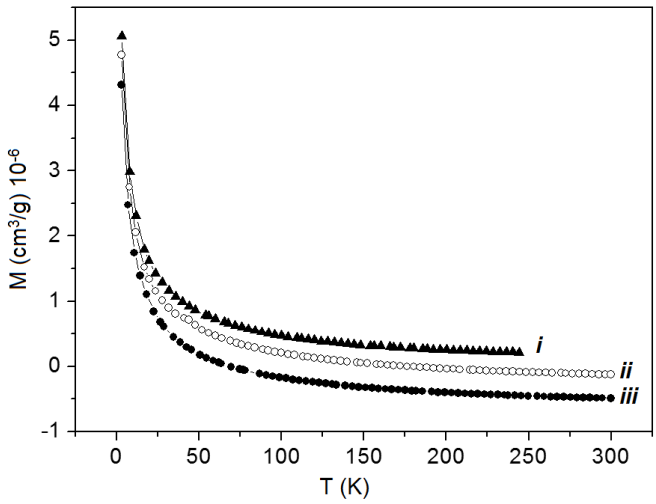

Fig. 4.2. M(T) dependences for the selected alloys of Cu, 2 % Be and 6 % (***i***), 4 % (***ii***), 0.5 % (***iii***) Ti in 500 Oe. *The data were acquired together with Dr. Vadim Ksenofontov (Johannes Gutenberg University Mainz).*

The high-pressure cell was placed into a cryostat and cooled down to 200 K (within the temperature range of liquid H_2S) and then H_2S gas was put through a capillary into a rim around the diamond anvil where it liquefied (see reprint in Chapter 4.2) [104]. Then liquid H_2S was clamped in the gasket hole by pushing the piston of the DAC with the aid of screws outside the cryostat. Samples of diameter 50–100 mm and a thickness of a few micrometres were prepared to provide a sufficient signal. After the clamping, the DAC was heated to 220 K to evaporate the rest of the H_2S, and then the pressure was further increased at this temperature. Pressure increase was monitored using Raman spectroscopy by the diamond vibration band. After pressurizing of hydrogen sulfide sample, magnetic susceptibility measurements were performed using conventional SQUID magnetometer. Magnetic susceptibility measurements using a high-pressure cell were performed using a background subtraction feature of the MPMS software of the SQUID magnetometer.

Experimental data [104] reveal that the H_2S superconductor is of type II. This fact is clearly supported by (i) a difference in temperature-dependent ZFC and FC magnetization, which is due to the Meissner effect (ZFC) and magnetic flux capture when the sample is cooled down from its normal state (FC); and (ii) the magnetic hysteresis curves. The magnetic hysteresis curves also have all the features of typical type II superconductors with a mixed state between B_{c1} and B_{c2}. A typical value of the coherence length ξ in the framework of the Ginzburg–Landau theory can be estimated on the basis of the upper critical field determined from the conductivity measurements. Using the experimental estimation 72(11) T and the relation:

$$\xi = \frac{1}{2}\sqrt{\frac{h}{\pi e B_{c2}}} \qquad (4.1)$$

the coherence length ξ = 2.15(15) nm can be found. This relatively short coherence length is of the same order as, for instance, the values for superconducting $YBa_2Cu_3O_7$ (1.3 nm) and Nb_3Sn (3.5 nm) [2]. The London penetration depth λ can be estimated from the relation between the lower critical field B_{c1} and the upper critical field B_{c2} for a type II superconductor:

$$\frac{B_{c1}}{B_{c2}} = \frac{\ln\kappa}{2\sqrt{2}\kappa}, \qquad (4.2)$$

where $\kappa = \lambda/\xi$. Considering the experimental value of the first critical field of 300 kOe, the London penetration depth $\lambda \sim 125$ nm. According to Bean's model, the magnetic critical current density of the superconductor can be estimated from the distance between the direct and the returning branches of the magnetic hysteresis loop at a given magnetic field. Provided grain radii are about 0.1 μm, the intra-grain critical current J_c is about 10^{-7} A·cm^{-2}.

Observation of the Meissner effect is a direct evidence of superconductivity in sulfur hydride under pressure. However, the particular compound responsible for the high T_c is not obvious. One of the possible scenarios is the decomposition of H_2S into higher hydrides and elemental sulphur. Calculations [105] support this hypothesis, showing that at pressures above 180 GPa hydrogen sulphide forms an *Im*3*m* structure with H_3S stoichiometry. The predicted $T_c \sim 190$ K and its pressure dependences are close to the experimental values [106]. The hypothesis of the transformation of H_2S to the higher hydride H_3S, where each S atom is surrounded by 6 hydrogen atoms, is strongly supported by further calculations [107-108]. Alternative calculations suggested that perovskite-like $(H_3S)(SH)$ phase might be responsible for superconductivity under pressure [109], however, it was not supported by structural studies [110].

4.2. Reprint: Conventional superconductivity at 203 kelvin at high pressures in the sulfur hydride system

Published in: Nature, 525 (2015), 73.

Personal contribution: Observation of the Meissner effect (Fig. 4), magnetization measurements under pressure, including the design of the magnetization experiment, were done by the author personally. The author prepared part of the manuscript (paragraphs dedicated to the Meissner effect and caption of Fig. 4), performed calcualtions of the fundamental parameters of hydrogen sulfide superconductor, and participated in transport measurements.

[redacted] performed resistivity measurements under pressure (Figs. 1-2) and in external magnetic fields (Fig. 3), and contributed to writing the manuscript.

[redacted] designed the study, supervised the work, designed the high-pressure cell, and wrote the major part of the manuscript.

[redacted] participated in the resistivity measurements and data interpretation.

[redacted] co-supervised the work, and participated in magnetization experiments.

LETTER

doi:10.1038/nature14964

Conventional superconductivity at 203 kelvin at high pressures in the sulfur hydride system

A. P. Drozdov[1]*, M. I. Eremets[1]*, I. A. Troyan[1], V. Ksenofontov[2] & S. I. Shylin[2]

A superconductor is a material that can conduct electricity without resistance below a superconducting transition temperature, T_c. The highest T_c that has been achieved to date is in the copper oxide system[1]: 133 kelvin at ambient pressure[2] and 164 kelvin at high pressures[3]. As the nature of superconductivity in these materials is still not fully understood (they are not conventional superconductors), the prospects for achieving still higher transition temperatures by this route are not clear. In contrast, the Bardeen–Cooper–Schrieffer theory of conventional superconductivity gives a guide for achieving high T_c with no theoretical upper bound—all that is needed is a favourable combination of high-frequency phonons, strong electron–phonon coupling, and a high density of states[4]. These conditions can in principle be fulfilled for metallic hydrogen and covalent compounds dominated by hydrogen[5,6], as hydrogen atoms provide the necessary high-frequency phonon modes as well as the strong electron–phonon coupling. Numerous calculations support this idea and have predicted transition temperatures in the range 50–235 kelvin for many hydrides[7], but only a moderate T_c of 17 kelvin has been observed experimentally[8]. Here we investigate sulfur hydride[9], where a T_c of 80 kelvin has been predicted[10]. We find that this system transforms to a metal at a pressure of approximately 90 gigapascals. On cooling, we see signatures of superconductivity: a sharp drop of the resistivity to zero and a decrease of the transition temperature with magnetic field, with magnetic susceptibility measurements confirming a T_c of 203 kelvin. Moreover, a pronounced isotope shift of T_c in sulfur deuteride is suggestive of an electron–phonon mechanism of superconductivity that is consistent with the Bardeen–Cooper–Schrieffer scenario. We argue that the phase responsible for high-T_c superconductivity in this system is likely to be H_3S, formed from H_2S by decomposition under pressure. These findings raise hope for the prospects for achieving room-temperature superconductivity in other hydrogen-based materials.

A search for high- (room)-temperature conventional superconductivity is likely to be fruitful, as the Bardeen–Cooper–Schrieffer (BCS) theory in the Eliashberg formulation puts no apparent limits on T_c. Materials with light elements are especially favourable as they provide high frequencies in the phonon spectrum. Indeed, many superconductive materials have been found in this way, but only a moderately high $T_c = 39$ K has been found in this search (in MgB_2; ref. 11).

Ashcroft[5] turned attention to hydrogen, which has very high vibrational frequencies due to the light hydrogen atom and provides a strong electron–phonon interaction. Further calculations showed that metallic hydrogen should be a superconductor with a very high T_c of about 100–240 K for molecular hydrogen, and of 300–350 K in the atomic phase at 500 GPa (ref. 12). However, superconductivity in pure hydrogen has not yet been found, even though a conductive and probably semimetallic state of hydrogen has been recently produced[13]. Hydrogen-dominated materials such as covalent hydrides SiH_4, SnH_4, and so on might also be good candidates for showing high-T_c superconductivity[6]. Similarly to pure hydrogen, they have high Debye temperatures. Moreover, heavier elements might be beneficial as they contribute to the low frequencies that enhance electron–phonon coupling. Importantly, lower pressures are required to metallize hydrides in comparison to pure hydrogen. Ashcroft's general idea was supported in numerous calculations[7,10] predicting high values of T_c for many hydrides. So far only a low T_c (~17 K) has been observed experimentally[8].

For the present study we selected H_2S, because it is relatively easy to handle and is predicted to transform to a metal and a superconductor at a low pressure $P \approx 100$ GPa with a high $T_c \approx 80$ K (ref. 10). Experimentally, H_2S is known as a typical molecular compound with a rich phase diagram[14]. At about 96 GPa, hydrogen sulphide transforms to a metal[15]. The transformation is complicated by the partial dissociation of H_2S and the appearance of elemental sulfur at $P > 27$ GPa at room temperature, and at higher pressures at lower temperatures[14]. Therefore, the metallization of hydrogen sulphide can be explained by elemental sulfur, which is known to become metallic above 95 GPa (ref. 16). No experimental studies of hydrogen sulphide are known above 100 GPa.

In a typical experiment, we performed loading and the initial pressure increase at temperatures of ~200 K; this is essential for obtaining a good sample (Methods). The Raman spectra of H_2S and D_2S were measured as the pressure was increased, and were in general agreement with the literature data[17,18] (Extended Data Fig. 1). The sample starts to conduct at $P \approx 50$ GPa. At this pressure it is a semiconductor, as shown by the temperature dependence of the resistance and pronounced photoconductivity. At 90–100 GPa the resistance drops further, and the temperature dependence becomes metallic. No photoconductive response is observed in this state. It is a poor metal—its resistivity at ~100 K is $\rho \approx 3 \times 10^{-5}$ ohm m at 110 GPa and $\rho \approx 3 \times 10^{-7}$ ohm m at ~200 GPa.

During the cooling of the metal at pressures of about 100 GPa (Fig. 1a) the resistance abruptly drops by three to four orders of magnitude, indicating a transition to the superconducting state. At the next increase of pressure at low temperatures of $T < 100$ K, T_c steadily increases with pressure. However, at pressures of >160 GPa, T_c increases sharply (Fig. 1b). As higher temperatures of 150–250 K were involved in this pressure range, we supposed that the increase of T_c and the decrease of sample resistance during warming (Fig. 1a) could indicate a possible kinetic-controlled phase transformation. Therefore in further experiments, after loading and after the initial pressure increase at 200 K, we annealed all samples by heating them to room temperature (or above) at pressures of >~150 GPa (Fig. 2a, see also Extended Data Fig. 2). This allowed us to obtain stable results, to compare different isotopes, to obtain the dependence of T_c on pressure and magnetic field, and to prove the existence of superconductivity in our samples as follows. (We note that additional information on experimental conditions are given in the appropriate figure legends.)

[1]Max-Planck-Institut für Chemie, Hahn-Meitner-Weg 1, 55128 Mainz, Germany. [2]Institut für Anorganische Chemie und Analytische Chemie, Johannes Gutenberg-Universität Mainz, Staudingerweg 9, 55099 Mainz, Germany.

*These authors contributed equally to this work.

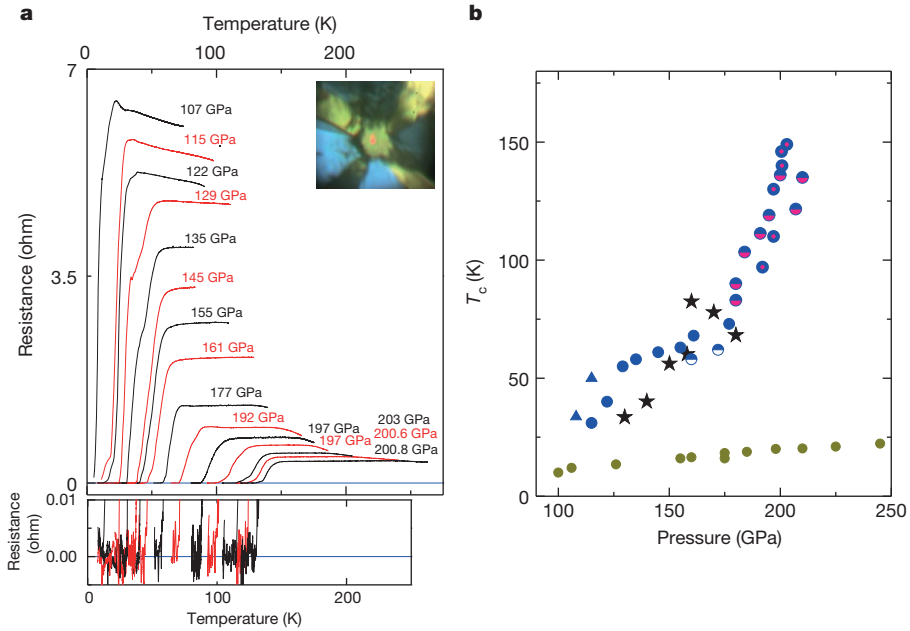

Figure 1 | Temperature dependence of the resistance of sulfur hydride measured at different pressures, and the pressure dependence of T_c. **a**, Main panel, temperature dependence of the resistance (R) of sulfur hydride at different pressures. The pressure values are indicated near the corresponding plots. At first, the sample was loaded at $T \approx 200$ K and the pressure was increased to ~100 GPa; the sample was then cooled down to 4 K. After warming to ~100 K, pressure was further increased. Plots at pressures <135 GPa have been scaled (reduced) as follows—105 GPa, by 10 times; 115 GPa and 122 GPa, by 5 times; and 129 GPa by 2 times—for easier comparison with the higher pressure steps. The resistance was measured with a current of 10 μA. Bottom panel, the resistance plots near zero. The resistance was measured with four electrodes deposited on a diamond anvil that touched the sample (top panel inset). The diameters of the samples were ~25 μm and the thickness was ~1 μm. **b**, Blue round points represent values of T_c determined from **a**. Other blue points (triangles and half circles) were obtained in similar runs. Measurements at $P > \sim 160$ GPa revealed a sharp increase of T_c. In this pressure range the $R(T)$ measurements were performed over a larger temperature range up to 260 K, the corresponding experimental points for two samples are indicated by adding a pink colour to half circles and a centred dot to filled circles. These points probably reflect a transient state for these particular P/T conditions. Further annealing of the sample at room temperature would require stabilizing the sample (Fig. 2a). Black stars are calculations from ref. 10. Dark yellow points are T_c values of pure sulfur obtained with the same four-probe electrical measurement method. They are consistent with literature data[30] (susceptibility measurements) but have higher values at $P > 200$ GPa.

(1) There is a sharp drop in resistivity with cooling, indicating a phase transformation. The measured minimum resistance is at least as low, $\sim 10^{-11}$ ohm m—about two orders of magnitude less than for pure copper (Fig. 1, Extended Data Fig. 3e) measured at the same temperature[19]. (2) A strong isotope effect is observed: T_c shifts to lower temperatures for sulfur deuteride, indicating phonon-assisted superconductivity (Fig. 2b, c). The BCS theory gives the dependence of T_c on atomic mass m as $T_c \propto m^{-\alpha}$, where $\alpha \approx 0.5$. Comparison of T_c values in the pressure range $P > 170$ GPa (Fig. 2c) gives $\alpha \approx 0.3$. (3) T_c shifts to lower temperatures with available magnetic field (B) up to 7 T

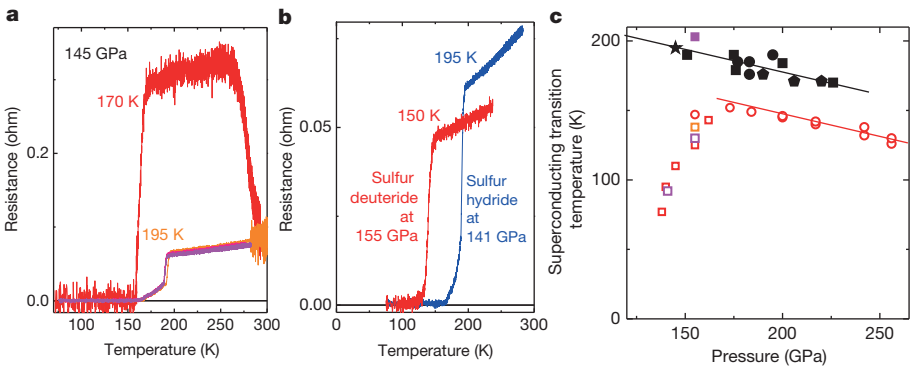

Figure 2 | Pressure and temperature effects on T_c of sulfur hydride and sulfur deuteride. **a**, Changes of resistance and T_c of sulfur hydride with temperature at constant pressure—the annealing process. The sample was pressurized to 145 GPa at 220 K and then cooled to 100 K. It was then slowly warmed at ~1 K min^{-1}; $T_c = 170$ K was determined. At temperatures above ~250 K the resistance dropped sharply, and during the next temperature run T_c increased to ~195 K. This T_c remained nearly the same for the next two runs. (We note that the only point for sulfur deuteride presented in ref. 9 was determined without sample annealing, and T_c would increase after annealing at room temperature.) **b**, Typical superconductive steps for sulfur hydride (blue trace) and sulfur deuteride (red trace). The data were acquired during slow warming over a time of several hours. T_c is defined here as the sharp kink in the transition to normal metallic behaviour. These curves were obtained after annealing at room temperature as shown in **a**. **c**, Dependence of T_c on pressure; data on annealed samples are presented. Open coloured points refer to sulfur deuteride, and filled points to sulfur hydride. Data shown as the magenta point were obtained in magnetic susceptibility measurements (Fig. 4a). The lines indicate that the plots are parallel at pressures above ~170 GPa (the isotope shift is constant) but strongly deviate at lower pressures.

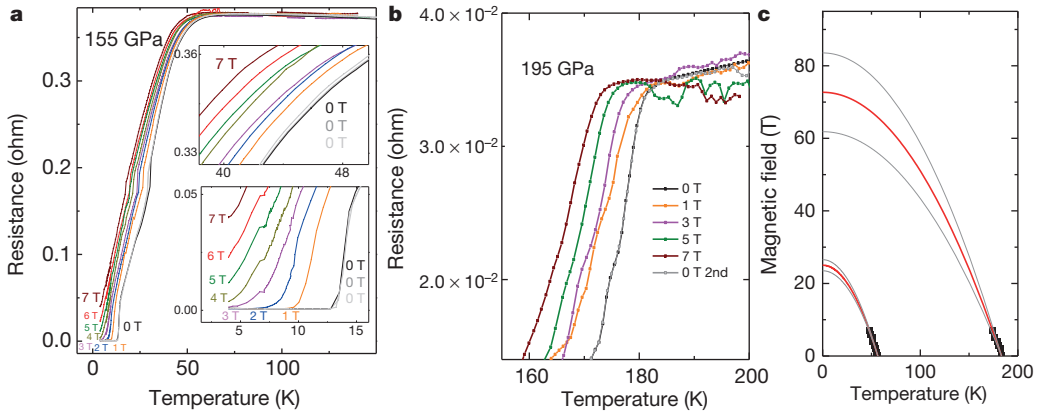

Figure 3 | Temperature dependence of the resistance of sulfur hydride in different magnetic fields. **a**, The shift of the ~60 K superconducting transition in magnetic fields of 0–7 T (colour coded). The upper and lower parts of the transition are shown enlarged in the insets (axes as in main panel). The temperature dependence of the resistance without an applied magnetic field was measured three times: before applying the field, after applying 1, 3, 5, 7 T and finally after applying 2, 4, 6 T (black, grey and dark grey colours). **b**, The same measurements but for the 185 K superconducting transition. **c**, The temperature dependence of the critical magnetic field strengths of sulfur hydride. T_c (black points deduced from **a**, **b**) are plotted for the corresponding magnetic fields. To estimate the critical magnetic field H_c, the plots were extrapolated to high magnetic fields using the formula $H_c(T) = H_{c0}(1 - (T/T_c)^2)$. The extrapolation has been done with 95% confidence (band shown as grey lines).

(Fig. 3). Much higher fields are required to destroy the superconductivity: extrapolation of $T_c(B)$ gives an estimate of a critical magnetic field as high as 70 T (Fig. 3). (4) Finally, in magnetic susceptibility measurements (Fig. 4) a sharp transition from the diamagnetic to the paramagnetic state (Fig. 4a) was observed for zero-field-cooled (ZFC) material. The onset temperature of the superconducting state $T_{onset} = 203(1)$ K, and the width of the superconducting transition is nearly the same as in electrical measurements (Fig. 4a). Magnetization measurements $M(H)$, where H is magnetic field, at different temperatures (Fig. 4c) revealed a pronounced hysteresis indicating type II superconductivity with the first critical field $H_{c1} \approx 30$ mT. The magnetization decreases sharply at temperatures above 200 K showing the onset of superconductivity at 203.5 K, in agreement with the susceptibility measurements (Fig. 4a). A list of key properties of the new superconductor is given in Methods.

We have presented purely experimental evidence of superconductivity in sulfur hydride. However the particular compound responsible for the high T_c is not obvious. The superconductivity measured in the

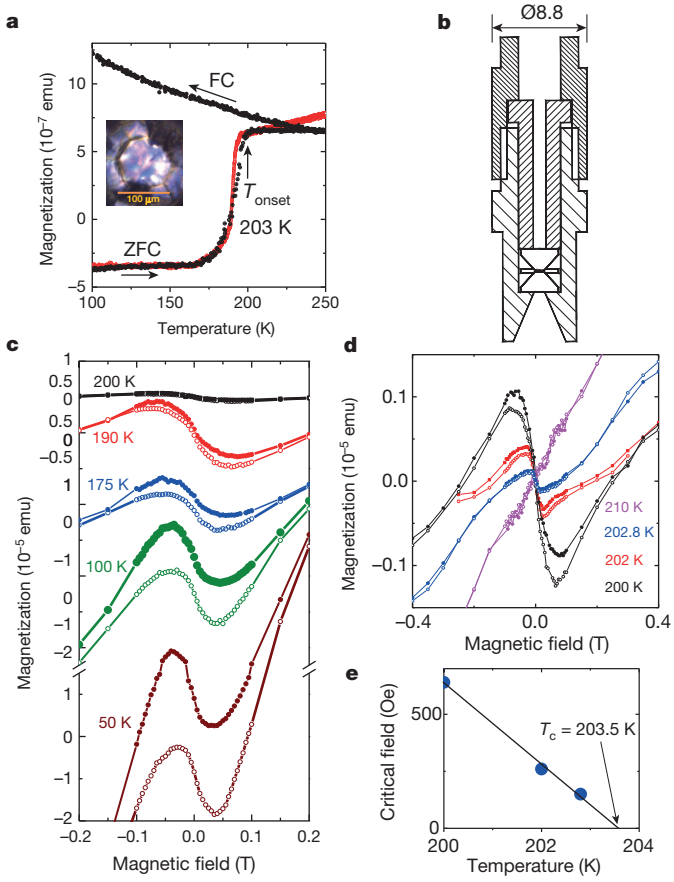

Figure 4 | Magnetization measurements. **a**, Temperature dependence of the magnetization of sulfur hydride at a pressure of 155 GPa in zero-field cooled (ZFC) and 20 Oe field cooled (FC) modes (black circles). The onset temperature is $T_{onset} = 203(1)$ K. For comparison, the superconducting step obtained for sulfur hydride from electrical measurements at 145 GPa is shown by red circles. Resistivity data ($T_{onset} = 195$ K) were scaled and moved vertically to compare with the magnetization data. Inset, optical micrograph of a sulfur hydride sample at 155 GPa in a $CaSO_4$ gasket (scale bar 100 μm). The high $T_{onset} = 203$ K measured from the susceptibility can be explained by a significant input to the signal from the periphery of the sample which expanded beyond the culet where pressure is smaller than in the culet centre (T_c increases with decreasing pressure (Fig. 2b)). **b**, Non-magnetic diamond anvil cell (DAC) of diameter 8.8 mm. **c**, Magnetization measurements $M(H)$ of sulfur hydride at a pressure of 155 GPa at different temperatures (given as curve labels). The magnetization curves show hysteresis, indicating a type II superconductor. The magnetization curves are however distorted by obvious paramagnetic input (which is also observed in other superconductors[31]). In our case, the paramagnetic signal is probably from the DAC, but further study of the origin of this input is required. The paramagnetic background increases when temperature is decreased. The minima of the magnetization curves (~35 mT) are the result of the diamagnetic input from superconductivity and the paramagnetic background. The first critical field $H_{c1} \approx 30$ mT can be roughly estimated as the point where magnetization deviates from linear behaviour. At higher fields, magnetization increases due to the penetration of magnetic vortexes. As the sign of the field change reverses, the magnetic flux in the Shubnikov phase remains trapped and therefore the back run (that is, with decreasing field) is irreversible—the returning branch of the magnetic cycle (shown by filled points) runs above the direct one. Hysteretic behaviour of the magnetization becomes more clearly visible as the temperature decreases. **d**, At high temperatures $T > 200$ K, the magnetization decreases sharply. **e**, Extrapolation of the pronounced minima at the magnetization curves to higher temperatures gives the onset of superconductivity at $T = 203.5$ K.

low-temperature runs (Fig. 1) possibly relates to H_2S, as it is generally consistent with calculations[10] for H_2S: both the value of $T_c \approx 80$ K and its pressure behaviour. However superconductivity with $T_c \approx 200$ K (Fig. 2) does not follow from these calculations. We suppose that it relates to the decomposition of H_2S, as high temperatures are required to reach the high T_c (Fig. 2b). Precipitation of elemental sulfur on decomposition could be expected (which is well known at low pressures of $P < 100$ GPa; ref. 14); however the superconducting transition in elemental sulfur occurs at significantly lower temperatures (Fig. 1b). Another expected product of decomposition of H_2S is hydrogen. However, the strong characteristic vibrational stretching mode from the H_2 molecule was never observed in our Raman spectra (nor was it observed in ref. 14). Therefore we suppose that the dissociation of H_2S is different and involves the creation of higher hydrides, such as $3H_2S \rightarrow H_6S + 2S$ or $2H_2S \rightarrow H_4S + S$. It is natural to expect these reactions, as sulfur can be not only divalent, but also exhibits higher valencies. In fact, calculations[10] indirectly support this hypothesis, as the dissociation $H_2S \rightarrow H_2 + S$ was shown to be energetically very unfavourable. We found further theoretical support in ref. 20. In that work, the van der Waals compound[21] $(H_2S)_2H_2$ was considered, and it was shown that at pressures above 180 GPa it forms an *Im*-3*m* structure with H_3S stoichiometry. The predicted $T_c \approx 190$ K and its pressure dependences are close to our experimental values (Fig. 2c). Our hypothesis of the transformation of H_2S to higher hydrides (in the H_3S stoichiometry each S atom is surrounded by 6 hydrogen atoms) is strongly supported by further calculations[22,23]. All the numerous works based on the *Im*-3*m* structure[23–27] are consistent in their prediction of $T_c > \sim 200$ K, which decreases with pressure. The hydrogen sublattice gives the main contribution to superconductivity[20,25,26]. Inclusion of zero point vibrations and anharmonicity in the calculations[24] corrected the calculated T_c to ~190 K, and the isotope coefficient from $\alpha = 0.5$ to $\alpha = 0.35$—both in agreement with the present work.

The highest T_c of 203 K that we report here has been achieved most probably in H_3S having the *Im*-3*m* structure. It is a good metal; interestingly, there is also strong covalent bonding between H and S atoms in this compound[20]. This is in agreement with the general assumption (see for instance ref. 28) that a metal with high T_c should have strong covalent bonding (as is realized in MgB_2; ref. 29) together with high-frequency modes in the phonon spectrum. This particular combination of bonding type and phonon spectrum would probably provide a good criterion when searching for the materials with high T_c at ambient pressure that are required for applications. There are many hydrogen-containing materials with strong covalent bonding (such as organics) but typically they are insulators. In principle, they could be tuned to a metallic state by doping or gating. Modern methods of structure prediction could facilitate exploration for the desired materials.

Online Content Methods, along with any additional Extended Data display items and Source Data, are available in the online version of the paper; references unique to these sections appear only in the online paper.

Received 25 June; accepted 22 July 2015.
Published online 17 August 2015.

1. Bednorz, J. G. & Mueller, K. A. Possible high T_C superconductivity in the Ba-La-Cu-O system. *Z. Phys. B* **64,** 189–193 (1986).
2. Schilling, A., Cantoni, M., Guo, J. D. &. Ott, H. R. Superconductivity above 130 K in the Hg-Ba-Ca-Cu-O system. *Nature* **363,** 56–58 (1993).
3. Gao, L. *et al.* Superconductivity up to 164 K in $HgBa_2Ca_{m-1}Cu_mO_{2m+2+\delta}$ (m=l, 2, and 3) under quasihydrostatic pressures. *Phys. Rev. B* **50,** 4260–4263 (1994).
4. Ginzburg, V. L. Once again about high-temperature superconductivity. *Contemp. Phys.* **33,** 15–23 (1992).
5. Ashcroft, N. W. Metallic hydrogen: A high-temperature superconductor? *Phys. Rev. Lett.* **21,** 1748–1750 (1968).
6. Ashcroft, N. W. Hydrogen dominant metallic alloys: high temperature superconductors? *Phys. Rev. Lett.* **92,** 187002 (2004).
7. Wang, Y. & Ma, Y. Perspective: Crystal structure prediction at high pressures. *J. Chem. Phys.* **140,** 040901 (2014).
8. Eremets, M. I., Trojan, I. A., Medvedev, S. A., Tse, J. S. & Yao, Y. Superconductivity in hydrogen dominant materials: silane. *Science* **319,** 1506–1509 (2008).
9. Drozdov, A. P., Eremets, M. I. & Troyan, I. A. Conventional superconductivity at 190 K at high pressures. Preprint at http://arXiv.org/abs/1412.0460 (2014).
10. Li, Y., Hao, J., Li, Y. & Ma, Y. The metallization and superconductivity of dense hydrogen sulfide. *J. Chem. Phys.* **140,** 174712 (2014).
11. Nagamatsu, J., Nakagawa, N., Muranaka, T., Zenitani, Y. & Akimitsu, J. Superconductivity at 39 K in magnesium diboride. *Nature* **410,** 63–64 (2001).
12. McMahon, J. M., Morales, M. A., Pierleoni, C. & Ceperley, D. M. The properties of hydrogen and helium under extreme conditions. *Rev. Mod. Phys.* **84,** 1607–1653 (2012).
13. Eremets, M. I. & Troyan, I. A. Conductive dense hydrogen. *Nature Mater.* **10,** 927–931 (2011).
14. Fujihisa, H. *et al.* Molecular dissociation and two low-temperature high-pressure phases of H_2S. *Phys. Rev. B* **69,** 214102 (2004).
15. Sakashita, M. *et al.* Pressure-induced molecular dissociation and metallization in hydrogen-bonded H_2S solid. *Phys. Rev. Lett.* **79,** 1082–1085 (1997).
16. Kometani, S., Eremets, M., Shimizu, K., Kobayashi, M. & Amaya, K. Observation of pressure-induced superconductivity of sulfur. *J. Phys. Soc. Jpn.* **66,** 2564–2565 (1997).
17. Shimizu, H. *et al.* Pressure-temperature phase diagram of solid hydrogen sulfide determined by Raman spectroscopy. *Phys. Rev. B* **51,** 9391–9394 (1995).
18. Shimizu, H., Murashima, H. & Sasaki, S. High-pressure Raman study of solid deuterium sulfide up to 17 GPa. *J. Chem. Phys.* **97,** 7137–7139 (1992).
19. Matula, R. A. Electrical resistivity of copper, gold, palladium, and silver. *J. Phys. Chem. Ref.* **8,** 1147–1298 (1979).
20. Duan, D. *et al.* Pressure-induced metallization of dense $(H_2S)_2H_2$ with high-T_c superconductivity. *Sci. Rep.* **4,** 6968 (2014).
21. Strobel, T. A., Ganesh, P., Somayazulu, M., Kent, P. R. C. & Hemley, R. J. Novel cooperative interactions and structural ordering in H_2S–H_2. *Phys. Rev. Lett.* **107,** 255503 (2011).
22. Duan, D. *et al.* Pressure-induced decomposition of solid hydrogen sulfide. *Phys. Rev. B* **91,** 180502(R) (2015).
23. Bernstein, N., Hellberg, C. S., Johannes, M. D., Mazin, I. I. & Mehl, M. J. What superconducts in sulfur hydrides under pressure, and why. *Phys. Rev. B* **91,** 060511(R) (2015).
24. Errea, I. *et al.* Hydrogen sulfide at high pressure: a strongly-anharmonic phonon-mediated superconductor. *Phys. Rev. Lett.* **114,** 157004 (2015).
25. Flores-Livas, J. A., Sanna, A. & Gross, E. K. U. High temperature superconductivity in sulfur and selenium hydrides at high pressure. Preprint at http://arXiv.org/abs/1501.06336v1 (2015).
26. Papaconstantopoulos, D. A., Klein, B. M., Mehl, M. J. & Pickett, W. E. Cubic H_3S around 200 GPa: an atomic hydrogen superconductor stabilized by sulfur. *Phys. Rev. B.* **91,** 184511 (2015).
27. Akashi, R., Kawamura, M., Tsuneyuki, S., Nomura, Y. & Arita, R. Fully non-empirical study on superconductivity in compressed sulfur hydrides. Preprint at http://arXiv.org/abs/1502.00936v1 (2015).
28. Cohen, M. L. in *BCS: 50 years* (eds Cooper, L. N. & Feldman, D.) 375–389 (World Scientific, 2011).
29. An, J. M. & Pickett, W. E. Superconductivity of MgB_2: covalent bonds driven metallic. *Phys. Rev. Lett.* **86,** 4366–4369 (2001).
30. Gregoryanz, E. *et al.* Superconductivity in the chalcogens up to multimegabar pressures. *Phys. Rev. B* **65,** 064504 (2002).
31. Senoussi, S., Sastry, P., Yakhmi, J. V. & Campbell, I. Magnetic hysteresis of superconducting $GdBa_2Cu_3O_7$ down to 1.8 K. *J. Phys.* **49,** 2163–2164 (1988).

Acknowledgements Support provided by the European Research Council under the 2010 Advanced Grant 267777 is acknowledged. We appreciate help provided in MPI Chemie by U. Pöschl. We thank P. Alireza and G. Lonzarich for help with samples of CuTi; J. Kamarad, S. Toser and C. Q. Jin for sharing their experience on SQUID measurements; K. Shimizu and his group for cooperation; P. Chu and his group for many discussions and collaboration, and L. Pietronero, M. Calandra and T. Timusk for discussions. V.K. and S.I.S. acknowledge the DFG (Priority Program No. 1458) for support. M.I.E. thanks H. Musshof and R. Wittkowski for precision machining of the DACs.

Author Contributions A.P.D. performed the most of the experiments and contributed to the data interpretation and writing the manuscript. M.I.E. designed the study, wrote the major part of the manuscript, developed the DAC for SQUID measurements, and participated in the experiments. I.A.T. participated in experiments. V.K. and S.I.S. performed the magnetic susceptibility measurements and contributed to writing the manuscript. M.I.E. and A.P.D. contributed equally to this paper.

Author Information Reprints and permissions information is available at www.nature.com/reprints. The authors declare no competing financial interests. Readers are welcome to comment on the online version of the paper. Correspondence and requests for materials should be addressed to M.I.E. (m.eremets@mpic.de).

5 Conclusions

Pressure has been shown to be “clean” method to tune the structural parameters and, consequently, electronic, magnetic and superconducting properties of the chalcogenide materials. These changes have been monitored using Mössbauer spectroscopy – the method that allows to detect the finest electronic effects at ^{57}Fe atoms, and magnetic susceptibility measurements. Both conventional and unconventional superconductors have been investigated. The main scientific results can be summarized as follows:

1. ^{57}Fe-Mössbauer spectroscopy studies of superconducting FeSe and its intercalates reveal a pronounced increase in electronic density near the Fermi level upon intercalation that is accompanied by drastic enhancement of T_c. Variation of the quadrupole splitting observed at 240 – 290 K in Li-containing FeSe superconductors evidences the thermal activation of the Li^+ ions motion. Detailed Mössbauer studies of $Li_x(NH_2)_y(NH_3)_{1-y}Fe_2Se_2$ (x=0.6; y=0.2) at low temperature point out the appearance of magnetic fluctuations in the vicinity of T_c = 42 K at ambient pressure. Pressure increase leads to the suppression of both dynamic magnetism and superconductivity, thereby, the leading role of spin fluctuations in superconducting pairing mechanism in Fe chalcogenides is supposed.

2. Structural, magnetic and Mössbauer studies of single-crystalline $FeSe_{0.5}Te_{0.5}$ reveal a dome-like pressure dependence of T_c: the latest grows from 13.5 to 20 K up to 1.3 GPa, remains stable in the 1.3 – 4.8 GPa region, decreases at higher pressures, and around 7 GPa superconductivity disappears completely. That is found to be associated with a first-order phase transition from superconducting tetragonal (PbO-type) to a non-superconducting hexagonal (NiAs-type) phase.

3. Using Mössbauer spectroscopy, phase separation in a selenide of $Rb_{0.8}Fe_{1.6}Se_2$ into the dominant antiferromagnetic matrix and minor paramagnetic “phase” is probed by Cu-doping and variation of stoichiometry. It is shown that the non-magnetic Fe sites of the compound, which are responsible for superconductivity, are very sensitive to chemical modification. It leads to a decrease of Fe population or induces magnetic ordering that in both cases suppresses superconductivity.

4. Correlation between hyperfine parameters of ^{57}Fe and superconducting transition temperature T_c in a series of FeSe-based compounds is established. It is a direct evidence of a T_c dependence on the density of states at the Fermi level, since the latest is mostly formed by the Fe 3*d* orbitals. Thus, the superconducting properties of chalcogenides can be estimated based on Mössbauer spectroscopy data.

5. A superconducting transition temperature as high as 203 K is achieved in H_2S under pressure of 155 GPa in the magnetization experiment. It is shown that H_2S under pressure is a conventional type-II superconductor, *i.e.* superconducting pairing is based on a classic phonon mechanism (BCS). Additionally to T_c, the fundamental parameters of H_2S superconductor are found: critical fields B_{c1} = 300 Oe and B_{c2} = 72(11) T, coherence length ξ = 2.15(15) nm, London penetration depth λ ~ 125 nm.

Bibliography

1. D. van Delft, P. Kes. The discovery of superconductivity. Phys. Today **63** (2010) 38–43.
2. V. L. Ginzburg. Superconductivity: the day before yesterday, yesterday, today, tomorrow. Russ. Phys. Rev. **170** (2000) 619–630.
3. H. Kamerlingh Onnes. Further experiments with liquid helium. C. On the change of electric resistance of pure metals at very low temperatures etc. IV. The resistance of pure mercury at helium temperatures. Commun. Phys. Lab. Univ. Leiden **120B** (1911) 1274–1276.
4. C. Kittel. Introduction to Solid State Physics. New York: John Wiley & Sons, 2004. P. 704
5. A. Schilling, M. Cantoni, J. D. Guo, H. R. Ott. Superconductivity above 130 K in the Hg–Ba–Ca–Cu–O system. Nature **363** (1993) 56–58.
6. L. Gao, Y.Y. Xue, F. Chen [et al.]. Superconductivity up to 164 K in $HgBa_2Ca_{m-1}Cu_mO_{2m+2+\delta}$ under quasihydrostatic pressures. Phys. Rev. B **50** (1994) 4260–4263.
7. H. Kamerlingh Onnes. The resistance of pure mercury at helium temperatures. . Commun. Phys. Lab. Univ. Leiden **160B** (1922) 12–16.
8. A. Ikushima, T. Mizusaki. Superconductivity in niobium and niobium-tantalum alloys. J. Phys. Chem. Solids **30** (1969) 873–879.
9. B. T. Matthias, T. H. Geballe, S. Geller, E. Corenzwit. Superconductivity of Nb_3Sn. Phys. Rev. **95** (1954) 1435.
10. A.R. Sweedler, D.E. Cox, S. Moehlecke [et al.]. Superconductivity and phase stability of Nb_3Ge. Journal of Low Temperature Physics **24** (1976) 645–661.
11. J. Bardeen, L. N. Cooper, J. R. Schrieffer. Microscopic Theory of Superconductivity. Phys. Rev. **106** (1957) 162–164.
12. J. G. Bednorz, K. A. Müller. Possible high-T_c superconductivity in the Ba−La−Cu−O system. Zeitschrift für Physik B Condensed Matter **64** (1986) 189–193.
13. M. K. Wu, J. R. Ashburn, C. J. Torng [et al.]. Superconductivity at 93 K in a new mixed-phase Y-Ba-Cu-O compound system at ambient pressure. Phys. Rev. Lett. **58** (1987) 908–910.
14. R. M. Hazen, C. T. Prewitt, R. J. Angel [et al.]. Superconductivity in the high-T_c Bi-Ca-Sr-Cu-O system: Phase identification. Phys. Rev. Lett. **60** (1988) 1174–1177.
15. Z. Z. Sheng, A. M. Hermann. Superconductivity in the rare-earth-free Tl–Ba–Cu–O system above liquid-nitrogen temperature. Nature **332** (1988) 55–58.
16. S. N. Putilin, E. V. Antipov, O. Chmaissem, M. Marezio. Superconductivity at 94 K in $HgBa_2CuO_{4+\delta}$. Nature **362** (1993) 226–228.
17. K. M. Shen, J. C. S. Davis. Cuprate high-T_c superconductors. Mat. Today **11** (2008) 14–21.
18. M. Nuñez-Regueiro, J.-L. Tholence, E. V. Antipov [et al.]. Pressure-Induced Enhancement of T_c above 150 K in Hg-1223. Science **262** (1993) 97–99.

19. Y. Kamihara, T. Watanabe, M. Hirano, H. Hosono. Iron-based layered superconductor $La[O_{1-x}F_x]FeAs$ (x = 0.05-0.12) with T_c = 26 K. J. Amer. Chem. Soc. **130** (2008) 3296–3297.
20. B. S. Chandrasekhar, J. K. Hulm. The electrical resistivity and superconductivity of some uranium alloys and compounds. J. Phys. Chem. Solids **7** (1958) 259–267.
21. H. F. Braun. Superconductivity of rare earth-iron silicides. Phys. Lett. A **75** (1980) 386–388.
22. H. Takahashi, K. Igawa, K. Arii, Y. Kamihara, M. Hirano, H. Hosono. Superconductivity at 43 K in an iron-based layered compound $LaO_{1-x}F_xFeAs$. Nature **453** (2008) 376–378.
23. G. Wu, Y.L. Xie, H. Chen [et al.]. Superconductivity at 56 K in samarium-doped SrFeAsF. J. Phys.: Cond. Matt. **21** (2009) 142203.
24. M. Rotter, M. Tegel, Dirk Johrendt. Superconductivity at 38 K in the iron arsenide $(Ba_{1-x}K_x)Fe_2As_2$. Phys. Rev. Lett. **101** (2008) 107006.
25. X. C. Wang, Q. Q. Liu, Y. X. Lv, W. B. Gao, L. X. Yang, R. C. Yu, F. Y. Li, C. Q. Jin. The superconductivity at 18 K in LiFeAs system. Solid State Commun. **148** (2008) 538–540.
26. R. Mittal, Y. Su, S. Rols, M. Tegel, S. L. Chaplot, H. Schober, T. Chatterji, D. Johrendt, T. Brueckel. Phonon dynamics in $Sr_{0.6}K_{0.4}Fe_2As_2$ and $Ca_{0.6}Na_{0.4}Fe_2As_2$ from neutron scattering and lattice-dynamical calculations. Phys. Rev. B **78** (2008) 224518.
27. F.-C. Hsu, J.-Y. Luo, K.-W. Yeh [et al.]. Superconductivity in the PbO-type structure α-FeSe. Proc. Nat. Acad. Sci. **105** (2008) 14262–14264.
28. T.M. McQueen, Q. Huang, V. Ksenofontov [et al.]. Extreme sensitivity of superconductivity to stoichiometry in $Fe_{1+\delta}Se$. Phys. Rev. B **79** (2009) 014522.
29. T.M. McQueen, A.J. Williams, P.W. Stephens [et al.]. Tetragonal-to-Orthorhombic Structural Phase Transition at 90 K in the Superconductor $Fe_{1.01}Se$. Phys. Rev. Lett. **103** (2009) 057002.
30. D. Chowdhury, E. Berg, S. Sachdev. Nematic order in the vicinity of a vortex in superconducting FeSe. Phys. Rev. B. **84** (2011) 205113.
31. E.-G. Moon, S. Sachdev. Competition between superconductivity and nematic order: Anisotropy of superconducting coherence length. Phys. Rev. B. **85** (2012) 184511.
32. A.V. Chubukov, R.M. Fernandes, J. Schmalian. Origin of nematic order in FeSe. Phys. Rev. B. **91** (2015) 201105.
33. S-H. Baek, D.V. Efremov, J.M. Ok [et al.]. Orbital-driven nematicity in FeSe. Nat. Mater. **14** (2015) 210–214.
34. S. Medvedev, T.M. McQueen, I.A. Troyan [et al.]. Electronic and magnetic phase diagram of β-$Fe_{1.01}Se$ with superconductivity at 36.7 K under pressure. Nat. Mater. **8** (2009) 630–633.
35. S. Margadonna, Y. Takabayashi, Y. Ohishi [et al.]. Pressure evolution of the low-temperature crystal structure and bonding of the superconductor FeSe (T_c=37 K). Phys. Rev. B. **80** (2009) 064506.
36. S. Margadonna, Y. Takabayashi, M.T. McDonald [et al.]. Crystal structure of the new $FeSe_{1-x}$ superconductor. Chem. Commun. **28** (2008) 5607–5609.

37. V. Ksenofontov, G. Wortmann, A.I. Chumakov [et al.]. Density of phonon states in superconducting FeSe as a function of temperature and pressure. Phys. Rev. B. **81** (2010) 184510.
38. T. Imai, K. Ahilan, F.L. Ning [et al.]. Why Does Undoped FeSe Become a High-T_c Superconductor under Pressure? Phys. Rev. Lett. **102** (2009) 177005.
39. A.J. Williams, T.M. McQueen, V. Ksenofontov [et al.]. The metal–insulator transition in $Fe_{1.01-x}Cu_xSe$. J. Phys.: Cond. Matt. **21** (2009) 305701.
40. S. Chadov, D. Schärf, G.H. Fecher [et al.]. Electronic structure, localization, and spin-state transition in Cu-substituted FeSe: $Fe_{1-x}Cu_xSe$. Phys. Rev. B **81** (2010) 104523.
41. L.M. Schoop, S.A. Medvedev, V. Ksenofontov [et al.]. Pressure-restored superconductivity in Cu-substituted FeSe. Phys. Rev. B. **84** (2011) 174505.
42. J. Guo, S. Jin, G. Wang [et al.]. Superconductivity in the iron selenide $K_xFe_2Se_2$ ($0 < x < 1.0$). Phys. Rev. B. **82** (2010) 180520.
43. A. Krzton-Maziopa, Z. Shermadini, E. Pomjakushina [et al.]. Synthesis and crystal growth of $Cs_{0.8}(FeSe_{0.98})_2$: a new iron-based superconductor with $T_c = 27$ K. J. Phys.: Cond. Matt. **23** (2011) 052203.
44. A.F. Wang, J.J. Ying, Y.J. Yan [et al.]. Superconductivity at 32 K in single-crystalline $Rb_xFe_{2-y}Se_2$. Phys. Rev. B. **83** (2011) 060512.
45. V. Tsurkan, J. Deisenhofer, A. Günther [et al.]. Anisotropic magnetism, superconductivity, and the phase diagram of $Rb_{1-x}Fe_{2-y}Se_2$. Phys. Rev. B. **84** (2011) 144520.
46. Y. Texier, J. Deisenhofer, V. Tsurkan [et al.]. NMR Study in the Iron-Selenide $Rb_{0.74}Fe_{1.6}Se_2$: Determination of the Superconducting Phase as Iron Vacancy-Free $Rb_{0.3}Fe_2Se_2$. Phys. Rev. Lett. **108** (2012) 237002.
47. W. Li, H. Ding, P. Deng [et al.]. Phase separation and magnetic order in K-doped iron selenide superconductor. Nat. Phys. **8** (2012) 126–130.
48. A. Ricci, N. Poccia, G. Campi [et al.]. Nanoscale phase separation in the iron chalcogenide superconductor $K_{0.8}Fe_{1.6}Se_2$ as seen via scanning nanofocused x-ray diffraction. Phys. Rev. B. **84** (2011) 060511.
49. R.H. Yuan, T. Dong, Y.J. Song [et al.]. Nanoscale phase separation of antiferromagnetic order and superconductivity in $K_{0.75}Fe_{1.75}Se_2$. Sci. Rep. **2** (2012) 221.
50. V. Ksenofontov, G. Wortmann, S.A. Medvedev [et al.]. Phase separation in superconducting and antiferromagnetic $Rb_{0.8}Fe_{1.6}Se_2$ probed by Mössbauer spectroscopy. Phys. Rev. B. **84** (2011) 180508.
51. V. Ksenofontov, S.A. Medvedev, L.M. Schoop [et al.]. Superconductivity and magnetism in $Rb_{0.8}Fe_{1.6}Se_2$ under pressure. Phys. Rev. B. **85** (2012) 214519.
52. L. Häggström, H.R. Verma, S. Bjarman [et al.]. Magnetic properties of $TlFe_{2-x}Se_2$. Journal of Solid State Chemistry **63** (1986) 401–408.
53. M. Burrard-Lucas, D.G. Free, S.J. Sedlmaier [et al.]. Enhancement of the superconducting transition temperature of FeSe by intercalation of a molecular spacer layer. Nat. Mater. **12** (2013) 15–19.

54. S.J. Sedlmaier, S.J. Cassidy, R.G. Morris [et al.]. Ammonia-Rich High-Temperature Superconducting Intercalates of Iron Selenide Revealed through Time-Resolved in Situ X-ray and Neutron Diffraction. J. Amer. Chem. Soc. **136** (2014) 630–633.
55. D. Guterding, H.O. Jeschke, P.J. Hirschfeld, R. Valenti. Unified picture of the doping dependence of superconducting transition temperatures in alkali metal/ammonia intercalated FeSe. Phys. Rev. B. **91** (2015) 041112.
56. T. Noji, T. Hatakeda, S. Hosono [et al.]. Synthesis and post-annealing effects of alkaline-metal-ethylenediamineintercalated superconductors $A_x(C_2H_8N_2)_yFe_{2-z}Se_2$ (A = Li, Na) with T_c = 45 K. Physica C: Superconductivity **504** (2014) 8–11.
57. A. Krzton-Maziopa, E.V. Pomjakushina, V.Yu. Pomjakushin [et al.]. Synthesis of a new alkali metal–organic solvent intercalated iron selenide superconductor with T_c ~ 45 K. J. Phys.: Cond. Matt. **24** (2012) 382202.
58. H-K. Mao, R.J. Hemley. Ultrahigh-pressure transitions in solid hydrogen. Rev. Mod. Phys. **66** (1994) 671–692.
59. N.W. Ashcroft. Metallic Hydrogen: A High-Temperature Superconductor? Phys. Rev. Lett. **21** (1968) 1748–1749.
60. E. Babaev, A. Sudbø, N.W. Ashcroft. A superconductor to superfluid phase transition in liquid metallic hydrogen. Nature **431** (2004) 666–668.
61. P. Loubeyre, F. Occelli, R. LeToullec. Optical studies of solid hydrogen to 320 GPa and evidence for black hydrogen. Nature **416** (2002) 613–616.
62. Y. Akahama, H. Kawamura, N. Hirao [et al.]. Raman scattering and x-ray diffraction experiments for phase III of solid hydrogen. J. Phys.: Conf. Ser. **215** (2010) 012056.
63. M.I. Eremets, I.A. Troyan. Conductive dense hydrogen. Nat. Mater. **10** (2011) 927–931.
64. J.M. McMahon, M.A. Morales, C. Pierleoni, D.M. Ceperley. The properties of hydrogen and helium under extreme conditions. Rev. Mod. Phys. **84** (2012) 1607–1653.
65. N.W. Ashcroft. Hydrogen Dominant Metallic Alloys: High Temperature Superconductors? Phys. Rev. Lett. **92** (2004) 187002.
66. M.I. Eremets, I.A. Trojan, S.A. Medvedev [et al.]. Superconductivity in Hydrogen Dominant Materials: Silane. Science **319** (2008) 1506–1509.
67. C.J. Pickard, M. Martinez-Canales, R.J. Needs. Decomposition and Terapascal Phases of Water Ice. Phys. Rev. Lett. **110** (2013) 245701.
68. Y. Li, J. Hao, H. Liu [et al.]. The metallization and superconductivity of dense hydrogen sulfide. J. Chem. Phys. **140** (2014) 174712.
69. H. Fujihisa, H. Yamawaki, M. Sakashita [et al.]. Molecular dissociation and two low-temperature high-pressure phases of H_2S. Phys. Rev. B. **69** (2004) 214102.
70. M. Sakashita, H. Yamawaki, H. Fujihisa, K. Aoki. Pressure-Induced Molecular Dissociation and Metallization in Hydrogen-Bonded H_2S Solid. Phys. Rev. Lett. **79** (1997) 1082–1085.
71. S. Kometani, M.I. Eremets, K. Shimizu [et al.]. Observation of Pressure-Induced Superconductivity of Sulfur. J. Phys. Soc. Jap. **66** (1997) 2564–2565.
72. T.A. Strobel, P. Ganesh, M. Somayazulu [et al.]. Novel Cooperative Interactions and Structural Ordering in H_2S-H_2. Phys. Rev. Lett. **107** (2011) 255503.

73. J.A. Flores-Livas, A. Sanna, E.K.U. Gross. High temperature superconductivity in sulfur and selenium hydrides at high pressure. The European Physical Journal B **89** (2016) 63.
74. R. Szczęśniaka, T.P. Zemłab, D. Szczęśniak. Superconducting state in bromium halide at high pressure. Physica B: Cond. Matter. **495** (2016) 106–116.
75. K.V. Shanavas, L. Lindsay, D.S. Parker. Electronic structure and electron-phonon coupling in TiH_2. Sci. Rep. **6** (2016) 28102.
76. Y. Fu, X. Du, L. Zhang [et al.]. High-Pressure Phase Stability and Superconductivity of Pnictogen Hydrides and Chemical Trends for Compressed Hydrides. Chem. Mater. **28** (2016) 1746–1755.
77. R. Szczęśniak, A.P. Durajski. Superconductivity well above room temperature in compressed MgH_6. Frontiers of Physics **11** (2016) 117406.
78. P. Gütlich, A.B. Gaspar, Y. Garcia. Spin state switching in iron coordination compounds. Beilstein Journal of Organic Chemistry **9** (2013) 342–391.
79. R. H. Herber. The Mössbauer Effect and Its Application in Chemistry. Washington: American Chemical Society, 1967, P. 158.
80. R. R. Gainov, F. G. Vagizov, V. A. Golovan. Application of ^{57}Fe Mössbauer spectroscopy as a tool for mining exploration of bornite (Cu_5FeS_4) copper ore. Hyperfine Interactions **226** (2014) 51–55.
81. J. M. Byrne, N. Klueglein, C. Pearce [et al.]. Redox cycling of Fe(II) and Fe(III) in magnetite by Fe-metabolizing bacteria. Science **347** (2015) 1473–1476.
82. G. Klingelhöfer, R. V. Morris, B. Bernhardt [et al.]. Jarosite and hematite at Meridiani Planum from opportunity's Mössbauer spectrometer. Science **306** (2004) 1740–1745.
83. W. B. Gao, J. Lindén, X. C. Wang. Evolution of the hyperfine parameters of Fe in superconducting LiFeAs as observed by ^{57}Fe Mössbauer spectroscopy. Solid State Commun. **150** (2010) 1525–1528.
84. A. Khasanov, S. C. Bhargava, J. G. Stevens [et al.]. Mössbauer studies of the superconducting cobalt/nickel-doped $BaFe_2As_2$. Whither go the injected electron(s)? J. Phys.: Cond. Matter. **23** (2011) 202201.
85. A. Pogrebna, T. Mertelj, N. Vujičić [et al.]. Coexistence of ferromagnetism and superconductivity in iron based pnictides: a time resolved magnetooptical study. Sci. Rep. **5** (2015).
86. N. N. Greenwood, T. C. Gibb. Mössbauer Spectroscopy. London: Chapman and Hall Ltd, 1971, P. 659.
87. K. Lagarec, D. G. Rancourt. Extended Voigt-based analytic lineshape method for determining N-dimensional correlated hyperfine parameter distributions in Mössbauer spectroscopy. Nuc. Instrum. Meth. Phys. Res. B. **129** (1997) 266–280.
88. V. Potapkin, A. I. Chumakov, G. V. Smirnov [et al.]. The ^{57}Fe Synchrotron Mössbauer Source at the ESRF. J. Synch. Rad. **19** (2012) 559–569.
89. V. Vreshch. DiffractWD: an open-source program for powder pattern comparison and visualization. J. Appl. Crystallogr. **44** (2011) 219–220.
90. S. I. Shylin, V. Ksenofontov, S. J. Sedlmaier, S. J. Clarke, S. J. Cassidy, G. Wortmann, S. A. Medvedev, C. Felser. Intercalation effect on hyperfine parameters of Fe in FeSe superconductor with T_c = 42 K. EPL **109** (2015) 67004.

91. A. Gerard, F. Gradjean F. J. Phys. Chem. Sol. **36** (1975) 1365.
92. S. I. Shylin, V. Ksenofontov, P. G. Naumov, S. A. Medvedev, V. Tsurkan, J. Deisenhofer, A. Loidl, L. M. Schoop, T. Palasyuk, G. Wortmann, C. Felser. Pressure effect on superconductivity in $FeSe_{0.5}Te_{0.5}$. Phys. Status Solidi B **254** (2017) 1600161.
93. M.H. Fang, H.M. Pham, B. Qian [et al.]. Superconductivity close to magnetic instability in $Fe(Se_{1-x}Te_x)_{0.82}$. Phys. Rev. B. **78** (2008) 224503.
94. K-W. Yeh, T-W. Huang, Y-l. Huang [et al.]. Tellurium substitution effect on superconductivity of the α-phase iron selenide. EPL **84** (2008) 37002.
95. V. Tsurkan, J. Deisenhofer, A. Günther [et al.]. Physical properties of $FeSe_{0.5}Te_{0.5}$ single crystals grown under different conditions. The European Physical Journal B **79** (2011) 289–299.
96. R. W. Gómez, V. Marquina, J. L. Pérez-Mazariego [et al.]. Effects of Substituting Se with Te in the FeSe Compound: Structural, Magnetization and Mössbauer Studies. J. Supercond. Nov. Magnet. **23** (2010) 551–557.
97. B. C. Sales, A. S. Sefat, M. A. McGuire [et al.]. Bulk superconductivity at 14 K in single crystals of $Fe_{1+y}Te_xSe_{1-x}$. Phys. Rev. B. **79** (2009) 094521.
98. G. F. Chen, Z. G. Chen, J. Dong [et al.]. Electronic properties of single-crystalline $Fe_{1.05}Te$ and $Fe_{1.03}Se_{0.30}Te_{0.70}$. Phys. Rev. B. **79** (2009) 140509.
99. T. Taen, Y. Tsuchiya, Y. Nakajima, T. Tamega. Superconductivity at $T_c \sim 14$ K in single-crystalline $FeTe_{0.61}Se_{0.39}$. Phys. Rev. B. **80** (2009) 092502.
100. A. Subedi, L. Zhang, D. J. Singh, M. H. Du. Density functional study of FeS, FeSe, and FeTe: Electronic structure, magnetism, phonons, and superconductivity. Phys. Rev. B. **78** (2008) 134514.
101. M. Forthaus, K. Sengupta, O. Heyer, N. Christensen, A. Svane, K. Syassen, D. Khomskii, T. Lorenz, and M. Abd-Elmeguid. Superconductivity in SnO: A Nonmagnetic Analog to Fe-Based Superconductors? Phys. Rev. Lett. **105** (2010) 157001.
102. S. I. Shylin, V. Ksenofontov, S. A. Medvedev, V. Tsurkan, C. Felser. Phase Separation in $Rb_xFe_{2-y}Se_2$ Probed by Non-stoichiometry and Cu Doping. J. Supercond. Nov. Magnet. **28** (2015) 1315–1319.
103. S. I. Shylin, V. Ksenofontov, S. A. Medvedev, C. Felser. Correlation between T_c and Hyperfine Parameters of Fe in Layered Chalcogenide Superconductors. J. Supercond. Nov. Magnet. **29** (2016) 573–576.
104. A. P. Drozdov, M. I. Eremets, I. A. Troyan, V. Ksenofontov, S. I. Shylin. Conventional superconductivity at 203 kelvin at high pressures in the sulfur hydride system. Nature **525** (2015) 73–76.
105. D. Duan, Y. Liu, F. Tian, D. Li, X. Huang, Z. Zhao, H. Yu, B. Liu, W. Tian, T. Cui. Pressure-induced metallization of dense $(H_2S)_2H_2$ with high-Tc superconductivity. Sci. Rep. **4** (2014) 6968.
106. L. P. Gor'kov, V. Z. Kresin. Pressure and high-T_c superconductivity in sulfur hydrides. Sci. Rep. **6** (2016) 25608.
107. A. Bianconi, T. Jarlborg. Superconductivity above the lowest Earth temperature in pressurized sulfur hydride. EPL **112** (2015) 37001.

108. T. Jarlborg, A. Bianconi. Breakdown of the Migdal approximation at Lifshitz transitions with giant zero-point motion in the H_3S superconductor. Sci. Rep. **6** (2016) 24816.
109. E. E. Gordon, K. Xu, H. Xiang, R. K. Kremer, A. Simon, J. Köhler, M.-H. Whangbo. Structure and Composition of the 200 K-Superconducting Phase of H_2S at Ultrahigh Pressure: The Perovskite (SH^-)(H_3S^+). Angew. Chem. Int. Ed. **128** (2016) 3746–3748.
110. M. Einaga, M. Sakata, T. Ishikawa, K. Shimizu, M. I. Eremets, A. P. Drozdov, I. A. Troyan, N. Hirao, Y. Ohishi. Crystal structure of the superconducting phase of sulfur hydride. Nat. Phys. **12** (2016) 835–838.